

Entanglement entropies of an interval for the massless scalar field in the presence of a boundary

Benoit Estienne^a, Yacine Ikhlef^a, Andrei Rotaru^a and Erik Tonni^b

^a *Sorbonne Université, CNRS, Laboratoire de Physique Théorique et Hautes Énergies, LPTHE,
F-75005 Paris, France*

^b *SISSA and INFN Sezione di Trieste, via Bonomea 265, 34136, Trieste, Italy*

Abstract

We study the entanglement entropies of an interval for the massless compact boson either on the half line or on a finite segment, when either Dirichlet or Neumann boundary conditions are imposed. In these boundary conformal field theory models, the method of the branch point twist fields is employed to obtain analytic expressions for the two-point functions of twist operators. In the decompactification regime, these analytic predictions in the continuum are compared with the lattice numerical results in massless harmonic chains for the corresponding entanglement entropies, finding good agreement. The application of these analytic results in the context of quantum quenches is also discussed.

Contents

1	Introduction	3
2	BCFT expressions for the entanglement entropies	5
2.1	Single interval either on the half line or on the segment	5
2.2	Entanglement entropies for the compact boson	8
3	Entanglement entropies in the unit disk	12
3.1	Partition function	12
3.2	Decompactification regime	19
4	Numerical results from harmonic chains	21
5	Quantum quenches	30
5.1	Global quench	31
5.2	Local quench	32
6	Conclusions	35
A	An insight from the six-vertex model	37
B	Period matrix	37
C	Green function in the presence of twist fields	39
D	Limiting regimes	42
D.1	Compactified boson	42
D.2	Decompactified boson	44
E	Details about the BCFT approach to quantum quenches	47
E.1	Global quench	48
E.2	Local quench	48

1 Introduction

Entanglement is a fascinating feature of quantum systems that is attracting the interest of a growing number of researchers from various fields of theoretical physics, including quantum gravity, condensed matter and quantum information (for further reading, we refer to the reviews [1–5]). The presence of physical boundaries influences the features of entanglement in highly non-trivial ways that have been explored in various contexts gaining important insights [6–12]. For instance, for the holographic entanglement entropy [13, 14] the analysis of the boundary effects [15–18] has recently provided a novel approach to the information paradox [19–23]. In the context of topological phases of matter, the entanglement entropy can be used to detect and identify edge modes at a boundary [24, 25] or more generally at an interface [26, 27].

The bipartite entanglement for a spatial bipartition can be studied by considering a quantum system whose space is bipartite into a region A and its complement B and whose Hilbert space \mathcal{H} can be factorised accordingly as $\mathcal{H} = \mathcal{H}_A \otimes \mathcal{H}_B$. Denoting by ρ the density matrix of the system, the reduced density matrix $\rho_A \equiv \text{Tr}_B \rho$ for the subsystem A is introduced by taking its partial trace over \mathcal{H}_B . When the system is in a pure state $|\Psi\rangle$, and therefore $\rho = |\Psi\rangle\langle\Psi|$, it is well known that the entanglement entropy

$$S_A \equiv -\text{Tr}(\rho_A \log \rho_A) \quad (1.1)$$

is the unique measure of the bipartite entanglement. It satisfies $S_A = S_B$ and all the other properties characterising an entanglement measure [28, 29]. In order to evaluate (1.1), it is often convenient to introduce the Rényi entropies

$$S_A^{(n)} \equiv \frac{1}{1-n} \log(\text{Tr} \rho_A^n) \quad (1.2)$$

where the Rényi index n takes integer values $n \geq 2$. Since the normalization condition $\text{Tr} \rho_A = 1$ is assumed, by performing the analytic continuation $n \rightarrow 1$, one finds $S_A^{(n)} \rightarrow S_A$, and this is also known as the replica limit in the context of entanglement. The entanglement entropy (1.1) and the moments $\text{Tr} \rho_A^n$ of the reduced density matrix ρ_A can be evaluated more directly also through the entanglement spectrum, i.e. the multiset made by the eigenvalues $\lambda_j \in (0, 1)$ of the reduced density matrix. The largest eigenvalue λ_{\max} of the entanglement spectrum provides the single copy entanglement $S_A^{(\infty)}$ [30–32], which can be obtained also as the limit $n \rightarrow \infty$ of the Rényi entropies

$$S_A^{(\infty)} \equiv -\log(\lambda_{\max}) = \lim_{n \rightarrow \infty} S_A^{(n)}. \quad (1.3)$$

The entanglement entropies correspond to the quantities (1.1), (1.2) and (1.3).

The entanglement entropies are usually evaluated through the replica method [6, 33, 34], which naturally leads to write the moments of ρ_A as follows

$$\text{Tr} \rho_A^n = \frac{\mathcal{Z}_n}{\mathcal{Z}^n} \quad (1.4)$$



Figure 1: Spatial bipartitions considered in this manuscript: the interval A (red segment) is either on the half line (left panel) or on the segment of finite length L (right panel), where the b.c. is labelled by α . The same b.c. is imposed at both the endpoints of the segment.

where \mathcal{Z} is the partition function of the model and \mathcal{Z}_n is the partition function of the same model defined on a n -sheeted branched covering. The determination of analytic expressions for (1.4) in quantum field theories is typically a difficult task.

Focussing on critical systems in one spatial dimension, we can employ the powerful framework of Conformal Field Theory (CFT) [35] and of Boundary Conformal Field Theory (BCFT) [36–40] whenever physical boundaries occur. In [6, 41], it has been shown that the branch point twist fields [42–45] provide an insightful tool to investigate entanglement in quantum field theories. For instance, in one spatial dimension the Rényi entropies of an interval in the infinite line is given by the two-point function of twist fields located at the endpoints of the boundary. For a CFT on the line and in its ground state, this two-point function depends only on the central charge of the model. For a BCFT on the half line and in its ground state, the Rényi entropies of an interval adjacent to the boundary are given by the one-point function of a twist field [6] and they encode also the boundary entropy introduced by Affleck and Ludwig [46], which characterises the boundary condition (b.c.) through the conformal boundary state. This boundary entropy allows to explore the boundary renormalisation group flows induced by the change of boundary conditions [47, 48].

The entanglement entropies of more complicated bipartitions encode more detailed information about the underlying quantum field theory. A paradigmatic example is given by the Rényi entropies of two disjoint intervals for a CFT on a line and in its ground state, which can be expressed as the four point function of twist fields, or equivalently as the partition function on a genus $n - 1$ Riemann surface obtained as a n -sheeted branched covering of the sphere through (1.4). The entanglement quantifiers encompass a significant amount of CFT data beyond the central charge [49–59]. Some analytic results have been obtained and they have been also checked through various numerical analysis in the proper lattice models. The replica limit $n \rightarrow 1$ of these analytic expressions is typically very difficult; hence the numerical extrapolation method discussed in [60, 61] can be useful.

All the challenges and characteristic features arising in a translation invariant space when the subsystem A is made by the union of two disjoint regions also occur when the model has a physical boundary and its spatial bipartition is given by a region not adjacent to it. In the case of a BCFT on a segment where the same conformally invariant b.c. has been imposed at both its endpoints (or on the half line) and in its ground state, the Rényi entropies of an interval located at finite distance from the boundary (see Fig. 1) can be expressed as either the partition function on a sphere with n disks removed or as a two-point function of twist fields on the unit disk. These quantities probe a significant amount of BCFT data beyond the

central charge and the boundary entropy. For instance, the Rényi entropy with $n = 2$ encodes the entire annulus partition function [62]. However, for $n > 2$ very few results are available in the literature. The case of an interval for the free massless Dirac field on the half line, which is the prototypical fermionic BCFT with $c = 1$, has been analyzed in [63] (see [64] for a lattice computation) and later extended to an arbitrary number of intervals [65]. Another important BCFT with $c = 1$ to explore is the massless compact boson either on the half line or on the segment. For this model, the Rényi entropies of an interval in the segment have been investigated in [66], where, in the case of Dirichlet b.c., an implicit expression has been found and evaluated numerically. This result has been checked through lattice calculations in the XXZ chain [67]. In the same setup, explicit analytic BCFT expressions for both Dirichlet b.c. and Neumann b.c. have been obtained for the special case of $n = 2$ in [62].

In this manuscript we consider the compact massless scalar field either on the half line or on the segment where the same b.c. are imposed at both its endpoints. Both Dirichlet b.c. and Neumann b.c. are investigated. By combining the twist field method [42, 52] with some results involving the branched covering of Riemann surfaces [68–75], we obtain analytic expressions for the Rényi entropies of an interval which is not adjacent to the boundary. In the special case of $n = 2$, the results of [62] are recovered. Furthermore, in the case of Dirichlet b.c., we have checked numerically that our expression agrees with the one obtained in [66]. In the decompactification limit, we have compared our analytic results with the corresponding numerical outcomes obtained for the harmonic chains in the massless regime, finding a good agreement. Finally, the application of these analytic results in the context of the BCFT approach to the quantum quenches developed in [76, 77] has been also discussed.

The outline of this manuscript is as follows. Explicit formulas for the Rényi entropies are reported and discussed in Sec. 2. In Sec. 3 the BCFT computations underlying these results are described. Sec. 4 contains a comparison of our analytical results in the decompactification limit with the lattice data obtained numerically for the corresponding semi-infinite and finite harmonic chains in the massless regime. In Sec. 5 the application of our analytic expressions within the BCFT approach to the quantum quenches is discussed. In Sec. 6 we summarise our results and mention some future directions. The Appendices A, B, C, D and E contain technical details and further discussions.

2 BCFT expressions for the entanglement entropies

In this section we discuss the procedure of our BCFT calculation and describe the main analytic results, both at finite compactification radius R and in the decompactification limit $R \rightarrow \infty$.

2.1 Single interval either on the half line or on the segment

We are interested in calculating the entanglement entropy of an interval for a one dimensional quantum critical system in its ground state defined either on a segment of finite length L or on the half line. In the latter case, we restrict to models where the same b.c. are imposed

at both ends of the system and its limit $L \rightarrow \infty$ provides the former one. The critical point is assumed to be governed by a BCFT and we denote by α the label identifying the allowed conformally invariant boundary conditions.

We investigate the spatial bipartition of the system given by an interval $A = (u, v)$ and its complement when A is not adjacent to the boundary, namely when $0 < u < v < L$, as shown in Fig. 1. The moments of the reduced density matrix ρ_A read

$$M_{A;\alpha}^{(n)} \equiv \text{Tr} \rho_A^n = \langle \tau_n(u) \tau_n^\dagger(v) \rangle \quad (2.1)$$

where τ_n and τ_n^\dagger stand for the microscopic twist operators, which are defined e.g. on a lattice. In the scaling limit, the lattice operator τ_n can be expanded into a linear combination of scaling fields in the corresponding CFT model and the most relevant among these primaries is the twist operator \mathcal{T}_n , a spinless primary field with scaling dimension [6]

$$\Delta_n = \frac{c}{12} \left(n - \frac{1}{n} \right). \quad (2.2)$$

Hence [41, 78, 79]

$$\tau_n = C_n \epsilon^{\Delta_n} \mathcal{T}_n + \dots \quad (2.3)$$

where the dots correspond to less relevant fields whose contribution to $\text{Tr} \rho_A^n$ matters when finite size corrections are taken into account. The prefactor C_n is a non universal constant coming from the normalization of the microscopic operator τ_n and ϵ is a UV cutoff, like e.g. the lattice spacing. Thus, the moments of the reduced density matrix $M_{A;\alpha}^{(n)}$ in (2.1) can be written as

$$M_{A;\alpha}^{(n)} = C_n^2 \epsilon^{2\Delta_n} \langle \mathcal{T}_n(u) \mathcal{T}_n^\dagger(v) \rangle_{\mathbb{S}} \quad (2.4)$$

where $\mathbb{S} = \{w \in \mathbb{C}; 0 < \text{Re}(w) < L\}$ is the infinite strip (with imaginary time running along the imaginary axis) of width L with the same boundary condition α imposed on both sides of the strip. Because of conformal invariance, the two-point function on the strip can be written in the following form

$$M_{A;\alpha}^{(n)} \equiv \text{Tr} \rho_A^n = C_n^2 \frac{\mathcal{F}_n^{(\alpha)}(r)}{\mathcal{P}(u, v)^{\Delta_n}} \quad (2.5)$$

where

$$\mathcal{P}(u, v) \equiv \frac{s(2u) s(2v) s(v-u)^2}{\epsilon^2 s(v+u)^2} \quad r \equiv \left(\frac{s(v-u)}{s(v+u)} \right)^2 \quad s(w) \equiv \frac{2L}{\pi} \sin\left(\frac{\pi w}{2L}\right) \quad (2.6)$$

and $\mathcal{F}_n^{(\alpha)}$ depends on the specific BCFT model, which is characterised also by the boundary conditions labelled by α and it is related to the partition functions on the Riemann sphere with n boundary components. In particular, $\mathcal{F}_2^{(\alpha)}(r)$ is given by the partition function of the BCFT model on the annulus [62].

From the moments (2.5), one obtains the Rényi entropies (1.2) of an interval A for a BCFT on the strip \mathbb{S}

$$S_{A;\alpha}^{(n)} = \frac{\Delta_n}{n-1} \log[\mathcal{P}(u, v)] + \frac{\log[C_n^2 \mathcal{F}_n^{(\alpha)}(r)]}{1-n} \quad (2.7)$$

whose analytic continuation $n \rightarrow 1$ provides the corresponding entanglement entropy (1.1), which reads

$$S_{A;\alpha} = \frac{c}{6} \log[\mathcal{P}(u, v)] + 2 C'_1 + \mathcal{G}_1^{(\alpha)}(r) \quad (2.8)$$

where we have defined $C'_1 \equiv -\lim_{n \rightarrow 1} \frac{\log C_n}{n-1}$ and

$$\mathcal{G}_1^{(\alpha)}(r) \equiv -\lim_{n \rightarrow 1} \partial_n \left(\log \mathcal{F}_n^{(\alpha)}(r) \right) \quad (2.9)$$

while the corresponding single copy entanglement (1.3) is given by

$$S_{A;\alpha}^{(\infty)} = \frac{c}{12} \log[\mathcal{P}(u, v)] + \lim_{n \rightarrow \infty} \frac{\log[C_n^2 \mathcal{F}_n^{(\alpha)}(r)]}{1-n}. \quad (2.10)$$

Instead, when A is adjacent to the boundary, i.e. $u = 0$, we have [6]

$$\text{Tr} \rho_A^n = C_n \epsilon^{\Delta_n} \frac{g_\alpha^{1-n}}{s(2v)^{\Delta_n}} \quad (2.11)$$

where g_α is related to the Affleck-Ludwig boundary entropy [46], that plays a crucial role in the analysis of the boundary renormalisation group flows [47, 48].

The expressions (2.4) and (2.5) for the moments of the reduced density matrix naturally lead to introduce two kinds of ratios that are UV finite. A first type of ratios can be defined for an assigned boundary condition α as follows

$$R_{A;\alpha}^{(n)} \equiv \frac{M_{A;\alpha}}{M_{A_u;\alpha} M_{A_v;\alpha}} \quad (2.12)$$

where $A_u \equiv [0, u]$ and $A_v \equiv [0, v]$ (see Fig. 1). For the BCFT we are considering, by using the expressions in (2.5)-(2.6), this ratio becomes

$$R_{A;\alpha}^{(n)} = g_\alpha^{2(n-1)} \frac{\mathcal{F}_n^{(\alpha)}(r)}{r^{\Delta_n}}. \quad (2.13)$$

From (2.12) and (1.2), the following UV finite combination of entanglement entropies can be introduced

$$\mathcal{I}_{A;\alpha}^{(n)} \equiv S_{A_u;\alpha}^{(n)} + S_{A_v;\alpha}^{(n)} - S_{A;\alpha}^{(n)}. \quad (2.14)$$

For a BCFT on a segment, by using (2.7), one finds that this UV finite combination becomes

$$\mathcal{I}_{A;\alpha}^{(n)} = -\frac{c}{12} \left(1 + \frac{1}{n} \right) \log(r) + \frac{\log[\mathcal{F}_n^{(\alpha)}(r)]}{n-1} + 2 \log g_\alpha \quad (2.15)$$

which is a function of the harmonic ratio r in (2.6).

Another type of UV finite ratios can be defined only through the interval A , without employing the entanglement entropies of intervals adjacent to the boundary; but it needs two different conformally invariant boundary conditions α_1 and α_2 . From (2.4) and (2.5), these ratios are

$$\frac{M_{A;\alpha_1}^{(n)}}{M_{A;\alpha_2}^{(n)}} = \frac{\mathcal{F}_n^{(\alpha_1)}(r)}{\mathcal{F}_n^{(\alpha_2)}(r)} \quad (2.16)$$

which naturally lead to the following difference of Rényi entropies

$$S_{A;\alpha_1}^{(n)} - S_{A;\alpha_2}^{(n)} = \frac{1}{1-n} \log \left(\frac{\mathcal{F}_n^{(\alpha_1)}(r)}{\mathcal{F}_n^{(\alpha_2)}(r)} \right) \quad (2.17)$$

where we have denoted by $S_{A;\alpha}^{(n)}$ the Rényi entropies (1.2), in order to highlight its dependence on the boundary condition α . We remark that the above expressions hold for a BCFT on a segment and that the corresponding ones for the BCFT on the half line are obtained by taking $L \rightarrow \infty$.

The CFT quantities we are considering are related to the two-point functions of twist fields $\langle \mathcal{T}_n(u) \mathcal{T}_n^\dagger(v) \rangle_{\mathbb{S}}$ on the strip $\mathbb{S} \equiv \{w \in \mathbb{C}; 0 < \text{Re}(w) < L\}$. Since the strip is conformally equivalent to the unit disk $\mathbb{D} \equiv \{z \in \mathbb{C}; |z| \leq 1\}$ via the map $w \mapsto z = \frac{s(w-u)}{s(w+u)}$, we have

$$\langle \mathcal{T}_n(u) \mathcal{T}_n^\dagger(v) \rangle_{\mathbb{S}} = \frac{\langle \mathcal{T}_n(0) \mathcal{T}_n^\dagger(x) \rangle_{\mathbb{D}}}{s(u+v)^{2\Delta_n}} \quad x = \frac{s(v-u)}{s(u+v)} \quad (2.18)$$

where the same boundary condition imposed on both the boundaries of \mathbb{S} holds also on the boundary of \mathbb{D} . In the case of the BCFT on the half line, we have to consider the right half plane $\mathbb{H} \equiv \{z \in \mathbb{C}; \text{Re}(z) \geq 0\}$ instead of the strip. The corresponding two-point functions of twist fields can be studied by taking $L \rightarrow \infty$ in (2.18), finding

$$\langle \mathcal{T}_n(u) \mathcal{T}_n^\dagger(v) \rangle_{\mathbb{H}} = \frac{\langle \mathcal{T}_n(0) \mathcal{T}_n^\dagger(x) \rangle_{\mathbb{D}}}{(u+v)^{2\Delta_n}} \quad x = \frac{v-u}{v+u}. \quad (2.19)$$

Thus, the Rényi entropies we are interested in can be obtained from the two-point function of twist fields $\langle \mathcal{T}_n(0) \mathcal{T}_n^\dagger(x) \rangle_{\mathbb{D}}$ on the unit disk, with $0 < x < 1$. This two-point function is equivalent to the following ratio of partition functions [6]

$$\langle \mathcal{T}_n(0) \mathcal{T}_n^\dagger(x) \rangle_{\mathbb{D}} = \mathcal{Z}_n(x) / \mathcal{Z}_1^n \quad (2.20)$$

where $\mathcal{Z}_n(x)$ is the BCFT partition function on the n -sheeted covering of the unit disk with branch points at 0 and x , while \mathcal{Z}_1 is simply the BCFT partition function on the unit disk.

Few explicit analytic expressions for $\mathcal{F}_n^{(\alpha)}$ in (2.5) are available in the literature: for the massless Dirac field, where $\mathcal{F}_n^{(\alpha)} = 1$ identically for any value of n and independently of the (conformally invariant) boundary conditions [63], and for the massless compactified scalar when $n = 2$ and a generic conformally invariant boundary condition [62], in terms of the annulus partition function [62]. In this manuscript we extend the latter result for the massless compactified scalar to a generic value of the Rényi index n , focussing on Dirichlet and Neumann boundary conditions.

2.2 Entanglement entropies for the compact boson

We consider a gapless one dimensional quantum system belonging to the Luttinger liquid universality class, whose low energy behaviour is captured by the massless compact real boson, which is a specific CFT with $c = 1$. A prototypical example is the spin- $\frac{1}{2}$ XXZ spin chain (see

Appendix A). The Euclidean action of the massless compact real boson on a generic Riemann surface \mathcal{M} equipped with metric $g_{\mu\nu}$ whose target space is a circle of radius R reads

$$S[\phi] = \frac{1}{8\pi} \int_{\mathcal{M}} g^{\mu\nu} \partial_\mu \phi \partial_\nu \phi \sqrt{|g|} d^2x \quad \phi \sim \phi + 2\pi R. \quad (2.21)$$

Considering the BCFT given by this model either on the half line or on the segment with the same b.c. at both its endpoints, the main results of this manuscript are the analytic expressions for $\mathcal{F}_n^{(\alpha)}$ when α corresponds to either Dirichlet (D) or Neumann (N) b.c., which are respectively

$$\mathcal{F}_n^{(D)}(r) = \frac{\Theta(\boldsymbol{\tau}(r)/R^2)}{\Theta(\boldsymbol{\tau}(r))} \quad \mathcal{F}_n^{(N)}(r) = \frac{\Theta(R^2 \boldsymbol{\tau}(r)/4)}{\Theta(\boldsymbol{\tau}(r))} \quad (2.22)$$

where $r \in (0, 1)$, in terms of the Siegel theta function defined as follows

$$\Theta(\mathbf{h}) \equiv \sum_{\mathbf{m} \in \mathbb{Z}^g} e^{i\pi \mathbf{m}^t \cdot \mathbf{h} \cdot \mathbf{m}} \quad (2.23)$$

which is a function of a $g \times g$ symmetric matrix \mathbf{h} having positive definite imaginary part. In our analysis, the matrix $\boldsymbol{\tau}(r)$ in (2.22) is the $(n-1) \times (n-1)$ period matrix found in [52], which occurs in the entanglement entropies of two disjoint intervals on the infinite line for the massless compact scalar in its ground state. Its matrix elements are

$$\tau_{i,j}(r) \equiv i \frac{2}{n} \sum_{k=1}^{n-1} \sin(\pi k/n) \frac{F_{k/n}(1-r)}{F_{k/n}(r)} \cos[2\pi k(i-j)/n] \quad (2.24)$$

where $1 \leq i, j \leq n-1$ and $F_{k/n}(y) \equiv {}_2F_1(k/n, 1-k/n; 1; y)$ is a particular hypergeometric function. The results of [62] are recovered by specialising the expressions in (2.22) to $n=2$.

When the bipartition on the infinite line is given by the union A of two disjoint intervals [52], the moments $\text{Tr} \rho_A^n$ are obtained as the partition function of the model on the n -sheeted Riemann surface $\mathcal{M} = \mathcal{M}_n$, which is a special Riemann surface with genus $g = n-1$ obtained through the replica construction (see the Appendix A of [53]). For a CFT, this special Riemann surface is characterised by the harmonic ratio of the endpoints of the two intervals, which is a real parameter in $(0, 1)$. For instance, \mathcal{M}_4 has genus $g = 3$ and it is shown in the left panel of Fig. 2 for the special case of two equal intervals. Further analyses and generalisations of \mathcal{M}_n have been discussed e.g. in [53, 56, 59].

The method of the images allows to find the n -sheeted Riemann surface $\mathcal{M} = \mathcal{S}_n$ for a BCFT on the half line and in its ground state as follows. Consider \mathcal{M}_n for two equal intervals (when $n=4$, see the left panel of Fig. 2), which exhibits a \mathbb{Z}_2 symmetry (a reflection) with respect to a plane (see the black plane in the middle panel of Fig. 2). The n -sheeted Riemann surface \mathcal{S}_n corresponds to one of the two halves identified by this reflection plane, whose union gives \mathcal{M}_n . Thus, \mathcal{S}_n has the topology of a sphere with n boundaries, which has genus $g = 0$ and Euler characteristic $\chi = 2 - n$ (for $n=4$, see the right panel of Fig. 2).

Upon examining (2.5), (2.6), and (2.22), one can readily observe that the BCFT expressions for the moments of the reduced density matrix remain unchanged when u and v are exchanged,

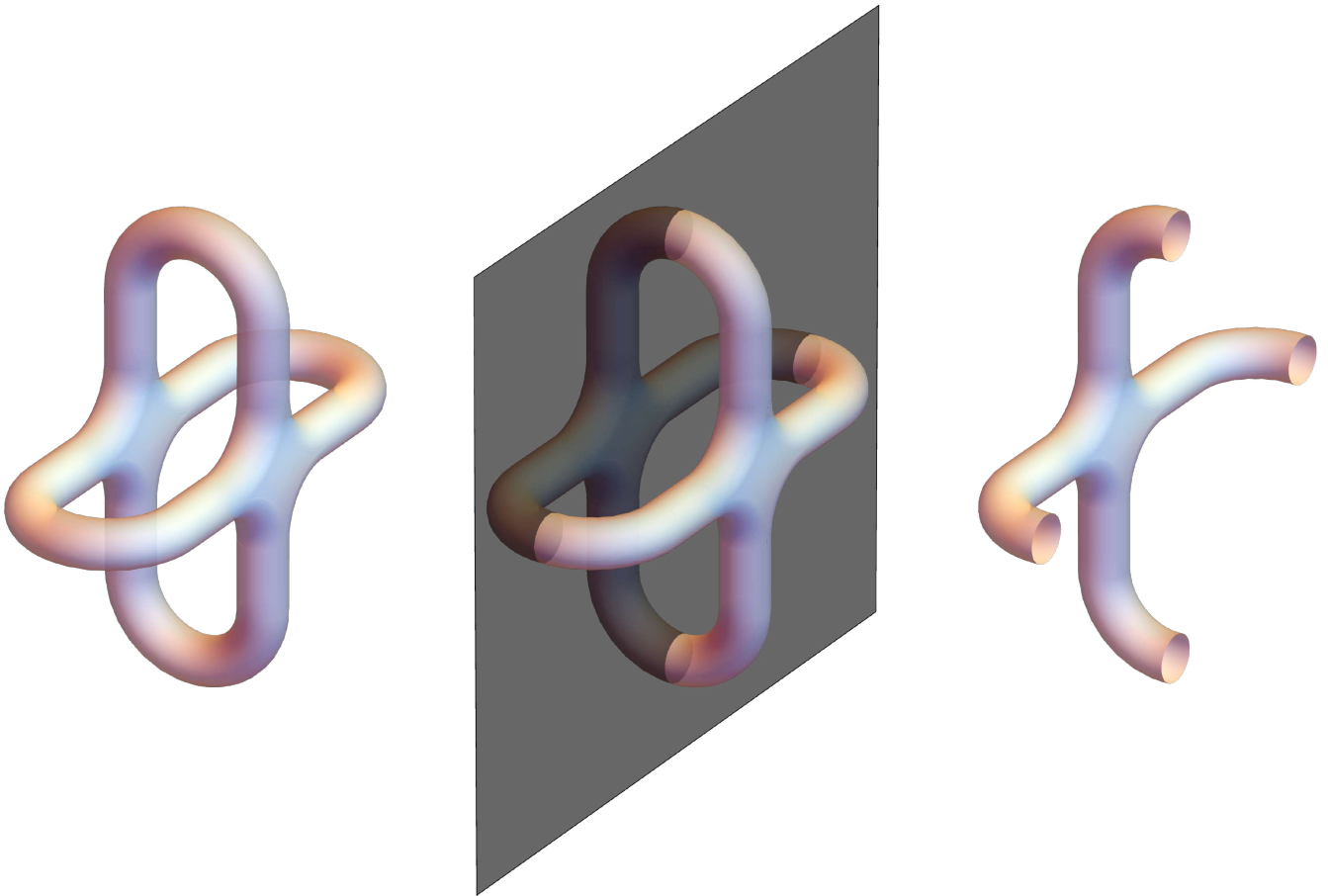


Figure 2: The Riemann surface \mathcal{S}_4 (right panel) is topologically a sphere with four boundaries. It is obtained as one of the two halves of \mathcal{M}_4 for two equal intervals (left panel) determined by its reflection symmetry with respect to a plane (the black plane in the middle panel).

which corresponds to the exchange of \mathcal{T}_n with \mathcal{T}_n^\dagger . This symmetry exchange is a consistency check for our analytic results.

Furthermore, since the entire system is in a pure state, it is well known that $S_A^{(n)} = S_B^{(n)}$ for any value of n . In our analysis, this is verified because the computation of the $S_A^{(n)}$ and of $S_B^{(n)}$ involve the same n -sheeted branched covering of the strip (or of the half plane).

By employing (1.4), (2.4), (2.5) and (2.22), we observe that the following relation occurs between the partition functions corresponding to Dirichlet b.c. and Neumann b.c.

$$\mathcal{Z}_n^{(N)}(R) = \mathcal{Z}_n^{(D)}(2/R). \quad (2.25)$$

This provides a non trivial consistency check of the dependence on the compactification radius R in (2.22); indeed, for the compact massless boson this T-duality relation is expected to hold, as discussed in [80] for the annulus (i.e. for the $n = 2$ case) and in [81] for a generic Riemann surfaces with boundaries.

As a further consistency check, in the Appendix D.1 we recover the known result for $S_A^{(n)}$ when the interval A is adjacent to the boundary [6] as a limiting case.

Summarising, for the massless compact scalar field on the segment with the same b.c. at its endpoints, which is a BCFT with $c = 1$, the moments of the reduced density matrix of an interval not adjacent to the boundary (see the right panel of Fig. 1) are given by (2.5) with $c = 1$ and $\mathcal{F}_n^{(\alpha)}(r)$ replaced by the function in (2.22) associated to the proper boundary condition. The corresponding expressions for the interval in the half line (see the left panel of Fig. 1) can be obtained by taking the limit $L \rightarrow +\infty$.

The Rényi entropies for the massless scalar field in the case of Dirichlet b.c. and the spatial bipartition in the right panel of Fig. 1 have been already studied in [66], where implicit results have been found. This analysis has been developed further in [67] for inhomogeneous systems. In order to apply the outcomes of these works, linear integral equations must be solved and, since analytic solutions have not been found, approximate results can be obtained numerically by discretising the interval A , as discussed in [66]. This provides an important benchmark for the analytic BCFT expression we obtain for Dirichlet b.c.: we checked¹ that it is compatible with the one obtained numerically in [66]. In particular, for $n \leq 5$ and various sizes for the interval, we found numerical agreement between the period matrix $\boldsymbol{\tau}$ in (2.24) and the matrix \mathcal{M} of [66], once the difference in the notations has been taken into account. Also the compatibility for the Rényi entropies when $n \leq 5$ and for various values of the compactification radius $R \in (0.5, 3)$ has been checked. As n increases, higher accuracy in the discretisation procedure is needed to find agreement with our BCFT result in the continuum.

2.2.1 Decompactification regime

The decompactification regime as defined as the limit of large compactification radius $R \rightarrow \infty$ and it corresponds to the case where the target space is the infinite line. Taking the limit $R \rightarrow \infty$ and rescaling by appropriate powers of R to obtain a finite result, we find that the moments $\text{Tr}\rho_A^n$ of the interval $A = [u, v]$ on the strip of length L for Dirichlet b.c. and Neumann b.c. become respectively

$$M_{A;D}^{(n)} = \frac{C_n^2}{\mathcal{P}(u, v)^{\Delta_n}} \tilde{\mathcal{F}}_n^{(D)}(r) \quad M_{A;N}^{(n)} = \frac{C_n^2}{\mathcal{P}(u, v)^{\Delta_n}} \tilde{\mathcal{F}}_n^{(N)}(r) \quad (2.26)$$

where we have introduced

$$\tilde{\mathcal{F}}_n^{(D)}(r) \equiv \frac{1}{\sqrt{\prod_{k=1}^{n-1} F_{k/n}(1-r)}} \quad \tilde{\mathcal{F}}_n^{(N)}(r) \equiv \frac{1}{\sqrt{\prod_{k=1}^{n-1} F_{k/n}(r)}} \quad (2.27)$$

and C_n are non-universal constants. The moments $\text{Tr}\rho_A^n$ for the interval on the half line with either Dirichlet b.c. and Neumann b.c. are obtained by taking $L \rightarrow \infty$ in (2.26). Notice that the constant C_n is assumed to relate the twist fields in the \mathbb{Z}_n orbifold of the non-compact boson BCFT and the lattice twist operators in a harmonic chain model, that is properly regularized both in the UV and in the IR. In the case of Dirichlet b.c., C_n has the same UV origin as in (2.3), while the case of Neumann boundary conditions is more subtle because the lattice model requires an IR regularization due to the occurrence of the zero mode.

¹We are grateful to Alvis Bastianello for having shared with us his Mathematica notebook for the numerical evaluation of the expression obtained in [66].

By using (2.26), the UV finite combination (2.17) in this regime reads

$$S_{A;D}^{(n)} - S_{A;N}^{(n)} = \frac{1}{2(n-1)} \sum_{k=1}^{n-1} \log \left(\frac{F_{k/n}(1-r)}{F_{k/n}(r)} \right). \quad (2.28)$$

In Sec. 4 the analytic expressions in (2.26) and (2.28) are compared with the corresponding results obtained numerically in the proper harmonic chains, finding a good agreement.

3 Entanglement entropies in the unit disk

In this section, we discuss the main BCFT calculation of this manuscript. As anticipated in Sec. 2, we employ the mirror trick to evaluate the partition function $\mathcal{Z}(\mathcal{S}_n)$ for the compact boson on the specific surface \mathcal{S}_n occurring in our problem because of the replica construction. Since the action is quadratic, the partition function factorizes into a classical part and a quantum part, which are evaluated separately.

3.1 Partition function

3.1.1 Mirror trick

In Sec. 2.2 we have qualitatively discussed that evaluating the Rényi entropies for the bipartitions in Fig. 1 corresponds to compute a partition function on a surface $\mathcal{M} = \mathcal{S}_n$ with boundary which is topologically equivalent to a sphere with n equal disks removed (for $n = 4$, see the right panel of Fig. 2). In a BCFT, this partition function can be obtained also as the two-point function $\langle \mathcal{T}_n(0) \mathcal{T}_n^\dagger(x) \rangle_{\mathbb{D}}$ of twist fields on the unit disk \mathbb{D} , placed at the origin and at x , with $0 < x < 1$.

The replica construction introduces the branched covering $\mathcal{M} = \mathcal{D}_n$, which is obtained by joining cyclically n copies of \mathbb{D} through the cut along the interval $(0, x)$. A standard approach to investigate partition functions on a Riemann surface \mathcal{M} with boundaries is to introduce the so-called *double* of \mathcal{M} , that we denote by $D(\mathcal{M})$ [82]. The double of \mathcal{M} is a compact Riemann surface endowed with an antiholomorphic involutive map σ (called a real structure) such that $\mathcal{M} = D(\mathcal{M})/\sigma$ and the boundary $\partial\mathcal{M}$ corresponds to the fixed points of σ . For instance, the double of the upper half plane is the whole plane with $\sigma(z) = \bar{z}$ and the double of the right half plane is the entire plane with real structure given by the reflection w.r.t. the vertical axis. The double of the unit disk \mathbb{D} is the Riemann sphere \mathbb{CP}^1 with real structure $\sigma(z) = 1/\bar{z}$. This construction is allowed when $\partial\mathcal{M}$ is analytic w.r.t. the complex structure induced by the metric and this condition is verified for \mathcal{D}_n . Thus, $D(\mathcal{D}_n)$ is simply the n -sheeted covering of the Riemann sphere \mathbb{CP}^1 with branch points at $0, x, 1/x$ and ∞ and the antiholomorphic involution is (a lift of) $\sigma(z) = 1/\bar{z}$. The case of the interval in the right half plane is considered in Fig. 2.

The first step of our analysis consists in constructing a canonical homology basis for the genus $n - 1$ surface $D(\mathcal{D}_n)$ that is compatible with the involution σ . Consider the cycles \mathcal{C}_1 and \mathcal{B}_1 shown in Fig. 3. The contour \mathcal{C}_1 is any cycle in the same homology class as the the unit

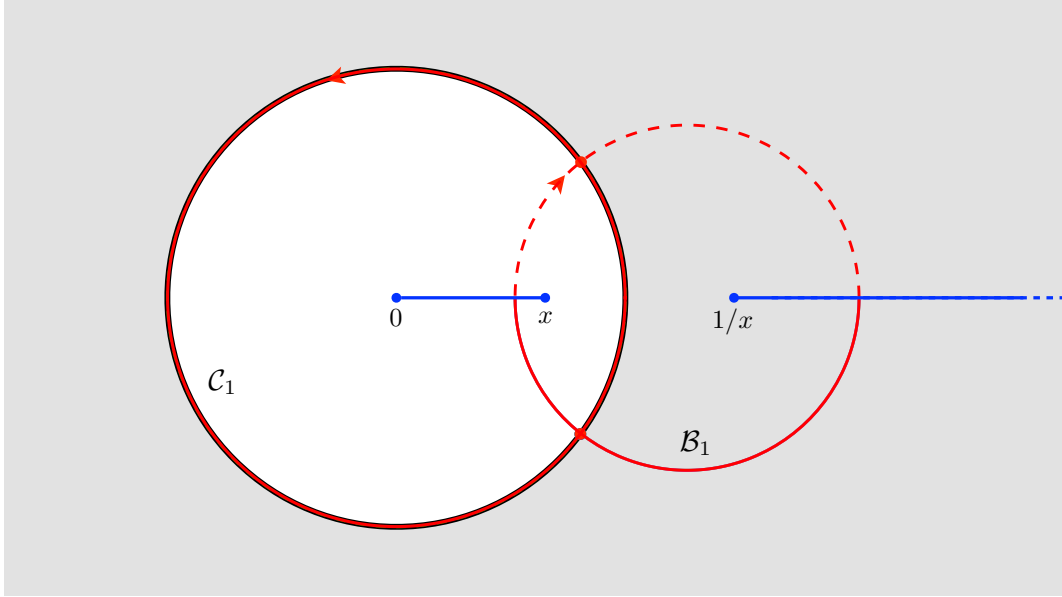


Figure 3: The cycles (red curves) discussed in Sec. 3.1.1. Solid curves lie in the first sheet, while dashed line stand for curves on the second sheet. The unit disk \mathbb{D} corresponds to the white region. The twist fields are located in the origin and in x .

circle. In particular, its homology class is invariant (even) under σ . On the other hand, the homology class of \mathcal{B}_1 is odd under σ ; indeed \mathcal{B}_1 can be chosen so that $\sigma(\mathcal{B}_1)$ is the same loop as \mathcal{B}_1 , but with the opposite orientation. These contours can be replicated on each sheet through the deck transformation f sending sheet j to $j + 1$, i.e. $\mathcal{C}_{j+1} = f(\mathcal{C}_j)$ and $\mathcal{B}_{j+1} = f(\mathcal{B}_j)$, for $1 \leq j \leq n - 1$. Since the deck transformation commutes with the real structure σ , the (homology class of the) cycles \mathcal{B}_j and \mathcal{C}_j are respectively odd and even under σ . Although the contours \mathcal{C}_j and \mathcal{B}_j for $1 \leq j \leq n - 1$ generate the whole homology group, they do not form a canonical basis because \mathcal{B}_j intersects both \mathcal{C}_j and \mathcal{C}_{j+1} . More precisely their intersection numbers are $\#(\mathcal{C}_i, \mathcal{B}_j) = \delta_{i,j} - \delta_{i,j+1}$. However, the cycles $\mathcal{A}_j = \mathcal{C}_1 + \dots + \mathcal{C}_j$ are such that $\#(\mathcal{A}_i, \mathcal{B}_j) = \delta_{i,j}$ (and $\#(\mathcal{A}_i, \mathcal{A}_j) = 0$) and therefore $(\mathcal{A}_j, \mathcal{B}_j)$ is a canonical homology basis. Furthermore, this basis satisfies $\sigma(\mathcal{A}_j) = \mathcal{A}_j$ and $\sigma(\mathcal{B}_j) = -\mathcal{B}_j$ (up to smooth deformations). Thus, under σ , each \mathcal{A}_j is invariant, while each \mathcal{B}_j just changes its orientation. The period matrix corresponding to this canonical homology basis is (2.24) and its derivation is discussed in Appendix B.

We are interested in the partition function of the real compact massless boson $\phi \sim \phi + 2\pi R$ on a compact Riemann surface \mathcal{M} with boundaries. The action (2.21) for this BCFT can be written also as follows

$$S[\phi] = \frac{1}{8\pi} \int_{\mathcal{M}} g(d\phi, d\phi) d\mu = \frac{1}{8\pi} \int_{\mathcal{M}} d\phi \wedge \star d\phi = \frac{i}{4\pi} \int \partial\phi \wedge \bar{\partial}\phi \quad (3.1)$$

where g is the metric tensor on \mathcal{M} , whose volume form is $d\mu = \sqrt{|g|} d^2x$, and \star is the Hodge star operator. In the last equality we introduced the Dolbeault operators $\partial = \frac{1}{2}(d + i\star d)$ and $\bar{\partial} = \frac{1}{2}(d - i\star d)$. The same b.c. are imposed on all the boundary components of $\partial\mathcal{M}$ and in our case they are either of Dirichlet or Neumann type. The action (3.1) is invariant

under Weyl rescaling $g \rightarrow e^\varphi g$. Such invariance can be made more manifest by introducing the decomposition $d\phi = \partial\phi + \bar{\partial}\phi$ and using that $\star dz = -idz$, $\star d\bar{z} = id\bar{z}$, which imply $\star d\phi = -i\partial\phi + i\bar{\partial}\phi$. This leads to the last expression in (3.1), that is manifestly independent of the metric (in a given conformal class). The partition function $\mathcal{Z} = \int [D\phi] e^{-S[\phi]}$ is obtained by performing the path integration over all field configurations satisfying the appropriate b.c. on $\partial\mathcal{M}$, which are either of Neumann or Dirichlet type in our analysis. A non compact real boson ϕ takes values in \mathbb{R} , while in the compact case that we are considering the real field ϕ takes values in the circle of radius R , i.e. in $\mathbb{R}/(2\pi R\mathbb{Z})$. In the latter case, the field configurations can be classified through their windings (or instanton sectors), meaning that

$$\int_{\mathcal{P}_j} d\phi = 2\pi n_j R \quad n_j \in \mathbb{Z} \quad (3.2)$$

where the integer n_j determines the winding number corresponding to the path \mathcal{P}_j , that can be either a non contractible cycle on the Riemann surface or an open path connecting two of its boundary components.

Following the standard procedure to deal with these windings discussed in [42], in the path integral for the partition function we decompose the field $\phi = \phi_{\text{cl}} + \phi_{\text{qu}}$ into the classical field ϕ_{cl} and a quantum part ϕ_{qu} . The classical solution ϕ_{cl} is a harmonic function $\phi_{\text{cl}} : \mathcal{M} \rightarrow \mathbb{R}/(2\pi R\mathbb{Z})$ satisfying (3.2) (hence it depends on the winding vector \mathbf{n} , whose j -th element is n_j), while the quantum field ϕ_{qu} has no windings.

The quadratic form of the action (3.1) combined with the fact that ϕ_{cl} is a solution of the equation of motion lead to decomposition $S[\phi] = S[\phi_{\text{cl}}] + S[\phi_{\text{qu}}]$, where only the classical term $S[\phi_{\text{cl}}]$ depends on the winding vector. This implies that the partition function on the Riemann surface \mathcal{M} factorises as follows

$$\mathcal{Z}(\mathcal{M}) = \mathcal{Z}_{\text{cl}}(\mathcal{M}; R) \mathcal{Z}_{\text{qu}}(\mathcal{M}) \quad (3.3)$$

where the classical and the quantum terms are defined respectively as

$$\mathcal{Z}_{\text{cl}}(\mathcal{M}; R) \equiv \sum_{\mathbf{n}} e^{-S[\phi_{\text{cl}}]} \quad \mathcal{Z}_{\text{qu}}(\mathcal{M}) \equiv \int [D\phi_{\text{qu}}] e^{-S[\phi_{\text{qu}}]}. \quad (3.4)$$

We remark that the quantum term $\mathcal{Z}_{\text{qu}}(\mathcal{M})$ is independent of the compactification radius R .

3.1.2 Classical term

We consider first the classical part $\mathcal{Z}_{\text{cl}}(\mathcal{M}; R)$ of the partition function in (3.3) when the Dirichlet b.c. $\phi = \phi_0$ is imposed, where ϕ_0 is a constant in $\mathbb{R}/(2\pi R\mathbb{Z})$. Crucially, we impose the same constant ϕ_0 on all the components of $\partial\mathcal{M}$ (see Appendix A). By exploiting the $U(1)$ invariance of the theory, we can assume that $\phi_0 = 0$ without loss of generality. Thus, the classical solutions of this Dirichlet problem are harmonic functions ϕ_{cl} that vanish on the boundary. Combining the vanishing (mod $2\pi R$) of ϕ_{cl} on $\partial\mathcal{M}$ with the fact that any harmonic function is (locally) the real part of an analytic function, ϕ_{cl} can be extended to the double $D(\mathcal{M})$ through the Schwarz reflection principle via the condition $\phi_{\text{cl}}(\sigma(p)) = -\phi_{\text{cl}}(p)$.

Hence the classical solutions ϕ_{cl} on \mathcal{M} satisfying vanishing Dirichlet b.c. are in one-to-one correspondence with the classical solutions on the double $D(\mathcal{M})$ that are odd under σ . This implies that $d\phi_{\text{cl}}$ is a harmonic form on $D(\mathcal{M})$ satisfying $\sigma^*d\phi_{\text{cl}} = -d\phi_{\text{cl}}$, where σ^* denote the pullback by σ .

On the other hand, the even harmonic forms on $D(\mathcal{M})$ are such that $\sigma^*d\phi_{\text{cl}} = d\phi_{\text{cl}}$ and their restriction to \mathcal{M} provide the classical solutions satisfying Neumann b.c. for all the components of $\partial\mathcal{M}$. In this case ϕ_{cl} can be extended to $D(\mathcal{M})$ via $\phi_{\text{cl}}(\sigma(p)) = \phi_{\text{cl}}(p)$. Alternatively, we can consider the dual field θ_{cl} , which is defined by $d\theta_{\text{cl}} = \star d\phi_{\text{cl}}$. When ϕ_{cl} satisfies Neumann b.c., the dual field θ_{cl} obeys Dirichlet b.c.; hence $\sigma^*d\theta_{\text{cl}} = -d\theta_{\text{cl}}$. Since σ_{cl} is an orientation reversing isometry, it anticommutes with the Hodge star operator and therefore $\sigma^*d\phi_{\text{cl}} = d\phi_{\text{cl}}$.

In the computation of the moments $\text{Tr } \rho_A^n$ for the bipartitions shown in Fig. 1, the Riemann surface $\mathcal{M} = \mathcal{D}_n$ is topologically equivalent to a sphere with n disks removed (for $n = 4$, see the right panel of Fig. 2). Its double $D(\mathcal{D}_n)$ is the compact Riemann sphere of genus $g = n - 1$ described in Sec. 3.1.1. When $n = 4$, the double $D(\mathcal{D}_n)$ is topologically equivalent to the Riemann surface shown in the left panel of Fig. 2. Consider the canonical homology basis $(\mathcal{A}_j, \mathcal{B}_j)$ discussed in Sec. 3.1.1. It is a standard result of Hodge theory [83] that there exists a unique dual basis (α_j, β_j) of real harmonic one-forms such that

$$\oint_{\mathcal{A}_i} \alpha_j = \delta_{i,j} \quad \oint_{\mathcal{B}_i} \alpha_j = 0 \quad \text{and} \quad \oint_{\mathcal{A}_i} \beta_j = 0 \quad \oint_{\mathcal{B}_i} \beta_j = \delta_{i,j}. \quad (3.5)$$

Since the homology class of \mathcal{A}_i and \mathcal{B}_i are respectively even and odd under sigma, the relations (3.5) are also satisfied by $\sigma^*\alpha_j$ and $-\sigma^*\beta_j$. Hence, uniqueness implies that $\sigma^*\alpha_j = \alpha_j$ and $\sigma^*\beta_j = -\beta_j$, meaning that, under σ , the one-forms α_j are even, while β_j are odd. For Dirichlet b.c. such that ϕ takes the same value (modulo $2\pi R$) on each boundary component of $\partial\mathcal{D}_n$, we have that

$$\int_{\mathcal{B}_j^+} d\phi_{\text{cl}} = 2\pi R m_j \quad m_j \in \mathbb{Z} \quad (3.6)$$

where $j \in \{1, \dots, n-1\}$ and \mathcal{B}_j^+ is defined as the part of \mathcal{B}_j that lies inside \mathcal{D}_n . Hence, \mathcal{B}_j^+ is a path connecting the j -th component to the $(j+1)$ -th component of $\partial\mathcal{D}_n$ (see Fig. 3). Thus, on $D(\mathcal{D}_n)$ we have that

$$\oint_{\mathcal{B}_j} d\phi_{\text{cl}} = 4\pi R m_j \quad m_j \in \mathbb{Z}. \quad (3.7)$$

Moreover, since ϕ is constant on each boundary component, $\oint_{\mathcal{A}_j} d\phi_{\text{cl}} = 0$ for all the allowed values of j . The analytic continuation of $d\phi_{\text{cl}}$ to $D(\mathcal{D}_n)$ involves only the odd harmonic forms β_j as follows

$$d\phi_{\text{cl}} = 4\pi R \sum_j m_j \beta_j. \quad (3.8)$$

The Riemann bilinear relation [83] provides the value of the action (3.1) for this classical solution. It reads

$$S[\phi_{\text{cl}}] = \frac{1}{8\pi} \int_{\mathcal{D}_n} d\phi_{\text{cl}} \wedge \star d\phi_{\text{cl}} = \frac{1}{16\pi} \int_{D(\mathcal{D}_n)} d\phi_{\text{cl}} \wedge \star d\phi_{\text{cl}} = \pi R^2 \mathbf{m}^t \cdot \boldsymbol{\tau}_2^{-1} \cdot \mathbf{m} \quad (3.9)$$

where $\boldsymbol{\tau}_2 \equiv \text{Im}(\boldsymbol{\tau})$ is the imaginary part of the $(n-1) \times (n-1)$ period matrix $\boldsymbol{\tau}$ of $D(\mathcal{D}_n)$ in the canonical homology basis $(\mathcal{A}_j, \mathcal{B}_j)$. In our case the period matrix is purely imaginary. Indeed,

given a basis of the holomorphic one-forms ω_k such that $\oint_{\mathcal{A}_j} \omega_k = \delta_{j,k}$, we have $\sigma^* \omega_k = \bar{\omega}_k$ and therefore

$$\bar{\tau}_{i,j} = \int_{\mathcal{B}_i} \bar{\omega}_j = \int_{\sigma(\mathcal{B}_i)} \omega_j = -\tau_{i,j}. \quad (3.10)$$

From (3.9) and the first expression in (3.4), for vanishing Dirichlet b.c. one obtains

$$\mathcal{Z}_{n,\text{cl}}^{(\text{D})} = \Theta(-R^2 \boldsymbol{\tau}^{-1}) \quad (3.11)$$

in terms of the Siegel theta function (2.23) and of the period matrix defined by (2.24), whose derivation is discussed in the Appendix B.

The case where Neumann b.c. are imposed on all the n boundary components of \mathcal{D}_n can be addressed by adapting the steps for Dirichlet b.c. described above. For Neumann b.c., the classical solutions can be extended to $D(\mathcal{D}_n)$ through the requirement $\phi_{\text{cl}} \circ \sigma = \phi_{\text{cl}}$, as already mentioned. Given the canonical homology base introduced above (see Sec. 3.1.1 and (3.5)), these classical solutions correspond to harmonic forms $d\phi_{\text{cl}}$ satisfying

$$\int_{\mathcal{A}_j} d\phi_{\text{cl}} = 2\pi n_j R \quad \int_{\mathcal{B}_j} d\phi_{\text{cl}} = 0 \quad n_j \in \mathbb{Z} \quad (3.12)$$

where $j \in \{1, \dots, n-1\}$ and the absence of winding over \mathcal{B}_j follows from the fact that $d\phi_{\text{cl}}$ is even under σ . Thus we have

$$d\phi_{\text{cl}} = 2\pi R \sum_j n_j \alpha_j. \quad (3.13)$$

Again, the Riemann bilinear relation allows to compute the action (3.1) for these classical solutions and the result is

$$S[\phi_{\text{cl}}] = \frac{\pi R^2}{4} \mathbf{n}^t \cdot \boldsymbol{\tau} \cdot \boldsymbol{\tau}_2^{-1} \cdot \bar{\boldsymbol{\tau}} \cdot \mathbf{n} = -i \frac{\pi R^2}{4} \mathbf{n}^t \cdot \boldsymbol{\tau} \cdot \mathbf{n} \quad (3.14)$$

where the last step has been obtained by using that $\boldsymbol{\tau}$ is pure imaginary, i.e. $\boldsymbol{\tau} = i\boldsymbol{\tau}_2$. Finally, we find

$$\mathcal{Z}_{n,\text{cl}}^{(\text{N})} = \Theta(R^2 \boldsymbol{\tau}/4) \quad (3.15)$$

in terms of the Siegel theta function (2.23).

3.1.3 Quantum term

The quantum part of the partition function in (3.3) and (3.4) for $\mathcal{M} = \mathcal{D}_n$ is independent of the compactification radius R . Rather than determining the quantum determinant of the Green function of the Laplacian on \mathcal{D}_n , we find it more convenient to adapt the analysis discussed in [52], which is based on the method introduced in [42]. In Sec. 3.1.1 the field ϕ has been decomposed into the sum $\phi = \phi_{\text{cl}} + \phi_{\text{qu}}$ and in the following analysis of the quantum term ϕ_{qu} is denoted just by ϕ to enlighten the expressions. Since $\mathcal{M} = \mathcal{D}_n$ is made by n copies of the unit disk joined cyclically along the cut $(0, x)$, the path integral in (3.4) can be rewritten by introducing a field ϕ_j on the j -th copy, with $1 \leq j \leq n$. The total action reads $S[\phi] = \sum_j S[\phi_j]$ and the fields on the consecutive copies are coupled through their boundary condition along the cut.

Following [84], it is useful to perform a discrete Fourier transform for the n bosonic fields in the different replicas and introduce

$$\tilde{\phi}_k = \frac{1}{\sqrt{n}} \sum_{j=1}^n e^{-2\pi i k j/n} \phi_j \quad 1 \leq k \leq n \quad (3.16)$$

which is a complex combination of fields; hence it is more convenient to replace the real bosons ϕ_j with the complex bosons Φ_j throughout the computation. The result for the real field is obtained by taking the square root of the final expression. The fields introduced through the transformation (3.16) are decoupled. However, the coupling of the original fields ϕ_j through the cut imposes the following twist condition around the origin

$$\tilde{\phi}_k(e^{2i\pi} z, e^{-2i\pi} \bar{z}) = e^{2\pi i k/n} \tilde{\phi}_k(z, \bar{z}) \quad (3.17)$$

and a similar one around the branch point at x , with the phase factor $e^{2\pi i k/n}$ in the r.h.s. replaced by its complex conjugate.

The partition function of a complex scalar on the Riemann sphere satisfying the above twisted boundary conditions around four branch points for an assigned value of k/n has been studied in [42]. In the case of the unit disk \mathbb{D} and of two branch points we are dealing with, this analysis tells us that the corresponding partition function can be written as the two-point function of particular twist fields $\mathcal{T}_{k/n}$ and $\mathcal{T}_{k/n}^\dagger$ placed at the endpoints of the branch cut. This leads us to write the quantum part of the partition function as the following product (up to normalization)

$$\mathcal{Z}_{n, \text{qu}}^2 = \prod_{k=1}^{n-1} \langle \mathcal{T}_{k/n}(0) \mathcal{T}_{k/n}^\dagger(x) \rangle_{\mathbb{D}} \quad (3.18)$$

where the mode corresponding to $k = n$ does not contribute because the corresponding twist field is the identity operator.

A method to determine $\langle \mathcal{T}_{k/n}(0) \mathcal{T}_{k/n}^\dagger(x) \rangle_{\mathbb{D}}$ was developed in [42] and it is based on the the expectation value of the stress-energy tensor $T(z)$ in the presence of the twist fields. In Appendix C we have adapted the analysis of [42] to the specific cases under investigation and the main results are presented below. We find that

$$\partial_x \log \langle \mathcal{T}_{k/n}(0) \mathcal{T}_{k/n}^\dagger(x) \rangle_{\mathbb{D}} = \text{Res}_{z \rightarrow x} \frac{\langle T(z) \mathcal{T}_{k/n}(0) \mathcal{T}_{k/n}^\dagger(x) \rangle_{\mathbb{D}}}{\langle \mathcal{T}_{k/n}(0) \mathcal{T}_{k/n}^\dagger(x) \rangle_{\mathbb{D}}} \quad (3.19)$$

$$= -2h_{k/n} \left(\frac{1}{x} + \frac{1}{x - 1/\bar{x}} \right) - \partial_x \log [E_{k/n}^{(\alpha)}(x)] \quad (3.20)$$

where

$$h_{k/n} \equiv \frac{1}{2} \frac{k}{n} \left(1 - \frac{k}{n} \right) \quad E_{k/n}^{(\alpha)}(x) \equiv \begin{cases} F_{k/n}(1 - |x|^2) & \text{Dirichlet b.c.} \\ F_{k/n}(|x|^2) & \text{Neumann b.c.} \end{cases} \quad (3.21)$$

(we remind that $F_{k/n}(y) \equiv {}_2F_1(k/n, 1 - k/n; 1; y)$). As for the quantum part of the partition function (3.18), this leads to

$$\partial_x \log \mathcal{Z}_{n, \text{qu}} = -\Delta_n \left(\frac{1}{x} + \frac{1}{x - 1/\bar{x}} \right) - \partial_x \log E_n^{(\alpha)}(x) \quad (3.22)$$

where we used that $\sum_{k=1}^{n-1} h_{k/n} = \Delta_n = \frac{1}{12}(n - 1/n)$ (see (2.2) with $c = 1$) and we introduced

$$E_n^{(\alpha)}(x) \equiv \sqrt{\prod_{k=1}^{n-1} E_{k/n}^{(\alpha)}(x)}. \quad (3.23)$$

From the relations reported in Appendix C of [52], the function $E_n^{(\alpha)}(x)$ can be expressed as a Siegel theta function as follows

$$\sqrt{\prod_{k=1}^{n-1} F_{k/n}(|x|^2)} = \Theta(\tau(|x|)) \quad \sqrt{\prod_{k=1}^{n-1} F_{k/n}(1 - |x|^2)} = \Theta(-\tau(|x|)^{-1}) \quad (3.24)$$

in terms of the Siegel theta (2.23) and of the period matrix $\tau(x)$ defined in (2.24). Then, integrating (3.22), for the quantum part of the partition function we get

$$\mathcal{Z}_{n,\text{qu}}(x) \propto \frac{1}{\mathcal{P}(x)^{\Delta_n} E_n^{(\alpha)}(x)} \quad \mathcal{P}(x) \equiv |x|^2(1 - |x|^2) \quad (3.25)$$

where

$$E_n^{(\alpha)}(x) \equiv \begin{cases} \Theta(\tau(|x|)) & \text{Dirichlet b.c.} \\ \Theta(-\tau(|x|)^{-1}) & \text{Neumann b.c.} \end{cases} \quad (3.26)$$

and the overall constant, which can depend both on n and on the b.c., will be fixed later.

3.1.4 Two-point functions of twist fields

Combining the classical part and the quantum part of the partition function, given by (3.11)-(3.15) and (3.25)-(3.26) respectively, we find that the two-point functions of the twist fields on the unit disk \mathbb{D} for the compactified massless scalar field with either Dirichlet b.c. or Neumann b.c. read respectively

$$\langle \mathcal{T}_n(0) \mathcal{T}_n^\dagger(x) \rangle_{\mathbb{D}}^{(\text{D})} \propto \frac{1}{\mathcal{P}(x)^{\Delta_n}} \frac{\Theta(-R^2 \tau(x)^{-1})}{\Theta(-\tau(x)^{-1})} = \frac{1}{R^{n-1} \mathcal{P}(x)^{\Delta_n}} \frac{\Theta(\tau(x)/R^2)}{\Theta(\tau(x))} \quad (3.27)$$

$$\langle \mathcal{T}_n(0) \mathcal{T}_n^\dagger(x) \rangle_{\mathbb{D}}^{(\text{N})} \propto \frac{1}{\mathcal{P}(x)^{\Delta_n}} \frac{\Theta(R^2 \tau(x)/4)}{\Theta(\tau(x))} \quad (3.28)$$

where $\mathcal{P}(x)$ has been defined in (3.25) and the last expression of (3.27) has been obtained by employing the following identity

$$\Theta(-\tau(x)^{-1}) = \sqrt{\det(-i\tau(x))} \Theta(\tau(x)) \quad (3.29)$$

which involves the Siegel theta function (2.23) and the period matrix (2.24).

In the limit $x \rightarrow 0$, for (2.24) we have $\tau(x)_{i,j} \rightarrow +i\infty$; hence $\Theta(\eta\tau(x)) \rightarrow 1$ for any constant $\eta > 0$, which implies that $\mathcal{F}_n^{(\alpha)}(x) \rightarrow 1$ as $x \rightarrow 0$ for any finite value of R . By applying this observation to (3.27) and (3.28), at the leading order we have that

$$\langle \mathcal{T}_n(0) \mathcal{T}_n^\dagger(x) \rangle_{\mathbb{D}}^{(\alpha)} \sim \frac{1}{|x|^{2\Delta_n}} \quad x \rightarrow 0 \quad \alpha \in \{\text{D}, \text{N}\} \quad (3.30)$$

which fixes the overall normalizations in (3.27) and (3.28). Thus, the final result for the two-point functions of twist fields on the unit disk with either Dirichlet b.c. or Neumann b.c. read respectively

$$\langle \mathcal{T}_n(0) \mathcal{T}_n^\dagger(x) \rangle_{\mathbb{D}}^{(D)} = \frac{1}{\mathcal{P}(x)^{\Delta_n}} \frac{\Theta(\tau(x)/R^2)}{\Theta(\tau(x))} \quad \langle \mathcal{T}_n(0) \mathcal{T}_n^\dagger(x) \rangle_{\mathbb{D}}^{(N)} = \frac{1}{\mathcal{P}(x)^{\Delta_n}} \frac{\Theta(R^2 \tau(x)/4)}{\Theta(\tau(x))}. \quad (3.31)$$

Finally, from (3.31) one obtains also the two-point functions of twist fields in the infinite strip and in the right half plane, which are given by (2.18) and (2.19) respectively, as discussed in the final part of Sec. 2.1.

3.2 Decompactification regime

An important regime to explore is given by the decompactification limit $R \rightarrow \infty$.

Taking this limit in (2.22) does not provide well defined finite expressions. A similar problem already arises for the conformal boundary states of the massless compact boson. Indeed, the boundary states corresponding to Dirichlet b.c. and Neumann b.c. can be constructed through the $|m, n\rangle\rangle$ Ishibashi states as follows [85]

$$|N\rangle_R = \sqrt{\frac{R}{2}} \sum_{n \in \mathbb{Z}} |(0, n)\rangle\rangle \quad |D\rangle_R = \sqrt{\frac{1}{R}} \sum_{m \in \mathbb{Z}} |(m, 0)\rangle\rangle \quad (3.32)$$

which do not have a well defined behaviour as $R \rightarrow \infty$. For these boundary states, a formal regularization scheme for the BCFT data of the massless compact boson (spectrum of primary fields, boundary states and structure constants) has been implemented [86, 87] to construct a well defined decompactification limit. However, extending this procedure to the \mathbb{Z}_n orbifold of the massless compact boson is beyond the scopes of our work.

Well defined expressions in the decompactification limit can be obtained as follows. By using that $\Theta(R^2 \tau(x)/4) \rightarrow 1$ and $\Theta(-R^2 \tau(x)^{-1}) \rightarrow 1$ as $R \rightarrow \infty$ and disregarding proportionality constants for the moment, it is straightforward to find that the two-point functions of twist fields in (3.27) and (3.28) become respectively

$$\langle \mathcal{T}_n(0) \mathcal{T}_n^\dagger(x) \rangle_{\mathbb{D}}^{(D)} \propto \frac{1}{\mathcal{P}(x)^{\Delta_n}} \tilde{\mathcal{F}}_n^{(D)}(x^2) \quad \langle \mathcal{T}_n(0) \mathcal{T}_n^\dagger(x) \rangle_{\mathbb{D}}^{(N)} \propto \frac{1}{\mathcal{P}(x)^{\Delta_n}} \tilde{\mathcal{F}}_n^{(N)}(x^2) \quad (3.33)$$

where the identities (3.24) and the functions (2.27) have been employed. The BCFT normalization in (3.33) needs a careful and slightly technical discussion of the $x \rightarrow 0$ limit that we report in the Appendix D.2.1. The final results for the two-point functions on the unit disk with either Dirichlet b.c. or Neumann b.c. in the decompactification regime are respectively

$$\langle \mathcal{T}_n(0) \mathcal{T}_n^\dagger(x) \rangle_{\mathbb{D}}^{(D)} = \frac{1}{\mathcal{P}(x)^{\Delta_n}} \tilde{\mathcal{F}}_n^{(D)}(x^2) \quad \langle \mathcal{T}_n(0) \mathcal{T}_n^\dagger(x) \rangle_{\mathbb{D}}^{(N)} = \frac{1}{\mathcal{P}(x)^{\Delta_n}} \tilde{\mathcal{F}}_n^{(N)}(x^2). \quad (3.34)$$

which provide the results reported in Sec. 2.2.1.

As for the Rényi entropies of an interval in the segment, from (2.7) we have

$$S_{A;\alpha}^{(n)} = \frac{\Delta_n}{n-1} \log[\mathcal{P}(u, v)] - \frac{\log(C_n)}{n-1} + \frac{1}{2(n-1)} \sum_{k=1}^{n-1} \log[F_{k/n}(y_\alpha)] \quad (3.35)$$

where we have introduced $y_D \equiv 1 - r$ for Dirichlet b.c. and $y_N \equiv r$ for Neumann b.c., and we remind that $F_{k/n}(y)$ has been defined in the text below (2.24). The corresponding result for the interval on the half line is obtained by taking the limit $L \rightarrow \infty$ in (3.35).

Finally, by using (2.15) and (3.35), we find the following UV finite quantity

$$\mathcal{I}_{A;\alpha}^{(n)} = \frac{\Delta_n}{1-n} \log(r) + \frac{1}{2(1-n)} \sum_{k=1}^{n-1} \log[F_{k/n}(y_\alpha)] \quad (3.36)$$

where we have also employed that $g_D = g_N = 1$ in our conventions, as shown in Sec. D.2.1 (see (D.33)) and in agreement with the existing results [88].

The analytic continuation $n \rightarrow 1$ of (3.35) can be studied by employing the following result obtained in [52]

$$\lim_{n \rightarrow 1} \partial_n \left(\sum_{k=1}^{n-1} \log[F_{k/n}(y)] \right) = \int_{-i\infty}^{i\infty} \frac{\pi z \log[F_z(y)]}{[\sin(\pi z)]^2} \frac{dz}{i} \equiv -\mathcal{D}'_1(y) \quad (3.37)$$

where the integral along the imaginary axis defining $\mathcal{D}'_1(y)$ is evaluated numerically. This leads to the following result for the entanglement entropy of the interval in the segment

$$S_{A;\alpha} = \frac{1}{6} \log[\mathcal{P}(u, v)] - \frac{\mathcal{D}'_1(y_\alpha)}{2} + 2C'_1 \quad (3.38)$$

where the non-universal constant shift is given by $C'_1 \equiv -\lim_{n \rightarrow 1} \frac{\log C_n}{n-1}$. The entanglement entropy of an interval on the half line is obtained by taking the $L \rightarrow \infty$ of (3.38).

From the UV finite quantity (3.36), we find it worth introducing

$$\widehat{\mathcal{I}}_{A;\alpha}^{(n)} \equiv \mathcal{I}_{A;\alpha}^{(n)} - \frac{\Delta_n}{1-n} \log(r) \quad (3.39)$$

whose analytic continuation $n \rightarrow 1$ can be written in terms of (3.37) as follows

$$\widehat{\mathcal{I}}_{A;\alpha}^{(1)} = \frac{\mathcal{D}'_1(y_\alpha)}{2}. \quad (3.40)$$

The limit $n \rightarrow \infty$ of (3.35) provides the single copy entanglement entropy in the decompactification regime. By introducing

$$\lim_{n \rightarrow \infty} \frac{1}{n-1} \sum_{k=1}^{n-1} \log[F_{k/n}(y)] = \int_0^1 \log[F_\kappa(y)] d\kappa \equiv \mathcal{S}(y) \quad (3.41)$$

where the integral defining $\mathcal{S}(y)$ can be evaluated numerically, for the single copy entanglement entropy of the interval in the segment one finds

$$S_{A;\alpha}^{(\infty)} = \frac{1}{12} \log[\mathcal{P}(u, v)] + \frac{\mathcal{S}(y_\alpha)}{2} + 2C'_\infty \quad (3.42)$$

where $C'_\infty \equiv -\lim_{n \rightarrow \infty} \frac{\log C_n}{n-1}$. The limit $L \rightarrow \infty$ of (3.42) gives the single copy entanglement entropy of the interval in the half line in the decompactification regime.

4 Numerical results from harmonic chains

In this section we compare the BCFT results reported in Sec. 2.2.1 and Sec. 3.2 for the decompactification regime with the entanglement entropies of a block of consecutive sites in the spatial bipartitions shown in Fig. 1 for harmonic chains defined either on the semi-infinite line or on the segment, when either Dirichlet b.c. or Neumann b.c. are imposed.

The Hamiltonian of a finite harmonic chain with nearest neighbour spring-like interactions made by $N - 1$ sites in the interior and two sites at its endpoints reads

$$\hat{H} = \sum_{i=0}^N \left(\frac{1}{2m} \hat{p}_i^2 + \frac{m\omega^2}{2} \hat{q}_i^2 \right) + \sum_{i=0}^{N-1} \frac{\kappa}{2} (\hat{q}_{i+1} - \hat{q}_i)^2 \quad (4.1)$$

in terms of the position and the momentum operators \hat{q}_i and \hat{p}_i , that are Hermitian operators satisfying the canonical commutation relations $[\hat{q}_i, \hat{q}_j] = [\hat{p}_i, \hat{p}_j] = 0$ and $[\hat{q}_i, \hat{p}_j] = i\delta_{i,j}$ (we set $\hbar = 1$). At the endpoints of the harmonic chain we impose the same boundary condition, which is either Dirichlet b.c.

$$\hat{q}_0 = \hat{q}_N = 0 \quad (4.2)$$

or Neumann b.c.

$$\hat{q}_1 - \hat{q}_0 = 0 \quad \hat{q}_N - \hat{q}_{N-1} = 0. \quad (4.3)$$

We consider these quadratic systems in their ground state, that is a Gaussian state. Since these are free systems, the crucial objects needed to perform our numerical analysis are the correlation matrices \mathbf{Q} and \mathbf{P} , whose generic elements are the two-point correlators in the ground state, which are given by $\langle \hat{q}_i \hat{q}_j \rangle$ and $\langle \hat{p}_i \hat{p}_j \rangle$ respectively [2–4, 89–94].

For the Dirichlet b.c. (4.2), the generic elements of the correlation matrices \mathbf{Q} and \mathbf{P} are respectively [95]

$$\langle \hat{q}_i \hat{q}_j \rangle = \frac{1}{N} \sum_{k=1}^{N-1} \frac{1}{m\omega_k} \sin(\pi k i/N) \sin(\pi k j/N) \quad (4.4)$$

$$\langle \hat{p}_i \hat{p}_j \rangle = \frac{1}{N} \sum_{k=1}^{N-1} m\omega_k \sin(\pi k i/N) \sin(\pi k j/N) \quad (4.5)$$

where the dispersion relation reads

$$\omega_k \equiv \sqrt{\omega^2 + \frac{4\kappa}{m} [\sin(\pi k/(2N))]^2} > \omega \quad 1 \leq k \leq N - 1. \quad (4.6)$$

In the massless regime (i.e. when $\omega = 0$) and in the thermodynamic limit $N \rightarrow \infty$, these correlators simplify respectively to [96]

$$\langle \hat{q}_i \hat{q}_j \rangle = \frac{1}{2\pi \sqrt{\kappa m}} \left(\psi(1/2 + i + j) - \psi(1/2 + i - j) \right) \quad (4.7)$$

$$\langle \hat{p}_i \hat{p}_j \rangle = \frac{2\sqrt{\kappa m}}{\pi} \left(\frac{1}{4(i+j)^2 - 1} - \frac{1}{4(i-j)^2 - 1} \right) \quad (4.8)$$

where $\psi(z)$ is the digamma function. These correlators can be employed to investigate the semi-infinite massless harmonic chain with Dirichlet b.c. imposed at its origin.

In the case of Neumann b.c. (4.3), the generic elements of the correlation matrices \mathbf{Q} and \mathbf{P} read respectively [97, 98]

$$\langle \hat{q}_i \hat{q}_j \rangle = \frac{1}{2} \sum_{k=1}^{N-1} \frac{1}{m\omega_k} V_{i,k} V_{j,k} \quad \langle \hat{p}_i \hat{p}_j \rangle = \frac{1}{2} \sum_{k=1}^{N-1} m\omega_k V_{i,k} V_{j,k} \quad (4.9)$$

where

$$\omega_k \equiv \sqrt{\omega^2 + \frac{4\kappa}{m} [\sin(\theta_k/2)]^2} \quad \theta_k \equiv \frac{\pi(k-1)}{N-1} \quad (4.10)$$

and

$$V_{i,k} = \sqrt{\frac{2 - \delta_{k,1}}{N-1}} \cos(\theta_k(i-1/2)). \quad (4.11)$$

The correlators in (4.9) can be written as $\langle \hat{q}_i \hat{q}_j \rangle = \frac{1}{2} M_{i,j}^{(1)}$ and $\langle \hat{p}_i \hat{p}_j \rangle = \frac{1}{2} M_{i,j}^{(-1)}$, where $M_{i,j}^{(\eta)}$ is defined as follows

$$M_{i,j}^{(\eta)} \equiv \frac{1}{(N-1)(m\omega)^\eta} + \frac{2}{N-1} \sum_{k=2}^{N-1} \frac{\cos[\theta_k(i-1/2)] \cos[\theta_k(j-1/2)]}{(2\sqrt{\kappa m})^\eta \{m\omega^2/(4\kappa) + [\sin(\theta_k/2)]^2\}^{\eta/2}}. \quad (4.12)$$

In the thermodynamic limit $N \rightarrow \infty$, this expression becomes

$$\begin{aligned} \mathcal{I}_{i,j}^{(\eta)} &\equiv \frac{2}{\pi (2\sqrt{\kappa m})^\eta} \int_0^\pi \frac{\cos[\theta(i-1/2)] \cos[\theta(j-1/2)]}{\{m\omega^2/(4\kappa) + [\sin(\theta/2)]^2\}^{\eta/2}} d\theta \\ &= \frac{1}{\pi (\sqrt{2\kappa m})^\eta [m\omega^2/(2\kappa) + 1]^{\eta/2}} \int_0^\pi \frac{\cos[\theta(i+j-1)] + \cos[\theta(i-j)]}{\{1 - [m\omega^2/(2\kappa) + 1]^{-1} \cos(\theta)\}^{\eta/2}} d\theta. \end{aligned} \quad (4.13)$$

By employing the following formula [99]

$$F(a, b; n, \tilde{a}^2) \equiv \frac{1}{\pi} \int_0^\pi \frac{\cos(n\theta)}{(1 - a \cos \theta)^b} d\theta = \frac{2^b \Gamma(n+b)}{a^b \Gamma(n+1) \Gamma(b)} \tilde{a}^{n+b} {}_2F_1(b, n+b; n+1; \tilde{a}^2) \quad (4.14)$$

with $\tilde{a} \equiv (1 - \sqrt{1 - a^2})/a$, the integral in the last step of (4.13) can be performed, finding

$$\mathcal{I}_{i,j}^{(\eta)} = \frac{1}{(\sqrt{2\kappa m} \tilde{\omega})^\eta} \left[F(1/\tilde{\omega}^2, \eta/2; i+j-1, \tilde{a}^2) + F(1/\tilde{\omega}^2, \eta/2; i-j, \tilde{a}^2) \right] \quad (4.15)$$

where $\tilde{\omega}^2 \equiv m\omega^2/(2\kappa) + 1$. This observation allows us to write the analytic expressions of the correlators in (4.9) in the thermodynamic limit in terms of (4.15) as follows

$$\langle \hat{q}_i \hat{q}_j \rangle = \frac{1}{2} \mathcal{I}_{i,j}^{(1)} \quad \langle \hat{p}_i \hat{p}_j \rangle = \frac{1}{2} \mathcal{I}_{i,j}^{(-1)}. \quad (4.16)$$

In the massless limit $\omega \rightarrow 0$, these expressions become respectively

$$\langle \hat{q}_i \hat{q}_j \rangle = -\frac{1}{2\pi\sqrt{\kappa m}} \left(\psi(|i-j| + \frac{1}{2}) + \psi(i+j + \frac{1}{2}) + \log(m\omega^2/\kappa) + 4\gamma + \log(4) + 2\psi(\frac{1}{2}) \right) \quad (4.17)$$

$$\langle \hat{p}_i \hat{p}_j \rangle = -\frac{\sqrt{\kappa m}}{2\pi} \left(\frac{1}{(i-j)^2 - 1/4} + \frac{1}{(i+j-1)^2 - 1/4} \right) \quad (4.18)$$

where $\gamma = -\psi(1) \simeq 0.5772$ is the Euler-Mascheroni constant. In all our numerical analyses we have set $\kappa = m = 1$.

We remark that all the finite correlation matrices \mathbf{Q} and \mathbf{P} introduced above are symmetric matrices satisfying $\mathbf{Q}\mathbf{P} = \frac{1}{4}\mathbf{1}$, where $\mathbf{1}$ is the identity matrix, as expected for the ground state.

An important feature to highlight is the occurrence of the zero mode, which is forbidden by the Dirichlet b.c. (4.2), while it is instead allowed by the Neumann b.c. (4.3). The zero mode has a significant impact on the behaviour of the correlators in the massless limit $\omega \rightarrow 0$. Indeed, while the correlators (4.4) and (4.5) satisfying Dirichlet b.c. yield finite results in this limit, the ones (4.9) characterised by Neumann b.c. are divergent because of the term corresponding to $k = 1$ in $\langle \hat{q}_i \hat{q}_j \rangle$. This crucial feature makes the analysis of the massless regime more complicated when Neumann b.c. hold. The occurrence of the zero mode induces to introduce a small but non-vanishing mass as regulator, but this introduces effects in the entanglement entropies that are challenging to quantify through analytic methods [100].

The entanglement entropies $S_A^{(n)}$ of a block A made by N_A consecutive sites can be computed through a well established method [2–4, 89–94]. The first step consists in introducing the reduced correlation matrices \mathbf{Q}_A and \mathbf{P}_A , whose generic elements are respectively $\langle \hat{q}_i \hat{q}_j \rangle$ and $\langle \hat{p}_i \hat{p}_j \rangle$, with $i, j \in A$. Then, the Rényi entropies $S_A^{(n)}$ are obtained as follows

$$S_A^{(n)} = \frac{1}{n-1} \sum_{j=1}^{N_A} \log \left[\left(\mu_j + \frac{1}{2} \right)^n - \left(\mu_j - \frac{1}{2} \right)^n \right] \quad (4.19)$$

where $\{\mu_1^2, \dots, \mu_{N_A}^2\}$ is the spectrum of the $N_A \times N_A$ matrix $\mathbf{Q}_A \mathbf{P}_A$ and provides the symplectic eigenvalues $\{\mu_1, \dots, \mu_{N_A}\}$ of the covariance matrix $\mathbf{Q}_A \oplus \mathbf{P}_A$. The limits $n \rightarrow 1$ and $n \rightarrow \infty$ of (4.19) give respectively the entanglement entropy

$$S_A = \sum_{j=1}^{N_A} \log \left[\left(\mu_j + \frac{1}{2} \right) \log \left(\mu_j + \frac{1}{2} \right) - \left(\mu_j - \frac{1}{2} \right) \log \left(\mu_j - \frac{1}{2} \right) \right] \quad (4.20)$$

and the single copy entanglement

$$S_A^{(\infty)} = \sum_{j=1}^{N_A} \log \left(\mu_j + \frac{1}{2} \right). \quad (4.21)$$

In the following we report some numerical results for the entanglement entropies of a block A made by N_A consecutive sites providing the bipartitions shown in Fig. 1, when either Dirichlet b.c. or Neumann b.c. are imposed and the whole harmonic chain is in its ground state. This leads to four possible setups for the harmonic chain: either an infinite chain on the semi-infinite line or a finite chain made by N consecutive sites on the segment, and either Dirichlet b.c. or Neumann b.c. (we stress that, in the case of the segment, the same b.c. is chosen at both its boundaries). The continuum limit of the lattice results for the semi-infinite chain and for the segment are compared against the corresponding BCFT expressions for the massless scalar field in the decompactification regime, either on the right half plane \mathbb{H} or on the strip \mathbb{S} respectively.

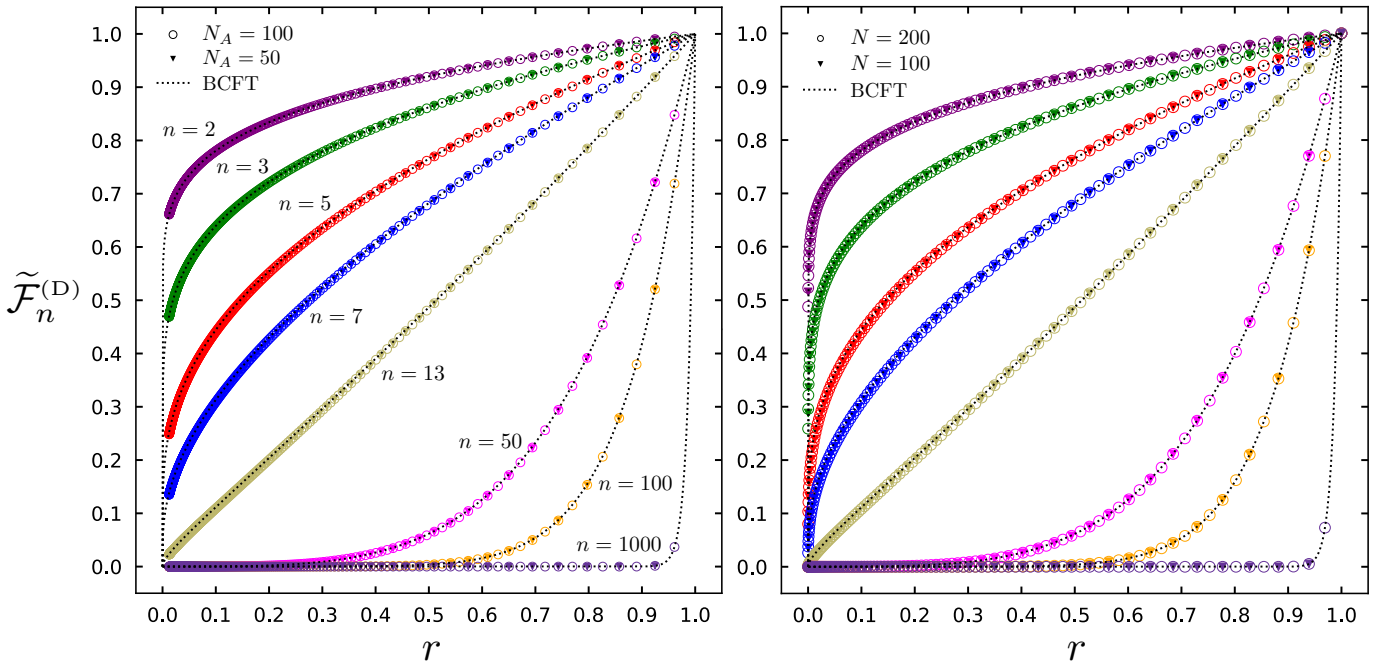


Figure 4: The function $\tilde{\mathcal{F}}_n^{(D)}$ for the bipartitions in Fig. 1 with Dirichlet boundary conditions. The black dotted lines correspond to the BCFT result given by the first expression in (2.27). The data points have been obtained for the block of N_A consecutive sites either in the semi-infinite chain (left panel) or on the finite chain made by N sites (right panel) with Dirichlet b.c. (see Sec. 4).

Unless stated otherwise, for the semi-infinite chains the interval size N_A is kept fixed while its distance from the boundary is varied in such a way that r covers the whole range $r \in (0, 1)$. Instead, in the finite chains of even size N , the whole range $r \in (0, 1)$ is spanned by keeping one endpoint of A fixed in the middle of the chain (this is not ambiguous for even values of N) while the interval grows towards one of the boundaries of the finite chain.

In the case of Dirichlet b.c., our lattice data are taken employing the correlators (4.4) with $\omega = 0$ and (4.7), which are well defined expressions. Instead, when Neumann b.c. are imposed, the first correlator in (4.9) diverges in the massless limit $\omega \rightarrow 0$ because of the occurrence of the zero mode corresponding to $k = 1$. To avoid this issue, we set the mass parameter ω to a small non-vanishing value. In our analysis we have chosen $\omega N_A \sim 10^{-10}$ for the semi-infinite chains and $\omega N \sim 10^{-10}$ for the finite chains, which are much smaller than the other scales. This procedure is the standard one in the case of periodic b.c. (or infinite chain), where the zero mode occurs as well.

For the harmonic chains on the semi-infinite line, when Dirichlet b.c. are chosen we have observed that block sizes $N_A \in \{50, 100\}$ are large enough to obtain a nice agreement with the BCFT predictions. Instead, for Neumann b.c. large sizes for the blocks are typically needed: we used $N_A \in \{200, 400\}$ for the semi-infinite chains and $N \in \{100, 200\}$ for the finite chains.

We find it worth remarking that, in all the figures of this manuscript, the lattice data corresponding to Dirichlet b.c. have not been shifted to be compared with the BCFT curves for all the UV finite quantities considered. Instead, for the ones corresponding to Neumann

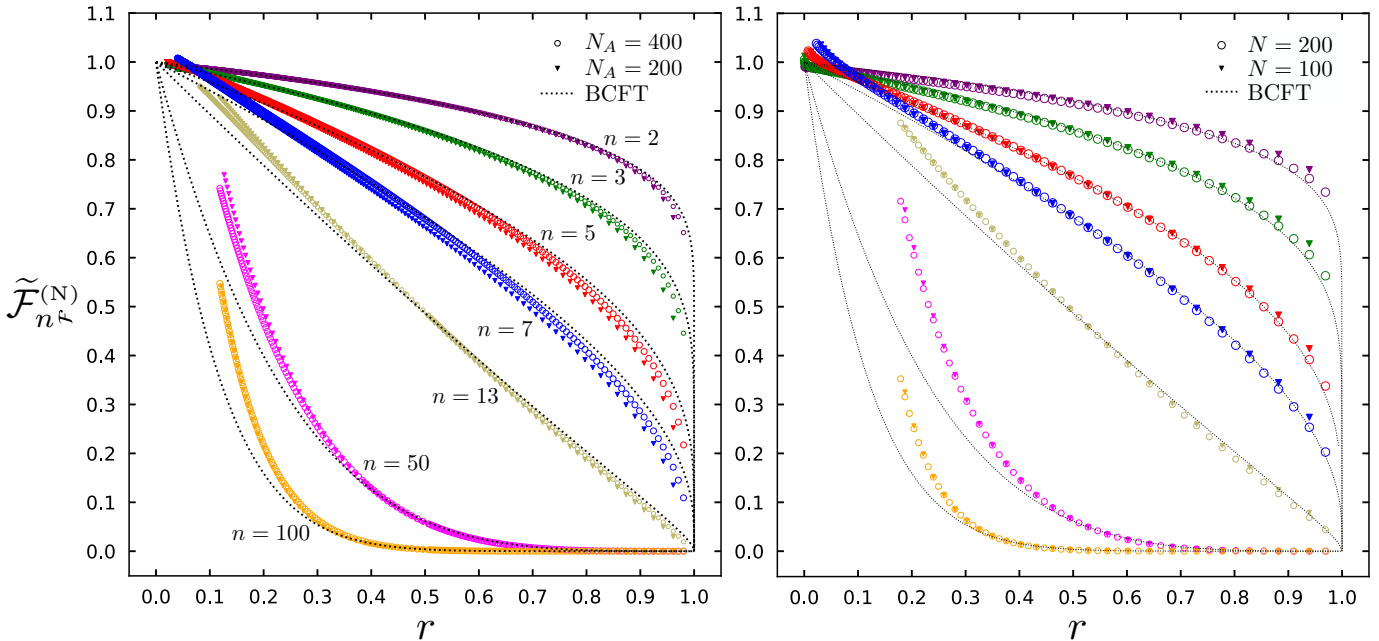


Figure 5: The function $\tilde{\mathcal{F}}_n^{(N)}$ for the bipartitions in Fig. 1 with Neumann boundary conditions. The black dotted lines correspond to the BCFT result given by the second expression in (2.27). The data points have been obtained for the block of N_A consecutive sites either in the semi-infinite chain (left panel) or on the finite chain made by N sites (right panel) with Neumann b.c., as discussed in Sec. 4.

b.c., we have to introduce a constant shift that we are not able to determine analytically which depend on the Rényi index and the lattice zero-mode regulator. It would be interesting to establish a quantitative relation between this shift and ω , if it exists (see e.g. [98, 100] for some results in this direction).

The subsystems $A = [u, v]$, $A_u = [0, u]$, and $A_v = [0, v]$ are used to construct the ratios (2.12), which represent combinations of entanglement entropies in (2.14). The expressions for the UV finite ratios (2.12) in BCFT are obtained by combining (2.13) and (2.27). Additionally, they suggest to consider $r^{\Delta_n} R_A^{(n)}$ for both finite and semi-infinite chains. From (2.6), we have that the ratio r is $r = [s(N_v - N_u)/s(N_v + N_u)]^2$ for the finite chains and $r = [(N_v - N_u)/(N_v + N_u)]^2$ for the semi-infinite chains. The numerical data for these quantities and the corresponding BCFT expressions are displayed in Fig. 4 for Dirichlet b.c., while the ones for Neumann b.c. are shown in Fig. 5 and Fig. 6. In the case of Dirichlet b.c., a remarkable agreement between the lattice data points in the scaling limit and the BCFT predictions is observed, for any value of r considered and even for very large values of the Rényi index n . Instead, when Neumann b.c. are imposed, we obtain a nice agreement for $n \leq 7$ and $r \in (0.5, 1)$. In order to understand these discrepancies, for Neumann b.c. we have reported also the UV finite ratio (2.12) in the cases of $n = 3$, $n = 13$ and $n = 50$ (see Fig. 6), with the same colour code adopted in Fig. 5. To get a better visibility of the data, the curves for different values of n have been vertically displaced. The relation between the BCFT expressions of the quantities considered in Fig. 5 and Fig. 6 is given in (2.13). The agreement

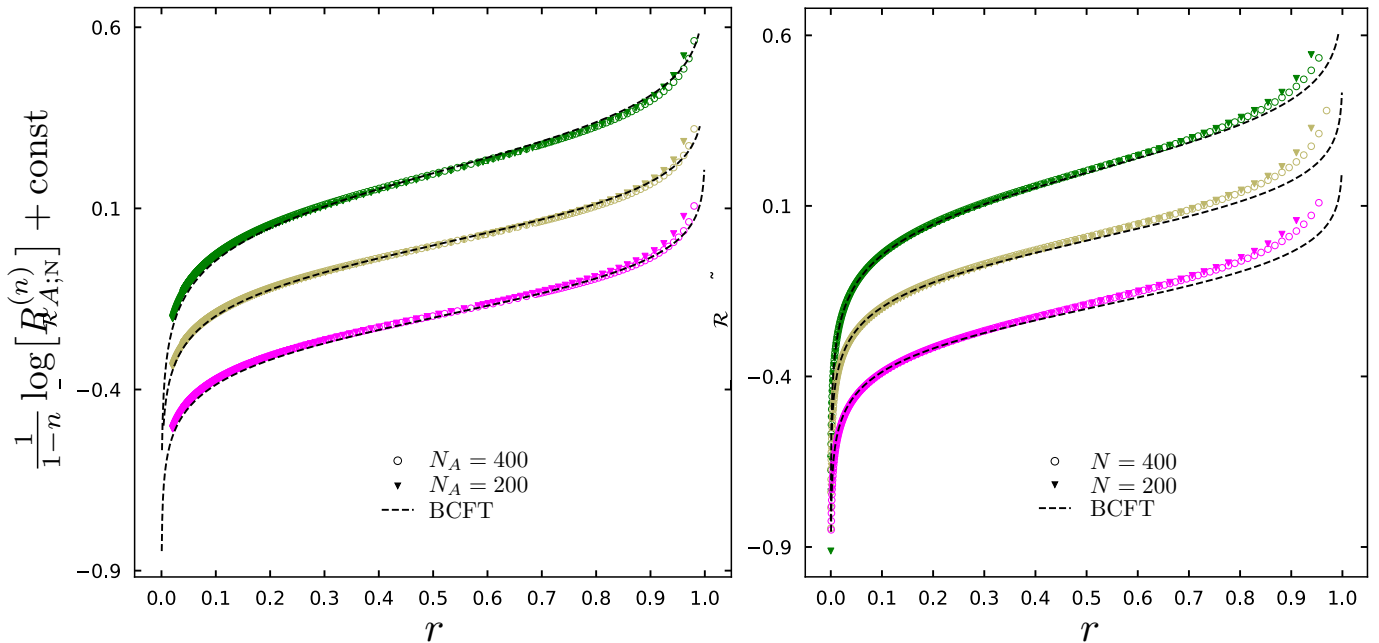


Figure 6: The UV finite ratio (2.12) for the bipartitions shown in Fig. 1 with Neumann b.c., either in the semi-infinite chains (left panel) or in the finite chains (right panel), and $n \in \{3, 13, 50\}$, with the same colour code of Fig. 5. Artificial vertical shifts of the curves for different values of n have been introduced for better visibility.

between the lattice data points and the BCFT curves in Fig. 6 suggests that larger blocks and system sizes are needed in Fig. 5 to obtain a better match with the BCFT predictions.

The occurrence of the zero mode in the case of Neumann b.c. could be another possible source of the discrepancy observed in Fig. 5. As n is increased to larger values at fixed N or N_A , one needs smaller values of ω to get a convergence of the lattice data points (up to shift). Notice that the data for $\tilde{\mathcal{F}}_n^{(N)}(r)$ is particularly sensitive to these effects, in contrast with the quantities shown in Fig. 6 and Fig. 11, which contain the same essential information. We leave the quantitative analysis of such discrepancies for future work.

In Sec. 2.1 we have observed that the difference (2.17) between the entanglement entropies corresponding to two different conformally invariant boundary conditions is another interesting UV finite quantity to investigate and it is a function of the harmonic ratio r . For the massless scalar field in the decompactification regime that we are exploring, we consider (2.28) and its analytic continuation $n \rightarrow 1$, which can be easily written by using (3.38). The results of our analyses for this UV finite quantity are shown in Fig. 7.

The collection of the lattice data has been performed by setting N_v to a constant value in both setups: we have chosen $N_v \in \{100, 200, 400\}$ for the semi-infinite chains, while we took $N_v = N/2$ with $N \in \{100, 200, 400\}$ for the finite chains. Then, we varied $N_u \in \{1, \dots, N_v - 1\}$ and plotted the entanglement entropy in terms of N_A/N_v and the entropy difference in terms of the corresponding cross ratio r in each case. For Neumann b.c., we have set $\omega N_v \sim 10^{-10}$ in both the semi-infinite and finite chains. In the case of Dirichlet b.c. we have considered $\omega = 0$, but we checked that introducing a small non-vanishing ω , such that $\omega N_v \sim 10^{-10}$,

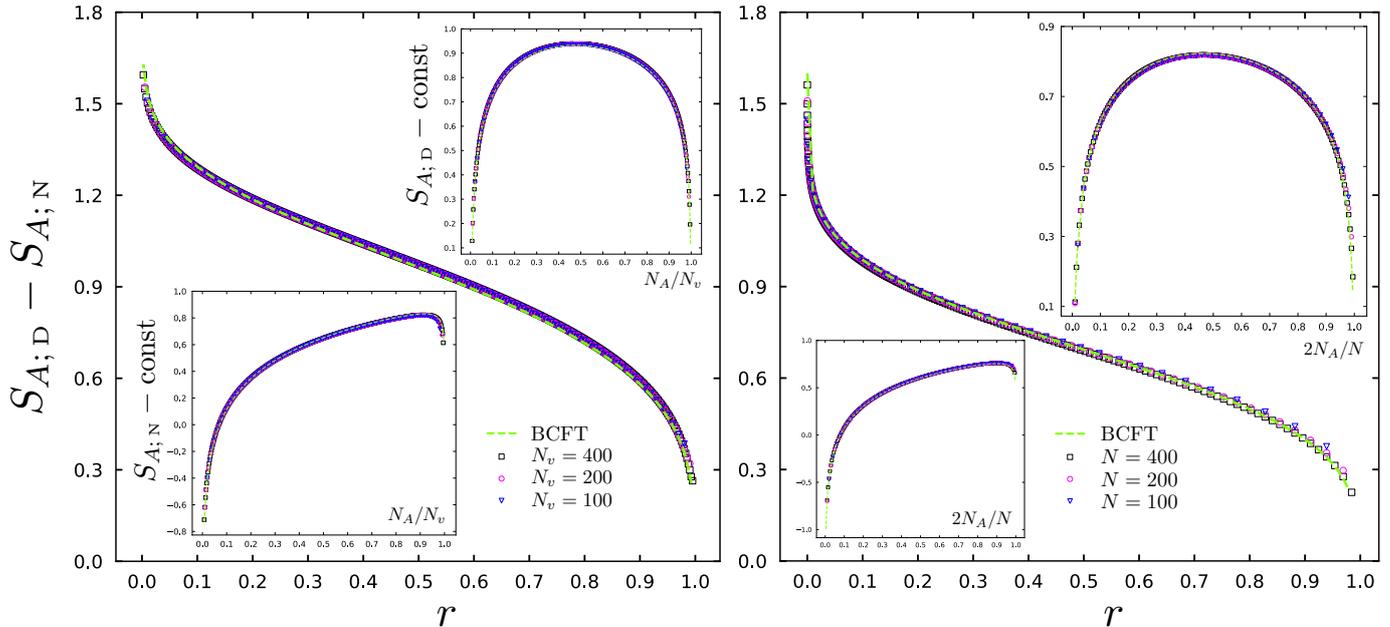


Figure 7: The difference between the entanglement entropy for Dirichlet b.c. and Neumann b.c. for the bipartitions of Fig. 1, either in the semi-infinite chains (left panel) or in the finite chains (right panel). The insets show the entanglement entropy for the two different boundary conditions. The BCFT curves have been obtained from (3.38).

does not lead to changes that can be observed. The agreement between the lattice data points and the corresponding BCFT predictions is excellent. In the insets of Fig. 7 we have reported $S_{A;\alpha} - \text{const}$, where the constant value that has been subtracted is $\frac{1}{6} \log(2N_v)$ for the semi-infinite chains (left panel) and $\frac{1}{3} \log(2N/\pi)$ for finite chains (right panel).

In Sec. 3.2 we have introduced the UV finite quantity (3.39), obtained from (2.13) and (2.14), which depends on the cross ratio r . Its limit $n \rightarrow 1$ is given by the following combination

$$\widehat{\mathcal{I}}_{A;\alpha}^{(1)} = \lim_{n \rightarrow 1} \frac{\log(r^{\Delta_n} R_A^{(n)})}{1-n} = S_{A_u} + S_{A_v} - S_A + \frac{1}{6} \log(r). \quad (4.22)$$

Our results for this UV finite quantity are reported in Fig. 8 and Fig. 9, for Dirichlet b.c. and Neumann b.c. respectively. The corresponding BCFT expressions are given by (3.40), which provide the dashed lines in these figures.

When imposing Dirichlet b.c., we observe an excellent agreement between the lattice data points and the BCFT prediction. Instead, for Neumann b.c. a slight discrepancy is found. It might be due to the occurrence of the zero mode, whose effect we are not able to characterize.

The numerical analysis discussed above allow to evaluate also the corresponding single copy entanglement (1.3) by applying (4.21). The resulting numerical data in the thermodynamic limit can be compared with the BCFT predictions given by (3.42) and (3.41). These comparisons are shown in Fig. 10 and Fig. 11, for Dirichlet and Neumann b.c. respectively (semi-infinite chains and finite chains made by N sites have been considered in the left and right panels respectively). In these figures, the harmonic chain data for $n \rightarrow \infty$ have been obtained through (4.21).

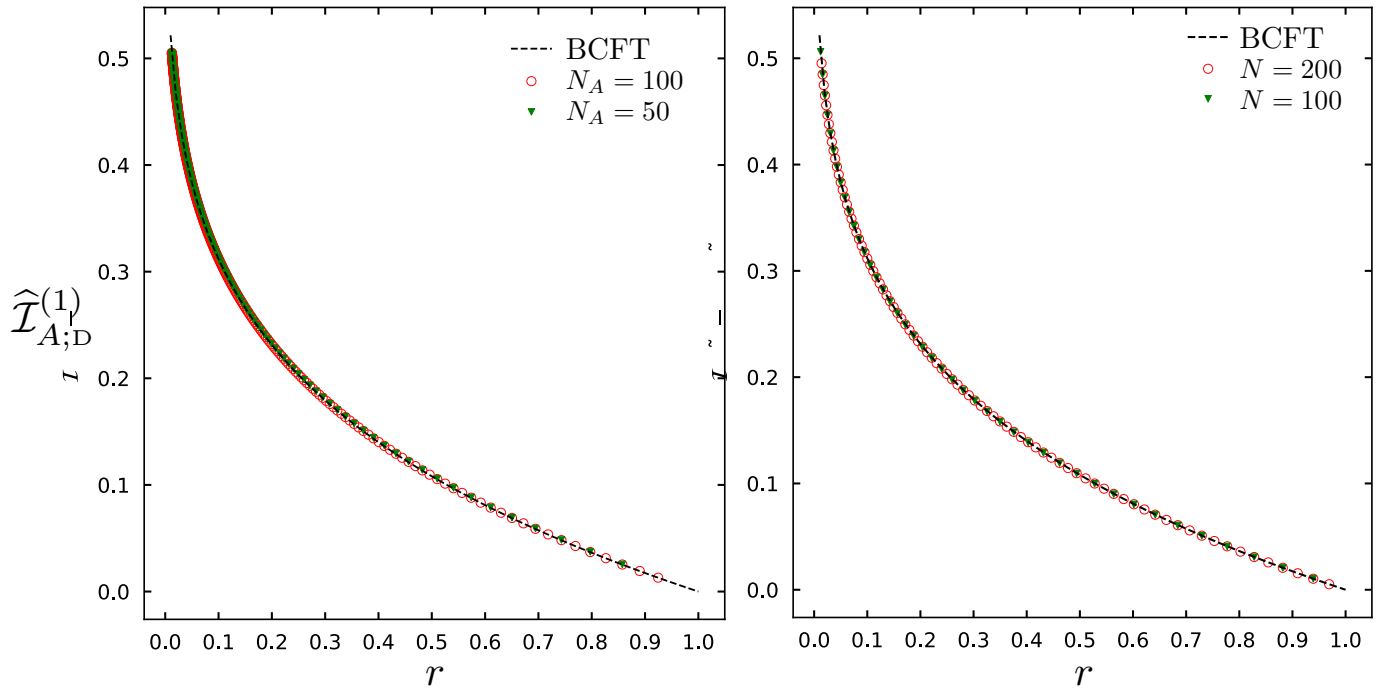


Figure 8: The UV finite quantity (4.22) for Dirichlet boundary conditions. The dashed curves correspond to the BCFT prediction (3.40). The results for the semi-infinite chains and for the finite chains made by N sites are reported in the left and right panel respectively.

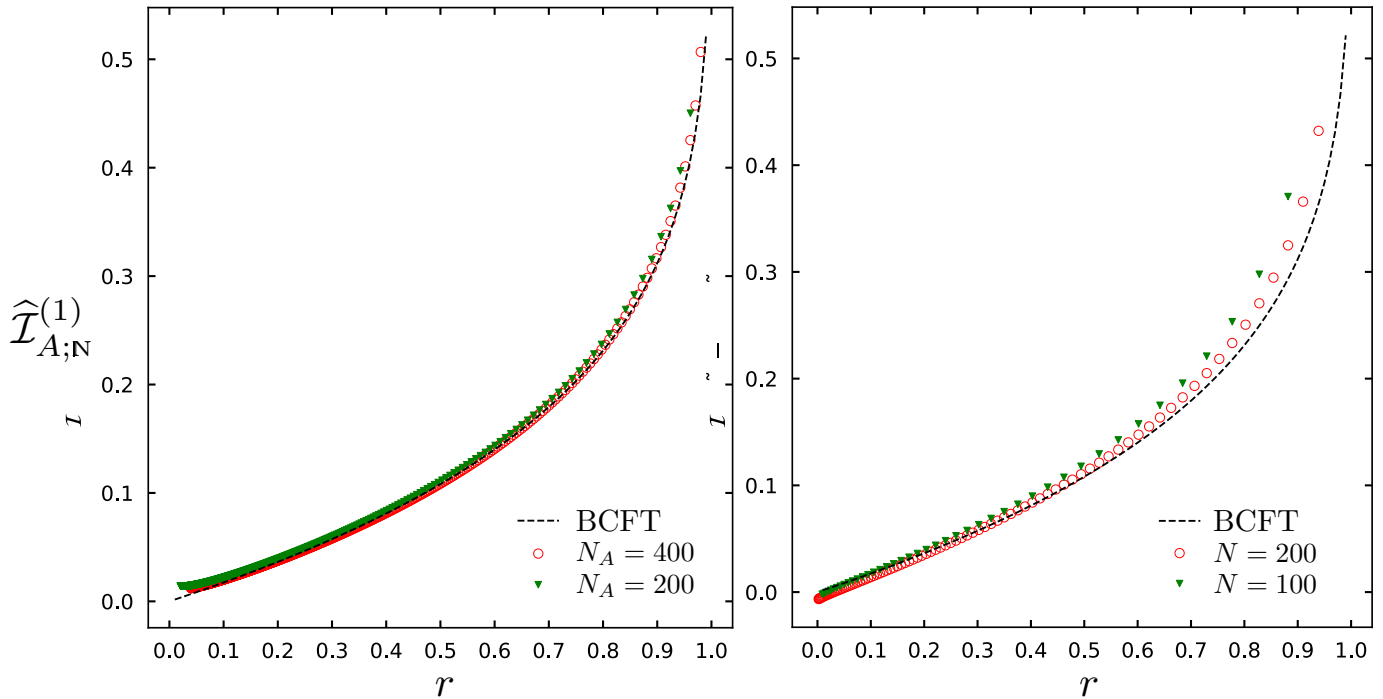


Figure 9: The UV finite quantity (4.22) for Neumann boundary conditions, with the same notation described in the caption of Fig. 8.

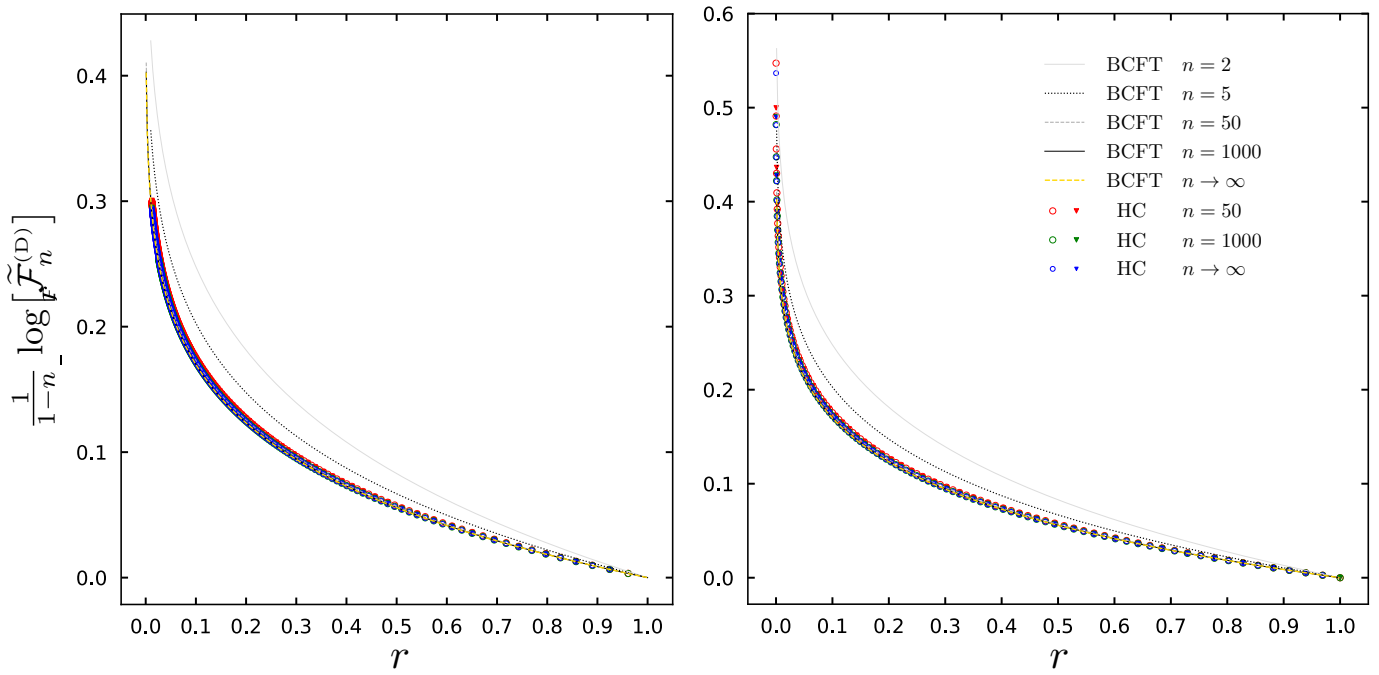


Figure 10: Single copy entanglement entropy for the bipartitions in Fig. 1 (see (4.23)) when Dirichlet b.c. are imposed. The same harmonic chains of Fig. 4 have been employed.

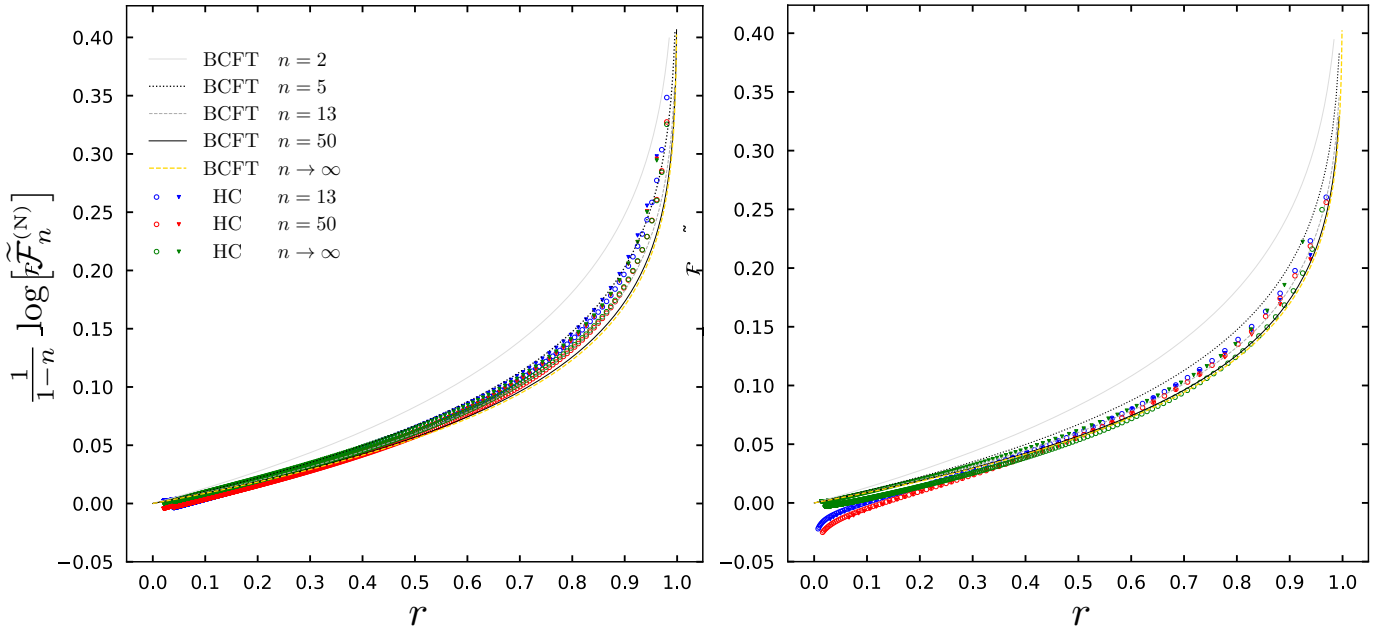


Figure 11: Single copy entanglement entropy for the bipartitions in Fig. 1 (see (4.23)) when Neumann b.c. are imposed. The same harmonic chains of Fig. 5 have been employed.

In particular, by using (2.13), one obtains

$$\lim_{n \rightarrow \infty} \frac{\log(r^{\Delta_n} R_A^{(n)})}{1-n} = S_A^{(\infty)} - S_{A_u}^{(\infty)} - S_{A_v}^{(\infty)} - \frac{1}{12} \log(r). \quad (4.23)$$

Also in this analysis we observe an excellent agreement between the lattice data points in the scaling limit and the corresponding BCFT predictions for Dirichlet b.c., while for Neumann b.c. some discrepancy occurs (see the right panel of Fig. 11, for small values of r).

5 Quantum quenches

A quantum quench is an efficient procedure to construct an out-of-equilibrium state. Given an initial state $|\psi_0\rangle$ (e.g. the ground state of some Hamiltonian H_0) at $t = 0$ and the Hamiltonian H such that $|\psi_0\rangle$ is not among its eigenstates, the evolution $|\psi(t)\rangle \equiv e^{iHt}|\psi_0\rangle$ for $t \geq 0$ provides an interesting out-of-equilibrium state to investigate. A global quench occurs e.g. when the Hamiltonian H is defined through a sudden change of a parameter in H_0 , which therefore occurs everywhere in the system. Instead, in a local quench protocol H is obtained through a sudden modification which is local in space [101]; e.g. when two initially separated systems are connected at $t = 0$.

We are interested in a class of quenches where H is the Hamiltonian of a CFT, which has been described by Calabrese and Cardy [1, 76, 77, 102]. These authors also proposed an approach based on BCFT to investigate the temporal evolutions of the entanglement entropies of an interval of length ℓ after either a global or local quench. This approach employs the two-point function of twist fields in the presence of a boundary; hence, it provides a natural setup to apply the results presented in Sec. 2. An important parameter in this approach is the extrapolation length τ_0 , which is related to the distance of the initial state $|\psi_0\rangle$ from a conformally invariant boundary state (we refer the reader to [102] for a detailed discussion). For the sake of completeness, in Appendix E we report the derivation of the main formulas of this BCFT analysis of quantum quenches that are employed in the following.

For both the global and local quenches, the relevant regimes to consider in terms of the harmonic ratio $r = |x|^2$ are $r \rightarrow 0^+$ and $r \rightarrow 1^-$. In the case of the compactified massless boson, for both Dirichlet b.c. and Neumann b.c., we have that $\mathcal{F}_n^{(\alpha)}(r) \rightarrow g_\alpha^{2(1-n)}$ as $r \rightarrow 1$ (see (D.4)) and $\mathcal{F}_n^{(\alpha)}(r) \rightarrow 1$ as $r \rightarrow 0$ (see Sec. 3.1.4, in the text before (3.30)). Instead, for the decompactified boson, the leading behaviours in the relevant regimes are

$$\tilde{\mathcal{F}}_n^{(D)}(r) \sim \frac{1}{\sqrt{n}} \left(\frac{2\pi}{|\log r|} \right)^{(n-1)/2} \quad \tilde{\mathcal{F}}_n^{(N)}(r) \sim 1 \quad r \rightarrow 0 \quad (5.1)$$

$$\tilde{\mathcal{F}}_n^{(D)}(r) \sim 1 \quad \tilde{\mathcal{F}}_n^{(N)}(r) \sim \frac{1}{\sqrt{n}} \left(\frac{2\pi}{|\log(1-r)|} \right)^{(n-1)/2} \quad r \rightarrow 1 \quad (5.2)$$

where the ones corresponding to Dirichlet b.c. can be read from (D.20) and (D.23), while the ones for Neumann b.c. are implied by (D.14) and (D.24). From these asymptotic behaviours for the decompactified boson, we have that $S_A^{(n)}$ diverge like $\frac{1}{2} \log |\log r|$ as $r \rightarrow 0$ when Dirichlet b.c. hold, while $S_A^{(n)}$ diverge like $\frac{1}{2} \log |\log(1-r)|$ as $r \rightarrow 1$ when Neumann b.c. are imposed.

5.1 Global quench

In the case of a global quench, for the temporal evolution of $\text{Tr}\rho_A^n$ for an interval A of length ℓ , the BCFT approach predicts the following result [1, 76]

$$\text{Tr}\rho_A^n \simeq \left(\frac{\pi}{2\tau_0}\right)^{2\Delta_n} \left[\frac{e^{\pi\ell/(2\tau_0)}(e^{\pi\ell/(2\tau_0)} + e^{-\pi\ell/(2\tau_0)} + 2 \cosh(\pi t/\tau_0))}{2(e^{\pi\ell/(2\tau_0)} - 1)^2 \cosh(\pi t/\tau_0)} \right]^{\Delta_n} \mathcal{F}_n^{(\alpha)}(r) \quad (5.3)$$

(whose derivation is discussed in the Appendix E.1), where an n -dependent normalization constant has been neglected and for the harmonic ratio we have²

$$r = \frac{(e^{\pi\ell/(2\tau_0)} - 1)^2}{e^{\pi\ell/(2\tau_0)}(e^{\pi\ell/(2\tau_0)} + 2 \cosh(\pi t/\tau_0) + e^{-\pi\ell/(2\tau_0)})} \sim \frac{e^{\pi\ell/(2\tau_0)}}{e^{\pi\ell/(2\tau_0)} + e^{\pi t/\tau_0}} \quad (5.4)$$

where the last expression corresponds to the regime where both $\ell/\tau_0 \gg 1$ and $t/\tau_0 \gg 1$. The explicit expression of $\mathcal{F}_n^{(\alpha)}(r)$ are given in (2.22) and the temporal dependence of (5.4) for a given value of ℓ/τ_0 is shown in the left panel of Fig. 14.

The expression (5.3) provides the temporal evolution of the Rényi entropies $S_{A;\alpha}^{(n)}$ after the global quench we are considering. When the contribution of $\mathcal{F}_n^{(\alpha)}(r)$ is neglected, which corresponds to set $\mathcal{F}_n^{(\alpha)}(r) = 1$ in (5.3), the resulting expression for the Rényi entropies is independent of the boundary conditions and in the regime where both $\ell/\tau_0 \gg 1$ and $t/\tau_0 \gg 1$ it reads [76]

$$S_A^{(n)} \simeq \frac{\pi c(n+1)}{12\tau_0 n} \left[t + \frac{\ell}{2} - \max(t, \ell/2) \right] \quad (5.5)$$

i.e. a temporal dependence given by a linear growth followed by a plateau, where the change between these two regimes occurs at $t/\ell = 1/2$.

In the left panel of Fig. 12, the temporal evolution of $\Delta S_{A;\alpha}^{(n)} \equiv S_{A;\alpha}^{(n)} - S_{A;\alpha}^{(n)}|_{t/\ell=1/10}$ when $n = 3$ is shown in the case of Dirichlet b.c., for $\ell \in \{100, 200\}$, $\tau_0 = 10$ and some values of R . The case of Neumann b.c. is obtained by replacing R with $2/R$; hence the same qualitative behaviour is observed for the temporal dependence. The choice of the subtraction constant corresponding to $t/\ell = 1/10$ is due to numerical issues that do not allow us to evaluate $S_{A;\alpha}^{(n)}$ at $t/\ell \simeq 0$. We remark that, for the compact boson, in the regime given by $t \gg \tau_0$ and $\ell \gg \tau_0$, the temporal evolution provided by (5.3) is compatible with (5.5) (see the dashed green curve in the left panel of Fig. 12), up to a constant. Such compatibility is due to the fact that $\mathcal{F}_n^{(\alpha)}(r)$ becomes a constant both when $r \rightarrow 0$ and when $r \rightarrow 1$, as already highlighted above. Thus, the factor $\mathcal{F}_n^{(\alpha)}(r)$ makes smooth the transition between the linear growth and the plateau regime. Notice that the height of the plateau in $\Delta S_{A;\alpha}^{(n)}$ depends on the value of the compactification radius R .

Instead, for the decompactified boson, the occurrence of a non-trivial $\mathcal{F}_n^{(\alpha)}(r)$ provides a new qualitative feature for the temporal evolution of the entanglement entropies. In the regime given by $t \gg \tau_0$ and $\ell \gg \tau_0$, by using (5.4), (5.1) and (5.2), for Neumann b.c. we find the following early time divergent behaviour

$$\frac{1}{1-n} \log \tilde{\mathcal{F}}_n^{(N)}(r) \approx \frac{1}{2} \log \left[\frac{\ell}{2\tau_0} \left(1 - \frac{2t}{\ell} \right) \right] + \text{const} \quad t/\ell \ll 1/2 \quad (5.6)$$

²The harmonic ratio (5.4) is different from the one chosen in [1].

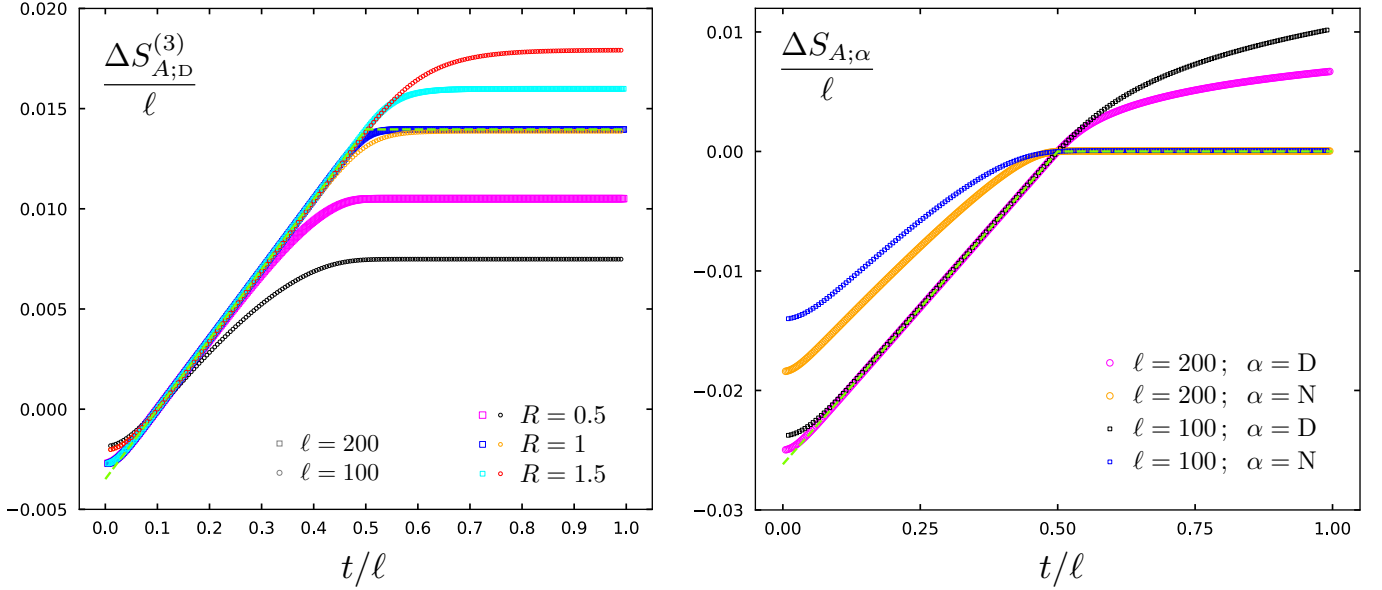


Figure 12: Temporal evolution of $\Delta S_{A;\alpha}^n$ after a global quench for an interval of length ℓ and $\tau_0 = 10$. Left: Compact boson with Dirichlet b.c. for $n = 3$. Right: Decompactified boson with either Dirichlet or Neumann b.c.. The dashed green line is given by (5.5) in both panels.

while for Dirichlet b.c. we observe the following late time divergent behaviour

$$\frac{1}{1-n} \log \tilde{\mathcal{F}}_n^{(D)}(r) \approx \frac{1}{2} \log \left[\frac{\ell}{2\tau_0} \left(\frac{2t}{\ell} - 1 \right) \right] + \text{const} \quad t/\ell \gg 1/2. \quad (5.7)$$

These divergencies are due to the fact that the limit of $\tilde{\mathcal{F}}_n^{(\alpha)}$ is not a constant both when $r \rightarrow 0$ and when $r \rightarrow 1$, as already highlighted above in (5.1) and (5.2). It would be interesting to observe these corrections to the temporal evolution after a global quench through numerical analyses in harmonic chains or other lattice models. In the right panel of Fig. 12, the difference $\Delta S_{A;\alpha}(t/\ell) \equiv S_{A;\alpha} - S_{A;\alpha}|_{t/\ell=1/2}$ is shown for both the types of b.c., and the same values for ℓ and τ_0 adopted in the left panel of the same figure. The deviations from the dashed green curve, which corresponds to (5.5), are due to the terms in (5.6) and (5.7).

5.2 Local quench

As for the local quench, in the following we consider the temporal evolution of $\text{Tr} \rho_A^n$ for an interval A of length ℓ , in the case where the first endpoint of the interval A coincides with the defect, which corresponds to the case III in the classification of local quenches introduced in [77] (the case IV can be also studied but we do not report it here for simplicity). For this bipartition the BCFT approach predicts the following result

$$\text{Tr} \rho_A^n = C_n^2 \epsilon^{2\Delta_n} \left(\frac{\sqrt{\ell^2 + \rho^2 - t^2} + 2\ell\rho \cosh \varphi - 2t\rho \sinh \varphi}{4\rho(1 + (t/\tau_0)^2)(\ell + \rho \cosh \varphi)} \right)^{\Delta_n} \frac{\mathcal{F}_n^{(\alpha)}(r)}{r^{\Delta_n}} \quad (5.8)$$

(whose derivation is discussed in the Appendix E.2), where

$$r = \frac{(\ell/\tau_0 - \sqrt{1 + (t/\tau_0)^2})^2 + (\rho/\tau_0)^2 + 2\rho/\tau_0 (\ell/\tau_0 - \sqrt{1 + (t/\tau_0)^2}) \cosh \varphi}{(\ell/\tau_0 + \sqrt{1 + (t/\tau_0)^2})^2 + (\rho/\tau_0)^2 + 2\rho/\tau_0 (\ell/\tau_0 + \sqrt{1 + (t/\tau_0)^2}) \cosh \varphi} \quad (5.9)$$

with

$$\rho^2 = \ell^2 \sqrt{[(\ell/\tau_0)^{-2} + 1 + (t/\ell)^2]^2 - 4(t/\ell)^2} \quad \varphi \equiv \frac{1}{4} \left| \log \left[\frac{(\ell/\tau_0 + t/\tau_0)^2 + 1}{(\ell/\tau_0 - t/\tau_0)^2 + 1} \right] \right| \quad (5.10)$$

hence the r.h.s. of (5.8) depends on the ratios t/ℓ , ℓ/τ_0 and t/τ_0 . The explicit expression of $\mathcal{F}_n^{(\alpha)}(r)$ are given in (2.22) and the temporal evolution of r in terms of t/ℓ , for some assigned values of ℓ/τ_0 , is shown in the right panel of Fig. 14.

In the regime given by $t \gg \tau_0$ and $\ell \gg \tau_0$, the expression (5.9) simplifies to

$$r \xrightarrow{t, \ell \gg \tau_0} \begin{cases} \frac{\ell - t}{\ell + t} & t < \ell \\ \frac{\tau_0^2 \ell^2}{4t^2(t^2 - \ell^2)} & t > \ell \end{cases} \quad (5.11)$$

and for the moments (5.8) in this regime one obtains

$$\text{Tr} \rho_A^n = \begin{cases} C_n^2 \left(\frac{\epsilon^2}{t^2} \frac{(\ell + t)^2}{t(\ell - t)} \frac{\tau_0}{4\ell} \right)^{\Delta_n} \mathcal{F}_n^{(\alpha)} \left(\frac{\ell - t}{\ell + t} \right) & t < \ell \\ C_n^2 \left(\frac{\epsilon}{\ell} \right)^{2\Delta_n} & t > \ell. \end{cases} \quad (5.12)$$

Hence, for the entanglement entropy in this regime we find

$$S_A = \begin{cases} \frac{c}{3} \log \frac{t}{\epsilon} + \frac{c}{6} \log \frac{\ell}{\tau_0} + \frac{c}{6} \log \frac{4(\ell - t)}{\ell + t} + \mathcal{G}_1^{(\alpha)} \left(\frac{\ell - t}{\ell + t} \right) + C'_1 & t < \ell \\ \frac{c}{3} \log \frac{\ell}{\epsilon} + 2C'_1 & t > \ell \end{cases} \quad (5.13)$$

where $C'_1 \equiv \lim_{n \rightarrow 1} \frac{\log C_n}{n-1}$ and $\mathcal{G}_1^{(\alpha)}(y)$ has been defined in (2.9). While for the compact boson $\mathcal{G}_1^{(\alpha)}(y)$ is not known, the decompactified boson can be studied by replacing $\mathcal{G}_1^{(\alpha)}(y)$ with $-D'_1(y_\alpha)/2$ in (5.13), where $D'_1(y)$ is given by (3.37).

The expression (5.8) provides the temporal evolution of the Rényi entropies $S_{A;\alpha}^{(n)}$ after the local quench we are considering. In the left panel of Fig. 13 we have shown the case $n = 3$ for the compact boson with Dirichlet b.c., $\ell = 200$, $\tau_0 = 0.001$ and some assigned values of the compactification radius $R \in \{0.5, 1, 1.5\}$. For Neumann b.c., the temporal evolution is qualitatively the same; hence we do not show it here.

In order to highlight the role of the factor $\mathcal{F}_n^{(\alpha)}$ in (5.8), (5.12) and (5.13), we find it worth considering also

$$\text{Tr} \rho_A^n \sim \begin{cases} \left(\frac{1}{t^2} \frac{\ell + t}{\ell - t} \frac{\tau_0}{4\ell} \right)^{\Delta_n} & t < \ell \\ \frac{1}{\ell^{2\Delta_n}} & t > \ell \end{cases} \quad (5.14)$$

which is obtained by setting $\mathcal{F}_n^{(\alpha)}$ equal to 1 identically in (5.12) and dropping the factors given by the powers of C_n and ϵ . The expression (5.14) provides the dashed cyan curve in both the panels of Fig. 13. In the left panel, when $R \neq 1$ we observe a significant deviation

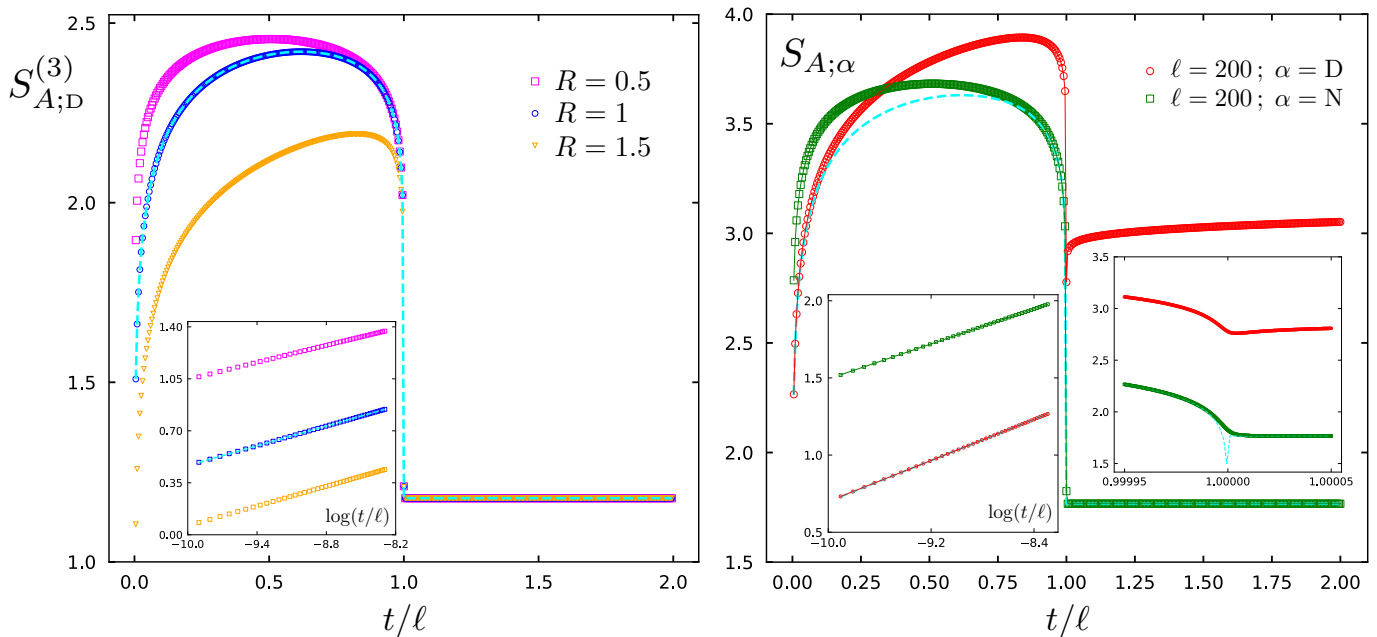


Figure 13: Temporal evolution of $S_{A;\alpha}^n$ after a local quench for an interval A of length ℓ whose first endpoint coincides with the defect, with $\tau_0 = 0.001$. Left: Compact boson with Dirichlet b.c. for $n = 3$ (the inset zooms in on the early time regime). Right: Decompactified boson with either Dirichlet or Neumann b.c. (the two insets zoom in on the early time regime and on $t/\ell \approx 1$). In both panels, the approximate results based on (5.14) correspond to the dashed cyan line.

with respect to (5.14), i.e. from the dashed cyan curve. Its inset zooms in on the initial regime $\tau_0 \ll t \ll \ell$, where $r \rightarrow 1$, showing the expected perfect match with (5.14) when $R = 1$ and the need of a vertical shift when $R \neq 1$, due to the fact that $\mathcal{F}_n^{(D)}(r) \rightarrow R^{n-1}$ as $r \rightarrow 1$.

As for the decompactified boson, we have that $\tilde{\mathcal{F}}_n^{(\alpha)}$ diverges logarithmically when $r \rightarrow 0$ for Dirichlet b.c and when $r \rightarrow 1$ for Neumann b.c. (see (5.1) and (5.2)). Hence, in the regime given by $t \gg \tau_0$ and $\ell \gg \tau_0$, for Neumann b.c. we get the following early time divergence

$$\frac{1}{1-n} \log \tilde{\mathcal{F}}_n^{(N)}(r) \approx \frac{1}{2} \log \left| \log \frac{2t}{\ell} \right| + \text{const} \quad t/\ell \ll 1 \quad (5.15)$$

while for Dirichlet b.c. we find a similar divergence, but at late time

$$\frac{1}{1-n} \log \tilde{\mathcal{F}}_n^{(D)}(r) \approx \frac{1}{2} \log \left| \log \frac{2t^2}{\ell\tau_0} \right| + \text{const} \quad t/\ell \gg 1. \quad (5.16)$$

It would be interesting to observe these corrections to the temporal evolution after a local quench through numerical analyses in harmonic chains or other lattice models. In the right panel of Fig. 13, we display the temporal evolution of the entanglement entropy after the local quench given by (5.13) (see the red and green curves) and also the same quantity (5.13) where the term $\mathcal{G}_1^{(\alpha)}$ has been removed (see the dashed cyan curve). Its first inset zooms in on the early time regime, where the curve corresponding to Dirichlet b.c. matches with the dashed cyan line, as expected from (5.2); while its second inset zooms in on $t/\ell \approx 1$, displaying a smooth crossover between $t < \ell$ and $t > \ell$.

6 Conclusions

In this paper we have employed BCFT techniques to calculate the leading behaviour of the entanglement entropies of an interval in a critical one-dimensional system belonging to the Luttinger liquid universality class in the presence of a boundary. We considered bipartitions characterised by an interval either on the half line or within a segment where the same b.c. are imposed at both its endpoints, which is not adjacent to the boundary, as shown in Fig. 1. Both Dirichlet b.c. and Neumann b.c. have been investigated.

Our main results are the analytic expressions for the entanglement entropies reported in (2.7), with the functions $\mathcal{F}_n^{(\alpha)}(r)$ given in (2.22), which are written in terms of the Siegel theta function and of the period matrix (2.24) occurring also for the entanglement entropies of two disjoint intervals on the line for the compact massless scalar field [52]. Our analysis extends to a generic value of the Rényi index n the one performed in [62], whose results are recovered when $n = 2$. Furthermore, in the case of Dirichlet b.c., we have checked numerically that our analytical expression is compatible with the implicit result reported in [66].

In the decompactification regime, the analytic expressions found through BCFT and reported in Sec. 3.2 have been compared with the corresponding numerical results obtained in harmonic chains (see Sec. 4). In the case of Dirichlet b.c. excellent agreement has been observed (see Fig. 4, Fig. 8 and Fig. 10), while for Neumann b.c. some discrepancies occur (see Fig. 5, Fig. 6, Fig. 9 and Fig. 11) that would be insightful to clarify in a quantitative way. However, we have also studied the UV finite quantity given by the difference between the entanglement entropy corresponding to different b.c. finding excellent agreement with the numerical data points from the harmonic chains (see Fig. 7).

Finally, we have explored the consequences of our analytic results within the context of the BCFT approach to the quantum quenches [1, 76, 77] (see Sec. 5). For global quenches (see Sec. 5.1) we find that, while in the case of the compact boson the main effect of the function $\mathcal{F}_n^{(\alpha)}$ is to smoothen the transition between the linear growth and the plateau regime (see the left panel of Fig. 12) for the decompactified boson it introduces a subleading logarithmic correction, either in the linear growth or in the plateau regime (see (5.6), (5.7) and the right panel of Fig. 12). For local quenches (see Sec. 5.2), the effect of $\mathcal{F}_n^{(\alpha)}$ is more relevant for the compact boson, as highlighted in the left panel of Fig. 13, and, in the case of the decompactified boson, a subleading log-log correction occurs (see (5.15) and (5.16)). Both for global and local quenches, it would be insightful to observe the above mentioned subleading corrections also from the numerical data corresponding to quantum quenches in some lattice models.

Possible extensions of our analysis for the compact scalar could involve mixed boundary conditions [103], or non-vanishing temperature for the entire system, or a non-vanishing mass [104], or a subsystem made by the union of a generic number of disjoint intervals [51, 56, 65], or spatially inhomogeneous backgrounds [66, 67, 105], or defects [106–110].

Regarding the lattice calculations in harmonic chains discussed in Sec. 4, a critical task is to gain an analytical understanding of the effects of the zero mode. Such understanding could shed light on the discrepancies observed between BCFT expressions and the harmonic chain results when Neumann b.c. are imposed.

The spatial bipartitions presented in Fig. 1 offer intriguing prospects for explorations in other compelling two-dimensional models, such as the Ising BCFT [37] and more complex interacting BCFT models like the Liouville field theory [111, 112].

Another intriguing direction of investigation involves going beyond the leading universal behavior of the entanglement entropy, which can be pursued for free fermions, like e.g. in the Schrödinger field theory at finite density [113–115]. Another approach to compute subleading, finite-size corrections involves the use of excited twist-fields [103].

For systems without boundaries, the application of Zamolodchikov’s recursion relation [116] to twist fields has been used to study the entanglement entropy of disjoint intervals on a line [117, 118]. Extending this analysis to the BCFT cases considered in our study would be a compelling endeavour. Other interesting cases where it is worth studying the two-point functions of twist fields in the presence of boundaries are suggested by further applications of the BCFT approach to quantum quenches (see e.g. the geometry considered in [119]).

Furthermore, exploring the effect of physical boundaries on other entanglement quantifiers like the entanglement Hamiltonians and their spectra [120–135], or the logarithmic negativity [96, 136–144], can provide further insights.

Lastly, exploring entanglement entropies in higher-dimensional BCFT models, where the shape of the subsystem plays a crucial role [145–150], is also relevant and opens new avenues for investigation.

Acknowledgements

We are grateful to Viktor Eisler, Paul Fendley, Mihail Mintchev, Giuseppe Mussardo, Ivan Kostov, Gregory Schehr and Barton Zwiebach for useful discussions. We thank in particular Alvis Bastianello for helpful correspondence. AR is grateful to SISSA for hospitality during part of this work. ET acknowledges the Galileo Galilei Institute (through the program *Reconstructing the Gravitational Hologram with Quantum Information*), the Institute Henri Poincaré, the Institut de Physique Théorique at Université Paris-Saclay, the Laboratoire de Physique Théorique et Hautes Energies at Sorbonne Université and the Center for Theoretical Physics at MIT for hospitality and financial support during part of this work.

A An insight from the six-vertex model

The Hamiltonian of the spin- $\frac{1}{2}$ XXZ spin chain with open b.c. is [151]

$$H_{\text{XXZ}} = \sum_{j=1}^{N-1} (\sigma_j^x \sigma_{j+1}^x + \sigma_j^y \sigma_{j+1}^y + \Delta \sigma_j^z \sigma_{j+1}^z) - h_1 \sigma_1^x - h_N \sigma_N^x \quad (\text{A.1})$$

where $\sigma_j^{x,y,z}$ denote the Pauli matrices acting on the j -th site, $\{h_1, h_N\}$ are boundary fields and the anisotropy parameter Δ lies in the critical regime $|\Delta| < 1$. The model (A.1) is a gapless one-dimensional quantum system belonging to the Luttinger liquid universality class. The related discrete 2D classical model is the six-vertex model on the square lattice with Boltzmann weights

a
 a
 b
 b
 c
 c

such that

$$\frac{a^2 + b^2 - c^2}{2ab} = \Delta. \quad (\text{A.2})$$

The six-vertex model is mapped to a height model on the dual lattice, with height values $\varphi(p) \in \mathbb{Z}$, through the following simple rule: for any pair on neighbouring faces p, p' , we set $\varphi(p') = \varphi(p) + 1$ (resp. $\varphi(p') = \varphi(p) - 1$) if p' is above or to the right of (resp. below or to the left of) p , following the reasoning of [152]. The arrow conservation around each vertex ensures that the height ϕ is well defined, up to an overall additive constant.

In the scaling limit, the height variable $\varphi(p)$ provides a real compact boson $\varphi(p) \rightarrow \phi(p)/(\pi R)$, with renormalized compactification radius $R = \sqrt{(2/\pi) \arccos(-\Delta)}$ [151]. Note also that setting free b.c. in the XXZ chain ($h_1 = h_N = 0$) corresponds to Dirichlet b.c. in the compact boson [153], while turning on the boundary fields leads to Neumann b.c. [151].

From the above mapping, we see that in any partition function the variation $\delta\phi$ along any trivial cycle is zero, whereas for non-trivial cycles or open paths joining two boundary points this variation $\delta\phi$ is a multiple of $2\pi R$ (by convention, we only consider lattices such that these non-trivial cycles and open paths have even length, so that the configuration with $\delta\phi = 0$ along each of these cycles and paths is allowed). In the scaling limit, this corresponds to (3.2).

B Period matrix

In this Appendix we discuss the derivation of the period matrix (2.24). This is a standard computation (see for instance [52]) that we report here for the sake of completeness.

We are interested in the period matrix of the Riemann surface Σ_n given by the n -sheeted covering surface over the Riemann sphere \mathbb{CP}^1 with four branch points at $0, x, 1/\bar{x}, \infty$ and two branch cuts: one connecting 0 to x and another one connecting $1/\bar{x}$ to ∞ . Without loss of generality, we could assume x real and positive. The Riemann surface Σ_n can be defined as the algebraic curve $w^n = z(z-x)(z-1/\bar{x})^{n-1}$ with $(z, w) \in \mathbb{C}^2$ (up to compactification

and resolution of the singularity at the origin by a blow-up). It is a compact Riemann surface with genus $n - 1$. This result can be obtained from the Riemann-Hurwitz theorem, which provides the Euler characteristics of the n -sheeted covering \mathcal{P}_n of a generic Riemann surface \mathcal{P}_1 as $\chi(\mathcal{P}_n) = n\chi(\mathcal{P}_1) - 4(n - 1)$, where $\chi(\mathcal{P}) = 2 - 2g$ is the Euler characteristic of a Riemann surface \mathcal{P} without boundaries. In our case $\Sigma_1 = \mathbb{C}\mathbb{P}^1$; hence $\chi(\Sigma_n) = 4 - 2n$.

A compact Riemann surface of genus g supports g linearly independent holomorphic one-forms. The ones for Σ_n have been constructed explicitly and read [42]

$$\omega_k = \frac{1}{z^{k/n}(z-x)^{(n-k)/n}(z-1/\bar{x})^{k/n}} dz \quad k \in \{1, \dots, n-1\}. \quad (\text{B.1})$$

This is the basis of holomorphic one-forms diagonalizing the holomorphic deck transformation f that sends the j -th sheet to the $(j+1)$ -th sheet. Indeed, we have $f^*\omega_k = e^{-2\pi ik/n} \omega_k$, being f^* defined as the pullback of the deck transformation.

We work with the cycles $\mathcal{A}_j, \mathcal{B}_j$ and \mathcal{C}_j described in Sec. 3.1.1 and depicted in Fig. 3. Then, the period matrix τ of Σ_n is

$$\tau = \mathbf{A}^{-1} \cdot \mathbf{B} \quad \mathbf{A}_{k,j} = \int_{\mathcal{A}_j} \omega_k \quad \mathbf{B}_{k,j} = \int_{\mathcal{B}_j} \omega_k. \quad (\text{B.2})$$

The integrals

$$\oint_{\mathcal{C}_j} \omega_k \quad \oint_{\mathcal{B}_j} \omega_k \quad (\text{B.3})$$

can be computed exactly [42]. Indeed, by using that $f^*\omega_k = e^{-2\pi ik/n} \omega_k$, we have

$$\oint_{\mathcal{C}_j} \omega_k = e^{-2\pi ik(j-1)/n} \oint_{\mathcal{C}_1} \omega_k \quad \oint_{\mathcal{B}_j} \omega_k = e^{-2\pi ik(j-1)/n} \oint_{\mathcal{B}_1} \omega_k \quad (\text{B.4})$$

which tell us that just two contour integrals in the r.h.s.'s must be evaluated. These integrals can be computed by deforming the contours down to the branch cut and using the integral representation of the Gauss hypergeometric function. This gives

$$\oint_{\mathcal{C}_1} \omega_k = 2i \sin(\pi k/n) \int_0^x \omega_k = 2\pi i \bar{x}^{k/n} F_{k/n}(|x|^2) \quad (\text{B.5})$$

and

$$\oint_{\mathcal{B}_1} \omega_k = -2\pi i \bar{x}^{k/n} e^{-\pi ik/n} F_{k/n}(1 - |x|^2) \quad (\text{B.6})$$

where we remind that $F_a(y) \equiv {}_2F_1(a, 1-a; 1; y)$. The final expression for the generic element of the $(n-1) \times (n-1)$ period matrix reads

$$\tau_{i,j}(|x|^2) = i \frac{2}{n} \sum_{k=1}^{n-1} \sin(\pi k/n) \frac{F_{k/n}(1 - |x|^2)}{F_{k/n}(|x|^2)} \cos[2\pi k(i-j)/n] \quad (\text{B.7})$$

which is the result obtained in [52]. The period matrix (B.7) satisfies the following relation

$$\tau(1 - |x|^2) = -\mathbf{T} \cdot \tau(|x|^2)^{-1} \cdot \mathbf{T}^t \quad (\text{B.8})$$

where the generic element of the matrix \mathbf{T} is $\mathbf{T}_{j,k} \equiv \delta_{j,k} - \delta_{j,k+1}$. Similar relations have been found also in the Appendix C.3.3 of [56] in the case of two disjoint intervals on the line.

C Green function in the presence of twist fields

Consider a non-compact complex scalar field Φ on the unit disk \mathbb{D} satisfying the following condition after a rotation of the complex coordinate z around a branch point at $z = 0$ [42] (see also (3.17))

$$\Phi(e^{2i\pi}z, e^{-2i\pi}\bar{z}) = e^{2\pi i k/n} \Phi(z, \bar{z}) \quad (\text{C.1})$$

and a similar condition with opposite phase after a rotation around $z = x \in (0, 1)$. In order to have a simpler notation and to prevent any potential confusion with the mirror image, we will use the notation $\Phi(z)$ instead of $\Phi(z, \bar{z})$. However, it is important to note that this does not imply that the field $\Phi(z)$ depends holomorphically on the position z .

These conditions define the occurrence of a twist field $\mathcal{T}_{k/n}$ at $z = 0$ and of its conjugate field $\mathcal{T}_{k/n}^\dagger$ at $z = x$. The holomorphic part of the stress energy tensor $T(z)$ for the complex boson we are considering is

$$T(z) = -\frac{1}{2} : \partial_z \Phi(z) \partial_z \bar{\Phi}(z) : = -\lim_{w \rightarrow z} \left[\frac{\partial_z \Phi(z) \partial_w \bar{\Phi}(w)}{2} + \frac{1}{(z-w)^2} \right]. \quad (\text{C.2})$$

By adapting the analysis of [42] to the case where a conformal boundary occurs, in the following we show that

$$\frac{\langle T(z) \mathcal{T}_{k/n}(0) \mathcal{T}_{k/n}^\dagger(x) \rangle_{\mathbb{D}}}{\langle \mathcal{T}_{k/n}(0) \mathcal{T}_{k/n}^\dagger(x) \rangle_{\mathbb{D}}} = \frac{h_{k/n} [x(1/\bar{x} - 2z) + z^2]^2}{z^2(z-x)^2(z-1/\bar{x})^2} - \frac{x(x-1/\bar{x})}{z(z-x)(z-1/\bar{x})} \partial_x \log E_{k/n}^{(\alpha)}(x) \quad (\text{C.3})$$

where $h_{k/n}$ and $E_{k/n}^{(\alpha)}(x)$ have been defined in (3.21). Then, taking the residue of (C.3) as $z \rightarrow x$ leads to (3.20).

Let us consider the following Green functions on the unit disk \mathbb{D}

$$G_{k/n}(z, w) = \frac{\langle \partial_z \Phi(z) \partial_w \bar{\Phi}(w) \mathcal{T}_{k/n}(0) \mathcal{T}_{k/n}^\dagger(x) \rangle_{\mathbb{D}}}{\langle \mathcal{T}_{k/n}(0) \mathcal{T}_{k/n}^\dagger(x) \rangle_{\mathbb{D}}} \quad (\text{C.4})$$

$$H_{k/n}(z, w) = \frac{\langle \partial_{\bar{z}} \Phi(z) \partial_w \bar{\Phi}(w) \mathcal{T}_{k/n}(0) \mathcal{T}_{k/n}^\dagger(x) \rangle_{\mathbb{D}}}{\langle \mathcal{T}_{k/n}(0) \mathcal{T}_{k/n}^\dagger(x) \rangle_{\mathbb{D}}} \quad (\text{C.5})$$

where $|z| \leq 1$, $|w| \leq 1$ and the boundary condition on $\partial\mathbb{D}$ reads

$$z \partial_z \Phi = \pm \bar{z} \partial_{\bar{z}} \Phi \quad (\text{C.6})$$

with $+$ and $-$ corresponding to Dirichlet b.c. and Neumann b.c. respectively. As remarked above, the notation $H_{k/n}(z, w)$ does not mean that $H_{k/n}$ is holomorphic in z (as a matter of fact, it is antiholomorphic in z). On the other hand, the function $G_{k/n}$ is holomorphic in z and w ; hence the Schwarz reflection principle can be employed to obtain its analytic continuation

to the whole Riemann sphere, via

$$G_{k/n}(z, w) = \begin{cases} \pm \frac{1}{z^2} \frac{\langle \partial_{\bar{z}} \Phi(1/\bar{z}) \partial_w \bar{\Phi}(w) \mathcal{T}_{k/n}(0) \mathcal{T}_{k/n}^\dagger(x) \rangle_{\mathbb{D}}}{\langle \mathcal{T}_{k/n}(0) \mathcal{T}_{k/n}^\dagger(x) \rangle_{\mathbb{D}}} & |z| \geq 1, |w| \leq 1 \\ \pm \frac{1}{w^2} \frac{\langle \partial_z \Phi(z) \partial_{\bar{w}} \bar{\Phi}(1/\bar{w}) \mathcal{T}_{k/n}(0) \mathcal{T}_{k/n}^\dagger(x) \rangle_{\mathbb{D}}}{\langle \mathcal{T}_{k/n}(0) \mathcal{T}_{k/n}^\dagger(x) \rangle_{\mathbb{D}}} & |z| \leq 1, |w| \geq 1 \\ \pm \frac{1}{w^2 z^2} \frac{\langle \partial_{\bar{z}} \Phi(1/\bar{z}) \partial_{\bar{w}} \bar{\Phi}(1/\bar{w}) \mathcal{T}_{k/n}(0) \mathcal{T}_{k/n}^\dagger(x) \rangle_{\mathbb{D}}}{\langle \mathcal{T}_{k/n}(0) \mathcal{T}_{k/n}^\dagger(x) \rangle_{\mathbb{D}}} & |z| \geq 1, |w| \geq 1. \end{cases} \quad (\text{C.7})$$

The Green function $H_{k/n}$, which is antiholomorphic in z and holomorphic in w , can be analytically continued in a similar way. Moreover, these two Green functions are related through a mirror relation as follows

$$G_{k/n}(z, w) = \pm \frac{1}{z^2} H_{k/n}(1/\bar{z}, w) \quad (\text{C.8})$$

whenever they are well defined functions, namely for $z \neq w$ and $z, w \notin \{0, x, 1/\bar{x}, \infty\}$. The r.h.s. of (C.8) is indeed holomorphic in z as $H_{k/n}(1/\bar{z}, w)$ is the composition of two antiholomorphic functions, namely $H_{k/n}(z, w)$ and $\sigma(z) = 1/\bar{z}$.

Now one observes that $z^{k/n}(z-x)^{1-k/n}(z-1/\bar{x})^{k/n} G_{k/n}(z, w)$ is holomorphic on the whole Riemann sphere except for $z = w$, where a second order pole occurs. Hence, for $G_{k/n}(z, w)$ we must have

$$G_{k/n}(z, w) = f_{k/n}(z) \left(\frac{\alpha_{k/n}}{(z-w)^2} + \frac{\beta_{k/n}}{(z-w)} + \gamma_{k/n} \right) \quad (\text{C.9})$$

where $\alpha_{k/n}, \beta_{k/n}$ and $\gamma_{k/n}$ are independent of z , while

$$f_{k/n}(z) = \frac{1}{z^{k/n}(z-x)^{(1-k/n)}(z-1/\bar{x})^{k/n}}. \quad (\text{C.10})$$

From the OPE of $\partial_z \Phi(z) \partial_w \bar{\Phi}(w)$ as $z \rightarrow w$, we have that $G_k(z, w) = -2/(z-w)^2 + O(1)$. This condition gives $\alpha_{k/n}$ and $\beta_{k/n}$, which can be plugged into (C.9), finding

$$G_{k/n}(z, w) = -\frac{2f_{k/n}(z)}{f_{k/n}(w)} \left(\frac{1}{(z-w)^2} - \frac{f'_{k/n}(w)/f_{k/n}(w)}{z-w} + f_{k/n}(w) f_{1-k/n}(w) \mu_{k/n}(w) \right) \quad (\text{C.11})$$

for some unknown function $\mu_{k/n}$. The same argument for the complex variable w leads to

$$G_{k/n}(z, w) = -\frac{2f_{1-k/n}(w)}{f_{1-k/n}(z)} \left(\frac{1}{(z-w)^2} - \frac{f'_{1-k/n}(z)/f_{1-k/n}(z)}{w-z} + f_{1-k/n}(z) f_{k/n}(z) \mu_{1-k/n}(z) \right). \quad (\text{C.12})$$

Comparing (C.11) and (C.12), one obtains

$$\mu_{k/n}(z) = \frac{k}{n}(z-x) + A_{k/n}(x) \quad A_{k/n} = A_{1-k/n}. \quad (\text{C.13})$$

Finally, combining (C.10)-(C.13), we arrive to

$$\begin{aligned} G_{k/n}(z, w) &= \tag{C.14} \\ &= -2 f_{k/n}(z) f_{1-k/n}(w) \left[\frac{k}{n} \frac{z(z-1/\bar{x})(w-x)}{(z-w)^2} + \left(1 - \frac{k}{n}\right) \frac{w(w-1/\bar{x})(z-x)}{(z-w)^2} + A_{k/n}(x) \right]. \end{aligned}$$

Then, from (C.2) it follows that

$$\frac{\langle T(z) \mathcal{T}_{k/n}(0) \mathcal{T}_{k/n}^\dagger(x) \rangle_{\mathbb{D}}}{\langle \mathcal{T}_{k/n}(0) \mathcal{T}_{k/n}^\dagger(x) \rangle_{\mathbb{D}}} = \frac{h_{k/n} [x(1/\bar{x} - 2z) + z^2]^2}{z^2(z-x)^2(z-1/\bar{x})^2} + \frac{A_{k/n}(x)}{z(z-x)(z-1/\bar{x})} \tag{C.15}$$

where the dependence on the boundary condition is encoded only in $A_{k/n}(x)$.

In the case of Neumann b.c., we can determine $A_{k/n}(x)$ by exploiting the fact that the field $\Phi(z)$ has no windings. In particular, the correlator $\langle \Phi(z) \partial_w \bar{\Phi}(w) \mathcal{T}_{k/n}(0) \mathcal{T}_{k/n}^\dagger(x) \rangle_{\mathbb{D}}$ must be a single-valued function of z . By using that $d\Phi = \partial_z \Phi dz + \partial_{\bar{z}} \Phi(z) d\bar{z}$ and comparing with (C.4) and (C.5), we find that the above condition implies

$$\oint_{\mathcal{C}_1} \left[G_{k/n}(z, w) dz + H_{k/n}(z, w) d\bar{z} \right] = 0. \tag{C.16}$$

To evaluate the l.h.s., one can first change variable to $\xi \equiv \sigma(z) = 1/\bar{z}$ and use (C.8) to get

$$\oint_{\mathcal{C}_1} H_{k/n}(z, w) d\bar{z} = \oint_{\mathcal{C}_1} H_{k/n}(1/\bar{\xi}, w) d(1/\xi) = \oint_{\mathcal{C}_1} G_{k/n}(\xi, w) d\xi \quad \text{Neumann b.c.} \tag{C.17}$$

where $\sigma(\mathcal{C}_1) = \mathcal{C}_1$ has been employed. Thus, the constraint (C.16) becomes

$$\oint_{\mathcal{C}_1} G_{k/n}(z, w) dz = 0 \quad \text{Neumann b.c.} \tag{C.18}$$

In the case of Dirichlet b.c., the constraint (C.16) is automatically satisfied; indeed the above change of variable leads to

$$\oint_{\mathcal{C}_1} H_{k/n}(z, w) d\bar{z} = - \oint_{\mathcal{C}_1} G_{k/n}(\xi, w) d\xi. \tag{C.19}$$

Now, since $\Phi(z)$ vanishes on all the components of the boundary, we have that

$$\int_{\mathcal{B}_1^+} \left[G_{k/n}(z, w) dz + H_{k/n}(z, w) d\bar{z} \right] = 0 \quad \text{Dirichlet b.c.} \tag{C.20}$$

where \mathcal{B}_1^+ is the part of \mathcal{B}_1 located inside the white region in Fig. 3, which connects the two red points located on two different components of the boundary. By using the above change of variable, the condition (C.20) becomes

$$\oint_{\mathcal{B}_1} G_{k/n}(z, w) dz = 0 \quad \text{Dirichlet b.c.} \tag{C.21}$$

where we exploit the fact that mirror image of \mathcal{B}_1^+ is the remaining part of \mathcal{B}_1 with the opposite orientation.

From (C.14), one finds that the constraints (C.18) and (C.21) become

$$\oint_{\mathcal{C}} f_{k/n}(z) \left[\frac{k}{n} \frac{z(z-1/\bar{x})(w-x)}{(z-w)^2} + \left(1 - \frac{k}{n}\right) \frac{w(w-1/\bar{x})(z-x)}{(z-w)^2} + A_{k/n}(x) \right] dz = 0 \quad (\text{C.22})$$

where the contour is either $\mathcal{C} = \mathcal{C}_1$ for Neumann b.c. or $\mathcal{C} = \mathcal{B}_1$ for Dirichlet b.c.; hence

$$\begin{aligned} A_{k/n}(x) \oint_{\mathcal{C}} f_{k/n}(z) dz &= \\ &= - \oint_{\mathcal{C}} f_{k/n}(z) \left[\frac{k}{n} \frac{z(z-1/\bar{x})(w-x)}{(z-w)^2} + \left(1 - \frac{k}{n}\right) \frac{w(w-1/\bar{x})(z-x)}{(z-w)^2} \right] dz. \end{aligned} \quad (\text{C.23})$$

The analysis of this equation has been already carried out in [42]. However, in the following we report a detailed derivation for the sake of completeness.

The first important feature to highlight is that the r.h.s. of (C.23) does not depend on w . This follows from the relation

$$\begin{aligned} \frac{\partial}{\partial w} \left[f_{k/n}(z) \left(\frac{k}{n} \frac{z(z-1/\bar{x})(w-x)}{(z-w)^2} + \left(1 - \frac{k}{n}\right) \frac{w(w-1/\bar{x})(z-x)}{(z-w)^2} \right) \right] &= \\ &= - \frac{\partial}{\partial z} \left[\frac{z(z-x)(z-1/\bar{x})f_{k/n}(z)}{(z-w)^2} \right]. \end{aligned} \quad (\text{C.24})$$

Since (C.23) is independent of w , we can choose convenient points for w on the Riemann sphere. In particular, for $w = x$ we obtain

$$A_{k/n}(x) \oint_{\mathcal{C}} f_{k/n}(z) dz = - \left(1 - \frac{k}{n}\right) x (x - 1/\bar{x}) \oint_{\mathcal{C}} \frac{f_{k/n}(z)}{z-x} dz. \quad (\text{C.25})$$

Now one observes that the definition of $f_{k/n}(z)$ in (C.10) straightforwardly leads to

$$\partial_x f_{k/n}(z) = \left(1 - \frac{k}{n}\right) \frac{f_{k/n}(z)}{z-x} \quad (\text{C.26})$$

which can be employed in (C.25), finding that

$$A_{k/n}(x) = - (x - 1/\bar{x}) x \partial_x \log \oint_{\mathcal{C}} f_{k/n}(z) dz. \quad (\text{C.27})$$

Since the integrals $\oint_{\mathcal{C}} f_{k/n}(z) dz$ have already been evaluated in (B.5) and (B.6), we arrive to

$$A_k(x) = - (x - 1/\bar{x}) x \partial_x \log E_{k/n}^{(\alpha)}(x) \quad (\text{C.28})$$

where $E_{k/n}^{(\alpha)}(x)$ has been defined in (3.21). This concludes the derivation of (C.3), whose residue at $z \rightarrow x$ leads to (3.20).

D Limiting regimes

D.1 Compactified boson

Let us consider the limiting regime where the interval is adjacent to the boundary.

The entanglement entropies of the interval $A = [0, v]$ for a BCFT with central charge c defined on the segment $[0, L]$ are [6] (see also (2.11))

$$S_A^{(n)} = \frac{c}{12} \left(1 + \frac{1}{n} \right) \log \left[\frac{2L}{\pi\epsilon} \sin \left(\frac{\pi v}{L} \right) \right] + \log(g) \quad (\text{D.1})$$

up to subleading terms, where g is the Affleck-Ludwig boundary entropy [46]. Considering the massless compact boson, which has $c = 1$, in the following we recover (D.1) for this model by taking the limit $u \rightarrow 0$ of $\langle \mathcal{T}_n(u) \mathcal{T}_n^\dagger(v) \rangle_s^{(\alpha)}$. This provides an important consistency check of our BCFT results in (2.22).

By employing (3.29), the expressions in (2.22) can be written respectively as follows

$$\mathcal{F}_n^{(\text{D})}(r) = R^{n-1} \frac{\Theta(-R^2 \tau(r)^{-1})}{\Theta(-\tau(r)^{-1})} \quad \mathcal{F}_n^{(\text{N})}(r) = \left(\frac{2}{R} \right)^{n-1} \frac{\Theta(-4\tau(r)^{-1}/R^2)}{\Theta(-\tau(r)^{-1})} \quad (\text{D.2})$$

where the prefactors can be expressed in terms of the ground state degeneracies [46] for this model, which are given by [85, 151]

$$g_{\text{D}} \equiv \sqrt{\frac{1}{R}} \quad g_{\text{N}} \equiv \sqrt{\frac{R}{2}} \quad (\text{D.3})$$

for Dirichlet b.c. and Neumann b.c. respectively.

From (2.6), we have that $r \rightarrow 1^-$ when $u \rightarrow 0^+$. Taking this limit in (D.2), one finds

$$\mathcal{F}_n^{(\text{D})}(r) \rightarrow g_{\text{D}}^{2(1-n)} \quad \mathcal{F}_n^{(\text{N})}(r) \rightarrow g_{\text{N}}^{2(1-n)}. \quad (\text{D.4})$$

The bulk-boundary Operator Product Expansion (OPE) of the twist field $\mathcal{T}_n(u)$ reads [154]

$$\mathcal{T}_n(u) \sim \frac{\mathcal{A}_{n;\mathbb{I}}^{(\alpha)}}{(2u)^{\Delta_n}} \mathbb{I} + \dots \quad u \rightarrow 0^+ \quad (\text{D.5})$$

where \mathbb{I} denotes the identity operator on the boundary, the dots indicate subleading contributions that have been neglected and $\mathcal{A}_{n;\mathbb{I}}^{(\alpha)}$ is the one-point structure constant, which can be expressed in terms of the ground state degeneracy g_α as $\mathcal{A}_{n;\mathbb{I}}^{(\alpha)} = g_\alpha^{1-n}$ [6, 154]. Combining this observation with (D.4), we have that $\mathcal{F}_n^{(\alpha)}(r) \rightarrow (\mathcal{A}_{n;\mathbb{I}}^{(\alpha)})^2$ as $r \rightarrow 1$, for $\alpha \in \{\text{D}, \text{N}\}$. Hence, by using also (2.5), one finds that

$$\langle \mathcal{T}_n(u) \mathcal{T}_n^\dagger(v) \rangle_s^{(\alpha)} \sim \frac{(\mathcal{A}_{n;\mathbb{I}}^{(\alpha)})^2}{(2u)^{\Delta_n} s(2v)^{\Delta_n}} + \dots \quad (\text{D.6})$$

From (D.5), it is straightforward to get that

$$\langle \mathcal{T}_n(u) \mathcal{T}_n^\dagger(v) \rangle_s^{(\alpha)} \sim \frac{\mathcal{A}_{n;\mathbb{I}}^{(\alpha)}}{(2u)^{\Delta_n}} \langle \mathcal{T}_n^\dagger(v) \rangle_s^{(\alpha)} + \dots \quad (\text{D.7})$$

Finally, consistency between (D.6) and (D.7) leads to $\langle \mathcal{T}_n^\dagger(v) \rangle_s^{(\alpha)} = g_\alpha^{(1-n)}/s(2v)^{\Delta_n}$, in agreement with (D.1) and (2.11).

The limiting regime of small x can be studied by employing the results of [52] in a straightforward way. For Dirichlet b.c., this leads to

$$\mathcal{F}_n^{(D)}(x) = 1 + n \left(\frac{x}{2n} \right)^{\frac{2}{R^2}} \sum_{j=1}^{n-1} \frac{1}{[\sin(\pi j/n)]^{2/R^2}} - \frac{x^2}{12} \left(n - \frac{1}{n} \right) + \dots \quad x \rightarrow 0 \quad (\text{D.8})$$

while for Neumann b.c. one finds

$$\mathcal{F}_n^{(N)}(x) = 1 + n \left(\frac{x}{2n} \right)^{\frac{R^2}{2}} \sum_{j=1}^{n-1} \frac{1}{[\sin(\pi j/n)]^{R^2/2}} - \frac{x^2}{12} \left(n - \frac{1}{n} \right) + \dots \quad x \rightarrow 0 \quad (\text{D.9})$$

where the dots correspond to subleading terms with respect to the ones reported in the r.h.s.'s, which have been neglected. These short distance expansions provide the two-point correlators of twist fields on the disk for small x ; indeed, $\langle \mathcal{T}_n(0) \mathcal{T}_n^\dagger(x) \rangle_{\mathbb{D}}^{(\alpha)} \sim \mathcal{F}_n^{(\alpha)}(x)/x^{2\Delta_n}$ as $x \rightarrow 0^+$.

D.2 Decompactified boson

D.2.1 Normalization of two-point function of twist fields

In the following we determine the overall normalization on the two-point function of twist fields for the decompactified boson. In the case of the compact boson, this constant has been fixed through the $x \rightarrow 0$ behaviour of this correlator and such criterion will be employed also for the decompactified boson. The most important difference to take into account with respect to the case of the compact boson is due to the continuous spectrum of primary operators, which is made by vertex operators $V_\gamma = :e^{i\gamma\phi(z,\bar{z})}:$ with scaling dimensions are $\Delta_\gamma = \gamma^2$, for $\gamma \in \mathbb{R}$. In the \mathbb{Z}_n orbifold of this model [155–157], the untwisted sector is built from the operators $\mathcal{V}_\gamma = V_{\gamma_1} \otimes \dots \otimes V_{\gamma_n}$ with $\gamma = \{\gamma_1, \dots, \gamma_n\}$ (only \mathbb{Z}_n invariant linear combinations of such fields are local in the orbifold but this subtlety can be ignored at this level) and the identity field $\mathbb{I} = \mathcal{V}_0$. Then, the leading $x \rightarrow 0$ behaviour in (3.33) will be obtained by considering the OPE of the twist fields, which can contain only fields of the above mentioned type because of the twist charge conservation and by their descendants, although the contribution of the latter ones is subleading the $x \rightarrow 0$ limit.

Since the spectrum of the untwisted primary fields is continuous, the OPE should be given by a weighted integral over the \mathcal{V}_γ operators. From previous works [155], we conjecture that the contribution of the untwisted primary operators to the OPE of conjugate twist fields reads

$$\mathcal{T}_n(0) \mathcal{T}_n^\dagger(x) \sim \frac{1}{x^{2\Delta_n}} \int_{\mathbb{R}^n} \prod_{i=1}^n d\gamma_i \delta\left(\sum_i \gamma_i\right) x^{\gamma^2} \mathcal{C}_{\mathcal{T}_n, \mathcal{T}_n^\dagger}^{\mathcal{V}_\gamma} \mathcal{V}_\gamma(0) \quad (\text{D.10})$$

where $\mathcal{C}_{\mathcal{T}_n, \mathcal{T}_n^\dagger}^{\mathcal{V}_\gamma}$ are structure constants and the Dirac δ function appears as a consequence of $U(1)$ charge conservation in the non-compact boson CFT. We work with the usual conventions where $\mathcal{C}_{\mathcal{T}_n, \mathcal{T}_n^\dagger}^{\mathbb{I}} = 1$.

Plugging (D.10) into the two-point functions (3.33) to find the primary fields contributions to the limit $x \rightarrow 0$, for Neumann b.c. and Dirichlet b.c. we find

$$\langle \mathcal{T}_n(0) \mathcal{T}_n^\dagger(x) \rangle_{\mathbb{D}}^{(\alpha)} \underset{x \rightarrow 0}{\sim} \frac{1}{x^{2\Delta_n}} \int_{\mathbb{R}^n} \prod_{i=1}^n d\gamma_i \delta\left(\sum_i \gamma_i\right) x^{\gamma^2} \mathcal{C}_{\mathcal{T}_n, \mathcal{T}_n^\dagger}^{\mathcal{V}_\gamma} \langle \mathcal{V}_\gamma(0) \rangle_{\mathbb{D}}^{(\alpha)}. \quad (\text{D.11})$$

Conveniently, the correlators in the r.h.s. factorize into one-point functions of the non-compact boson BCFT, namely

$$\langle \mathcal{V}_\gamma(0) \rangle_{\mathbb{D}}^{(\alpha)} = \prod_{i=1}^n \langle V_{\gamma_i}(0) \rangle_{\mathbb{D}}^{(\alpha)}. \quad (\text{D.12})$$

For Neumann b.c. and Dirichlet b.c. where $\phi = \phi_0$, we have respectively [88]

$$\langle \mathcal{V}_\gamma(0) \rangle_{\mathbb{D}}^{(N)} = \prod_{i=1}^n \delta(\gamma_i) = \delta(\gamma) \quad \langle \mathcal{V}_\gamma(0) \rangle_{\mathbb{D}}^{(D)} = \prod_{i=1}^n e^{i\phi_0 \gamma_i} = \exp\left(i\phi_0 \sum_{i=1}^n \gamma_i\right) = 1 \quad (\text{D.13})$$

where, in the case of Dirichlet b.c., the dependence on ϕ_0 cancels for the fields that contribute to the OPE (D.10), because of the $U(1)$ charge neutrality condition $\sum_{i=1}^n \gamma_i = 0$.

For Neumann b.c. we find

$$\langle \mathcal{T}_n(0) \mathcal{T}_n^\dagger(x) \rangle_{\mathbb{D}}^{(N)} \underset{x \rightarrow 0}{\sim} \frac{1}{x^{2\Delta_n}} + \dots \quad (\text{D.14})$$

which gives $C_n^{(N)} = 1$ after a comparison with the limit $x \rightarrow 0$ of (3.28).

For Dirichlet b.c., we have

$$\langle \mathcal{T}_n(0) \mathcal{T}_n^\dagger(x) \rangle_{\mathbb{D}}^{(D)} \underset{x \rightarrow 0}{\sim} \frac{1}{x^{2\Delta_n}} \int_{\mathbb{R}^n} \prod_{i=1}^n d\gamma_i \delta\left(\sum_i \gamma_i\right) x^{\gamma^2} \mathcal{C}_{\mathcal{T}_n, \mathcal{T}_n^\dagger}^{\mathcal{V}_\gamma} \quad (\text{D.15})$$

where the structure constant $\mathcal{C}_{\mathcal{T}_n, \mathcal{T}_n^\dagger}^{\mathcal{V}_\gamma}$ depends smoothly on γ . Indeed, it can be unfolded to a n -point correlator of vertex operators on the Riemann sphere in the non-compact boson CFT as follows

$$\mathcal{C}_{\mathcal{T}_n, \mathcal{T}_n^\dagger}^{\mathcal{V}_\gamma} = n^{-\sum_i \gamma_i^2/2} \langle V_{\gamma_1}(e^{2\pi i/n}) V_{\gamma_2}(e^{4\pi i/n}) \dots V_{\gamma_n}(1) \rangle_{\mathbb{C}}. \quad (\text{D.16})$$

By employing the following well known CFT result [158]

$$\langle V_{\gamma_1}(z_1) \dots V_{\gamma_n}(z_n) \rangle_{\mathbb{C}} = \prod_{i < j} |z_i - z_j|^{2\gamma_i \gamma_j} \quad (\text{D.17})$$

we find that the behaviour of the structure constants close to $\gamma_i = 0$ is

$$\mathcal{C}_{\mathcal{T}_n, \mathcal{T}_n^\dagger}^{\mathcal{V}_\gamma} \underset{\gamma_i \rightarrow 0}{\sim} 1 \quad (\text{D.18})$$

which provides the leading $x \rightarrow 0$ behaviour in (D.15) as follows. Integrating the Dirac delta function, we arrive to

$$\langle \mathcal{T}_n(0) \mathcal{T}_n^\dagger(x) \rangle_{\mathbb{D}}^{(D)} \underset{x \rightarrow 0}{\sim} \frac{1}{x^{2\Delta_n}} \int_{\mathbb{R}^{n-1}} \prod_{i=1}^{n-1} d\gamma_i \exp\left\{-\frac{1}{2} |\log x^2| \sum_{i,j=1}^{n-1} \gamma_i A_{i,j} \gamma_j\right\} \quad (\text{D.19})$$

where we have introduced the matrix $A_{i,j} \equiv 1 + \delta_{i,j}$, whose determinant is $\det A = n$. The Laplace's method allows us to find the leading $x \rightarrow 0$ asymptotic behaviour of this integral

$$\langle \mathcal{T}_n(0) \mathcal{T}_n^\dagger(x) \rangle_{\mathbb{D}}^{(D)} \underset{x \rightarrow 0}{\sim} \frac{1}{x^{2\Delta_n}} \frac{1}{\sqrt{n}} \left(\frac{2\pi}{|\log x^2|}\right)^{(n-1)/2}. \quad (\text{D.20})$$

The normalisation constant is obtained by comparing this result with the limit $x \rightarrow 0$ of (3.27), which can be found by observing that

$$\langle \mathcal{T}_n(0) \mathcal{T}_n^\dagger(x) \rangle_{\mathbb{D}}^{(D)} \underset{x \rightarrow 0}{\sim} \frac{1}{x^{2\Delta_n}} \frac{1}{\sqrt{\det(-i\boldsymbol{\tau})}} (C_n^{(D)} + \dots). \quad (\text{D.21})$$

By using the identities reported in Sec. 4.5 of [52] for $\det(-i\boldsymbol{\tau}(x))$ and (3.24), we get

$$\frac{1}{\sqrt{\det(-i\boldsymbol{\tau}(x))}} = \prod_{k=1}^{n-1} \sqrt{\frac{F_{k/n}(x^2)}{F_{k/n}(1-x^2)}} \underset{x \rightarrow 0}{\sim} \frac{1}{\sqrt{n}} \left(\frac{2\pi}{|\log x^2|} \right)^{(n-1)/2}. \quad (\text{D.22})$$

Finally, the comparison of (D.21) and (D.20) gives $C_n^{(D)} = 1$.

D.2.2 The $x \rightarrow 1$ regime

It is worth investigating also the behaviour of (3.33) as $x \rightarrow 1$ because it provides information about the one-point structure constants of the twist fields. From the normalized two-point functions in (3.34), since $\Theta(-\boldsymbol{\tau}^{-1}(x)) \rightarrow 1$ as $x \rightarrow 1$, for Dirichlet b.c. we have

$$\langle \mathcal{T}_n(0) \mathcal{T}_n^\dagger(x) \rangle_{\mathbb{D}}^{(D)} \underset{x \rightarrow 1}{\sim} \frac{1}{(1-x^2)^{\Delta_n}}. \quad (\text{D.23})$$

For Neumann b.c., by using (3.29) in the second equation of (3.34), we get

$$\langle \mathcal{T}_n(0) \mathcal{T}_n^\dagger(x) \rangle_{\mathbb{D}}^{(N)} \underset{x \rightarrow 1}{\sim} \frac{\sqrt{\det(-i\boldsymbol{\tau}(x))}}{(1-x^2)^{\Delta_n}} \quad (\text{D.24})$$

where, from (D.22), we have that

$$\det(-i\boldsymbol{\tau}(x)) = \prod_{k=1}^{n-1} \frac{F_{k/n}(1-x^2)}{F_{k/n}(x^2)} \underset{x \rightarrow 1}{\sim} \frac{1}{n} \left(\frac{2\pi}{|\log(1-x^2)|} \right)^{(n-1)}. \quad (\text{D.25})$$

Now we compare (D.24) with the corresponding $x \rightarrow 1$ behaviour coming from the bulk-boundary OPE of $\mathcal{T}_n^\dagger(x)$ fields. In this case, the OPE has contributions only from the untwisted boundary fields. This comparison is done by using some facts about the boundary field spectrum of the non-compact boson BCFT [88], which we denote $\psi^{(\alpha)}(e^{i\theta})$, where $\theta \in (0, 2\pi)$ is a coordinate parametrizing the boundary of the unit disk \mathbb{D} .

For Dirichlet b.c., the spectrum of the boundary operators only contains the boundary identity operator $\psi_0^{(D)}$ and its descendants; indeed, the constraint $\phi_0 = \text{const}$ holds along the boundary. For Neumann b.c., any boundary vertex operator $\psi_\gamma^{(N)} = :\exp[i\gamma\phi(e^{i\theta})]:$ with charge $\gamma \in \mathbb{R}$ and scaling dimension $\Delta_\gamma = \gamma^2/2$ is allowed. In the \mathbb{Z}_n orbifold of this BCFT, for Dirichlet b.c. the untwisted sector of primary boundary fields consists of the identity operator $\Psi_0^{(D)}$, while for Neumann b.c. we have $\Psi_\gamma^{(N)} = \psi_{\gamma_1}^{(N)} \otimes \dots \otimes \psi_{\gamma_n}^{(N)}$.

For Dirichlet b.c., the leading contribution to the bulk-boundary OPE of \mathcal{T}_n^\dagger is

$$\mathcal{T}_n^\dagger(x) \sim \frac{\mathcal{A}_{n,\mathbb{D}}^{(D)}}{(1-x^2)^{\Delta_n}} \mathbb{I}(1). \quad (\text{D.26})$$

In the case of Neumann b.c., there are issues with the continuous spectrum of boundary operators similar to the ones identified in the Appendix D.2.1 for Dirichlet boundary conditions. To bypass them, we conjecture the following bulk-boundary OPE

$$\mathcal{T}_n^\dagger(x) \sim \frac{1}{(1-x^2)^{\Delta_n}} \int_{-\infty}^{+\infty} \prod_{i=1}^n d\gamma_i \delta\left(\sum_i \gamma_i\right) (1-x^2)^{\gamma^2/2} \mathcal{A}_{n,\Psi_\gamma}^{(N)} \Psi_\gamma^{(N)}(1) \quad (\text{D.27})$$

where $\mathcal{A}_{n,\Psi_\gamma}^{(N)}$ are the bulk-boundary structure constants and the $U(1)$ charge neutrality on the boundary is manifest.

Plugging (D.26) and (D.27) into the corresponding correlators in (3.34), for Dirichlet b.c. we find

$$\langle \mathcal{T}_n(0) \mathcal{T}_n^\dagger(x) \rangle_{\mathbb{D}}^{(D)} \underset{x \rightarrow 1}{\sim} \frac{(\mathcal{A}_{n,\mathbb{I}}^{(D)})^2}{(1-x^2)^{\Delta_n}} \quad (\text{D.28})$$

where we used that [103]

$$\langle \mathcal{T}_n(0) \rangle_{\mathbb{D}}^{(\alpha)} = \mathcal{A}_{n,\mathbb{I}}^{(\alpha)}. \quad (\text{D.29})$$

The comparison of (D.28) and (D.23) fixes $(\mathcal{A}_{n,\mathbb{I}}^{(D)})^2 = 1$. For Neumann b.c., the result is more involved and reads

$$\langle \mathcal{T}_n(0) \mathcal{T}_n^\dagger(x) \rangle_{\mathbb{D}}^{(N)} \underset{x \rightarrow 1}{\sim} \frac{1}{(1-x^2)^{\Delta_n}} \int_{-\infty}^{+\infty} \prod_{i=1}^n d\gamma_i \delta\left(\sum_i \gamma_i\right) (1-x^2)^{\gamma^2/2} (\mathcal{A}_{n,\Psi_\gamma}^{(N)})^2 \quad (\text{D.30})$$

where we have used that [103]

$$\langle \mathcal{T}_n(0) \Psi_\gamma^{(\alpha)}(1) \rangle_{\mathbb{D}}^{(\alpha)} = \mathcal{A}_{n,\Psi_\gamma}^{(\alpha)}. \quad (\text{D.31})$$

The derivation is analogous to the one described in the Appendix D.2.1. The correlator in (D.31) unfolds to a n -point function of boundary vertex operators on the unit disk [103] which should be smooth in γ_i . Since we are only interested in the leading behaviour as $x \rightarrow 1$, we can approximate $\mathcal{A}_{n,\Psi_\gamma}^{(N)} \approx \mathcal{A}_{n,\mathbb{I}}^{(N)}$ for $\gamma_i \rightarrow 0$ small. Then, by evaluating the Gaussian integral as done in Appendix D.2.1, one arrives to

$$\langle \mathcal{T}_n(0) \mathcal{T}_n^\dagger(x) \rangle_{\mathbb{D}}^{(N)} \underset{x \rightarrow 1}{\sim} \frac{(\mathcal{A}_{n,\Psi_\gamma}^{(N)})^2}{(1-x^2)^{\Delta_n}} \left(\frac{2\pi}{|\log(1-x^2)|} \right)^{(n-1)/2} \quad (\text{D.32})$$

which can be compared with (D.24), finding that $(\mathcal{A}_{n,\Psi_\gamma}^{(N)})^2 = 1$.

Finally, by employing the fact that the one-point structure constants of twist fields are related to the ground state degeneracies g_α as $\mathcal{A}_{n,\mathbb{I}}^{(\alpha)} = g_\alpha^{1-n}$, we get

$$g_D = 1 \quad g_N = 1 \quad (\text{D.33})$$

which is compatible with well-established results in the literature [88].

E Details about the BCFT approach to quantum quenches

In this Appendix, we report the derivation of the main expressions on the quantum quenches reported and discussed in Sec. 5.

E.1 Global quench

In [76] the temporal evolution after a global quantum quench determined by a critical Hamiltonian has been studied through BCFT. The setup is given by a Euclidean BCFT defined in the strip $\mathbb{S}_{\tau_0} \equiv \{w \in \mathbb{C}; 0 < \text{Im}(w) < 2\tau_0\}$, with the same conformally invariant boundary condition α imposed both on $\text{Im}(w) = 0$ and on $\text{Im}(w) = 2\tau_0$. We are interested in the two-point function of twist fields in \mathbb{S}_{τ_0} placed at $w_1 = i\tau$ and $w_2 = i\tau + \ell$, with $\ell > 0$; i.e. (see (2.1) and (2.3))

$$\text{Tr}\rho_A^n = C_n^2 \epsilon^{2\Delta_n} \langle \mathcal{T}_n(w_1) \mathcal{T}_n^\dagger(w_2) \rangle_{\mathbb{S}_{\tau_0}}. \quad (\text{E.1})$$

The strip \mathbb{S}_{τ_0} is sent into the upper half plane $\mathbb{H} \equiv \{z \in \mathbb{C}; \text{Im}(z) \geq 0\}$ through the map $z = e^{\pi w/(2\tau_0)}$. As a consequence, the positions of the twist fields in \mathbb{H} are $z_1 = e^{i\theta}$ and $z_2 = fe^{i\theta}$, where $f \equiv e^{\pi\ell/(2\tau_0)}$.

In order to employ the two-point correlation function of twist fields in the unit disk \mathbb{D} given in (3.31) and (3.34), first we map the upper half plane \mathbb{H} into the unit disk (parameterised by the complex coordinate ζ) through $z \rightarrow \zeta = \frac{z-\bar{z}_1}{z-\bar{z}_2}$ and then we perform a global rotation by $\arg(\frac{z_2-z_1}{z_2-\bar{z}_1})$. This procedure leads to the following expression for the harmonic ratio $r = |x|^2$

$$r = \left| \frac{z_2 - z_1}{z_2 - \bar{z}_1} \right|^2 = \frac{(f-1)^2}{f^2 - 2f \cos(2\theta) + 1} = \frac{2[\sinh(\pi\ell/(4\tau_0))]^2}{\cosh(\pi\ell/(2\tau_0)) - \cosh(\pi\tau/\tau_0)} \quad (\text{E.2})$$

(the last expression agrees e.g. with the cross ratio $\eta_{1,2}$ in [159]) and the following expression for (E.1)

$$\text{Tr}\rho_A^n = C_n^2 \epsilon^{2\Delta_n} \frac{J}{[r(1-r)]^{\Delta_n}} \mathcal{F}_n^{(\alpha)}(r) \quad (\text{E.3})$$

in terms of the functions given in (2.22) for the compact boson and in (2.27) for the decompactified boson, where J includes all the jacobian terms associated to the various mappings and reads

$$J = \left(\frac{\pi}{2\tau_0} \right)^{2\Delta_n} \left| \frac{(z_2 - \bar{z}_2)(z_1 - \bar{z}_1)}{(z_2 - \bar{z}_1)^2 (z_1 - \bar{z}_2)^2} \right|^{\Delta_n} |z_1 z_2|^{\Delta_n}. \quad (\text{E.4})$$

The crucial step introducing the physical time t is the analytic continuation $\tau \rightarrow \tau_0 + it$. This brings (E.2) into (5.4), which is shown in the left panel of Fig. 14 for different values of ℓ/τ_0 . Notice that a step function is obtained when $\ell/\tau_0 \gg 1$. Performing the analytic continuation $\tau \rightarrow \tau_0 + it$ in (E.4), after some algebra one finds

$$J = \left(\frac{\pi}{2\tau_0} \right)^{2\Delta_n} \left(\frac{f}{f^2 + 2f \cosh(\pi t/\tau_0) + 1} \right)^{\Delta_n}. \quad (\text{E.5})$$

By using this expression and (5.4) in (E.3), we arrive to (5.3).

E.2 Local quench

As for the local quench, in the following we review the BCFT analysis performed in [77] and adapt it in order to employ the analytic expressions for the two-point functions of the twist fields reported in Sec. 2.

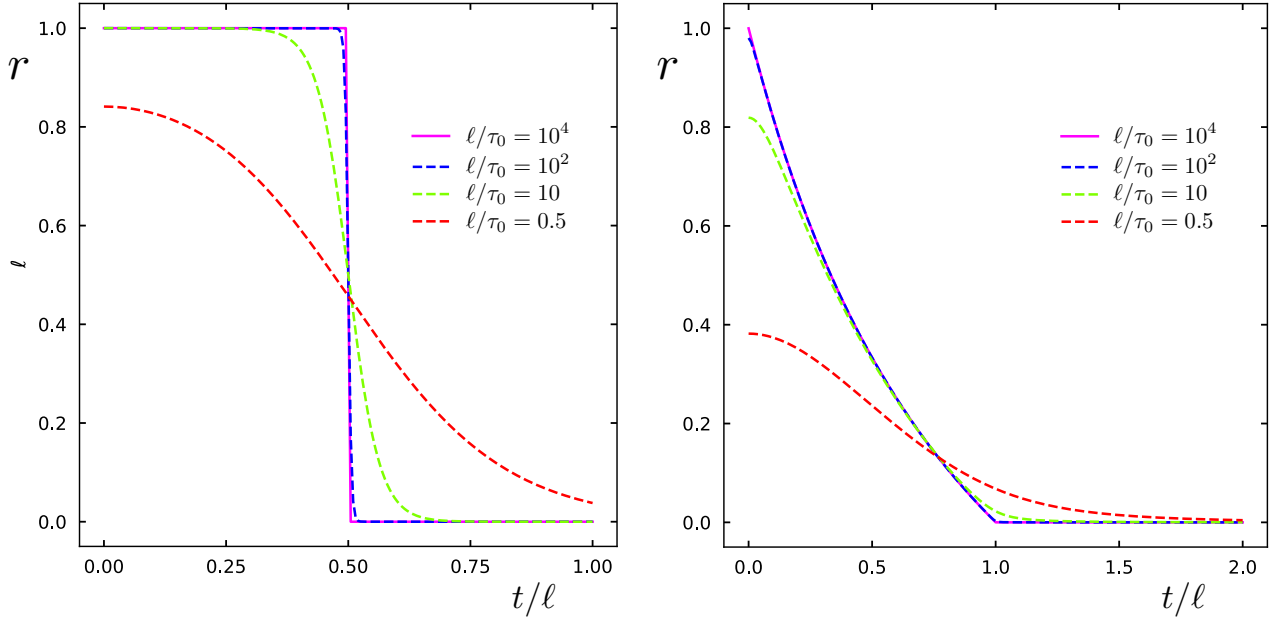


Figure 14: Temporal evolution of the harmonic ratio r for the global quench (left panel, see (5.4)) and for the local quench (right panel, see (5.9)), for different values of ℓ/τ_0 .

In [77] the temporal evolution after a local quench of the moments of the reduced density matrix ρ_A of an interval of length ℓ are investigated by considering the two-point correlator of twist fields in the Euclidean geometry \mathbb{C}_{τ_0} defined as the complex plane (parameterised by the complex coordinate w) where boundaries are introduced by removing the slits corresponding to $(-i\infty, -i\tau_0]$ and $[i\tau_0, +i\infty)$. In the case we are interested in, the defect coincides with the first endpoint of the interval; hence the twist fields are located at $w_1 = i\tau$ and $w_2 = \ell + i\tau$. Thus we have (see (2.1) and (2.3))

$$\text{Tr}\rho_A^n = C_n^2 \epsilon^{2\Delta_n} \langle \mathcal{T}_n(w_1) \mathcal{T}_n^\dagger(w_2) \rangle_{\mathbb{C}_{\tau_0}}. \quad (\text{E.6})$$

The domain \mathbb{C}_{τ_0} is mapped into the right half plane $\tilde{\mathbb{H}} \equiv \{z \in \mathbb{C}; \text{Re}(z) \geq 0\}$ through the following conformal map

$$z = \frac{w}{\tau_0} + \sqrt{\left(\frac{w}{\tau_0}\right)^2 + 1} \quad w = \tau_0 \frac{z^2 - 1}{2z} \quad (\text{E.7})$$

hence the positions of the twist fields in $\tilde{\mathbb{H}}$ are

$$z_1 = i\tau/\tau_0 + \sqrt{1 - (\tau/\tau_0)^2} \quad z_2 = \frac{\ell}{\tau_0} + \frac{i\tau}{\tau_0} + \frac{\rho}{\tau_0} e^{i\theta} \quad (\text{E.8})$$

where

$$\rho^2 \equiv \sqrt{(\tau_0^2 + \ell^2 - \tau^2)^2 + 4\ell^2\tau^2} \quad \theta \equiv \frac{1}{2} \arctan \frac{2\ell\tau}{\tau_0^2 + \ell^2 - \tau^2}. \quad (\text{E.9})$$

The factor coming from the Jacobians occurring in the transformation of the two-point correlator reads

$$\mathcal{J} \equiv \left| \frac{dz}{dw} \right|_{w_1}^{\Delta_n} \left| \frac{dz}{dw} \right|_{w_2}^{\Delta_n} = \left(\frac{\sqrt{(\ell + \rho \cos \theta)^2 + (\tau + \rho \sin \theta)^2}}{\tau_0 \rho \sqrt{\tau_0^2 - \tau^2}} \right)^{\Delta_n}. \quad (\text{E.10})$$

Then, one employs the conformal map $z \rightarrow \zeta = \frac{z-z_1}{z+\bar{z}_1}$, which sends the right half plane $\widetilde{\mathbb{H}}$ into the unit disk \mathbb{D} parameterised by the complex variable ζ . Hence the location of the twist fields in \mathbb{D} are the points $\zeta_1 = 0$ and $\zeta_2 = \frac{z_2-z_1}{z_2+\bar{z}_1}$ and the corresponding factor occurring in the transformation of the two-point function reads

$$\tilde{\mathcal{J}} \equiv \left| \frac{d\zeta}{dz} \right|_{z_1}^{\Delta_n} \left| \frac{d\zeta}{dz} \right|_{z_2}^{\Delta_n} = \frac{1}{|z_2 + \bar{z}_1|^{2\Delta_n}} = \left[\frac{\tau_0^2}{(\ell + \sqrt{\tau_0^2 - \tau^2})^2 + \rho^2 + 2\rho(\ell + \sqrt{\tau_0^2 - \tau^2}) \cos \theta} \right]^{\Delta_n}. \quad (\text{E.11})$$

Performing also a rotation by $\arg\left(\frac{z_2-z_1}{z_2+\bar{z}_1}\right)$, one arrives to the correlators in (3.31) in \mathbb{D} with the harmonic ratio given by

$$r = |x|^2 = \left| \frac{z_2 - z_1}{z_2 + \bar{z}_1} \right|^2 = \frac{(\ell - \sqrt{\tau_0^2 - \tau^2})^2 + \rho^2 + 2\rho(\ell - \sqrt{\tau_0^2 - \tau^2}) \cos \theta}{(\ell + \sqrt{\tau_0^2 - \tau^2})^2 + \rho^2 + 2\rho(\ell + \sqrt{\tau_0^2 - \tau^2}) \cos \theta}. \quad (\text{E.12})$$

By using also that $1 - r = \frac{(z_1 + \bar{z}_1)(z_2 + \bar{z}_2)}{|z_2 + \bar{z}_1|^2}$, we find that (E.6) can be written as

$$\langle \mathcal{T}_n(w_1) \mathcal{T}_n^\dagger(w_2) \rangle_{\mathbb{C}\tau_0} = \frac{\mathcal{J} \tilde{\mathcal{J}}}{[r(1-r)]^{\Delta_n}} \mathcal{F}_n^{(\alpha)}(r). \quad (\text{E.13})$$

The crucial step in the analysis of [77] which introduces the physical time t is the analytic continuation $\tau \rightarrow it$. By employing the identity $\arctan(z) = \frac{1}{2i} \log \frac{i-z}{i+z}$, we have that the expressions in (E.9) after the analytic continuation become respectively

$$\rho^2 = \sqrt{(\tau_0^2 + \ell^2 + t^2)^2 - 4\ell^2 t^2}, \quad \theta = \frac{i}{4} \log \left[\frac{(\ell/\tau_0 + t/\tau_0)^2 + 1}{(\ell/\tau_0 - t/\tau_0)^2 + 1} \right]. \quad (\text{E.14})$$

From these expressions and (E.12), one obtains (5.9) and (5.10). The temporal evolution of (5.9) is shown in the right panel of Fig. 14 for some assigned values of ℓ/τ_0 .

After the analytic continuation, (E.10) and (E.11) become respectively

$$\mathcal{J} = \left[\frac{\sqrt{\ell^2 + \rho^2 - t^2 + 2\ell\rho \cosh |\theta| - 2\rho t \sinh |\theta|}}{\tau_0 \rho \sqrt{\tau_0^2 + t^2}} \right]^{\Delta_n} \equiv \mathcal{R}^{\Delta_n} \quad (\text{E.15})$$

$$\tilde{\mathcal{J}} = \left[\frac{\tau_0^2}{(\ell + \sqrt{\tau_0^2 + t^2})^2 + \rho^2 + 2\rho(\ell + \sqrt{\tau_0^2 + t^2}) \cosh |\theta|} \right]^{\Delta_n} \equiv \tilde{\mathcal{R}}^{\Delta_n}. \quad (\text{E.16})$$

Combining the above results, we arrive to (5.8).

The result of [77] for the quench we are considering, i.e. the case III in their classification, is obtained from (5.8) by first setting $\mathcal{F}_n^{(\alpha)}(r)$ equal to 1 and then considering the regime where $t \gg \tau_0$ and $\ell \gg \tau_0$. Taking these limits in (5.9) and (5.10), one obtains

$$\rho \xrightarrow{t, \ell \gg \tau_0} \sqrt{|\ell^2 - t^2|} \quad \rho \cosh |\theta| \xrightarrow{t, \ell \gg \tau_0} \max(t, \ell) \quad \rho \sinh |\theta| \xrightarrow{t, \ell \gg \tau_0} \min(t, \ell) \quad (\text{E.17})$$

and

$$r \xrightarrow{t, \ell \gg \tau_0} \begin{cases} \frac{\ell - t}{\ell + t} & t < \ell \\ \frac{\tau_0^2 \ell^2}{(4t^2)(t^2 - \ell^2)} & t > \ell \end{cases} \quad 1 - r \xrightarrow{t, \ell \gg \tau_0} \begin{cases} \frac{2t}{\ell + t} & t < \ell \\ 1 & t > \ell. \end{cases} \quad (\text{E.18})$$

Similarly, in this limiting regime, from (E.15) and (E.16) we get respectively

$$\mathcal{R} \xrightarrow{t, \ell \gg \tau_0} \begin{cases} \frac{2}{\tau_0 t} & t < \ell \\ \frac{1}{t(t-\ell)} & t > \ell \end{cases} \quad \tilde{\mathcal{R}} \xrightarrow{t, \ell \gg \tau_0} \begin{cases} \frac{\tau_0^2}{4\ell(\ell+t)} & t < \ell \\ \frac{\tau_0^2}{4t(\ell+t)} & t > \ell. \end{cases} \quad (\text{E.19})$$

Combining these results, we arrive to

$$\frac{\mathcal{J} \tilde{\mathcal{J}}}{[r(1-r)]^{\Delta_n}} \xrightarrow{t, \ell \gg \tau_0} \begin{cases} \left(\frac{1}{t^2} \frac{\ell+t}{\ell-t} \frac{\tau_0}{4\ell} \right)^{\Delta_n} & t < \ell \\ \frac{1}{\ell^{2\Delta_n}} & t > \ell \end{cases} \quad (\text{E.20})$$

which is the expression reported in [77].

References

- [1] P. Calabrese and J. Cardy, “*Entanglement entropy and conformal field theory*”, *J. Phys. A* **42**, 504005 (2009), [arxiv:0905.4013](#).
- [2] V. Eisler and I. Peschel, “*Reduced density matrices and entanglement entropy in free lattice models*”, *J. Phys. A* **42**, 504003 (2009), [arxiv:0906.1663](#).
- [3] H. Casini and M. Huerta, “*Entanglement entropy in free quantum field theory*”, *J. Phys. A* **42**, 504007 (2009), [arxiv:0905.2562](#).
- [4] J. Eisert, M. Cramer and M. B. Plenio, “*Area laws for the entanglement entropy - a review*”, *Rev. Mod. Phys.* **82**, 277 (2010), [arxiv:0808.3773](#).
- [5] M. Rangamani and T. Takayanagi, “*Holographic Entanglement Entropy*”, Springer (2017).
- [6] P. Calabrese and J. L. Cardy, “*Entanglement entropy and quantum field theory*”, *J. Stat. Mech.* **0406**, P06002 (2004), [hep-th/0405152](#).
- [7] H.-Q. Zhou, T. Barthel, J. Fjaeretad and U. Schollwock, “*Entanglement and boundary critical phenomena*”, *Phys. Rev. A* **74**, 050305 (2006), [cond-mat/0511732](#).
- [8] I. Affleck, N. Laflorencie and E. S. Sorensen, “*Entanglement entropy in quantum impurity systems and systems with boundaries*”, *J. Phys. A* **42**, 504009 (2009), [arxiv:0906.1809](#).
- [9] C. Berthiere and S. N. Solodukhin, “*Boundary effects in entanglement entropy*”, *Nucl. Phys. B* **910**, 823 (2016), [arxiv:1604.07571](#).
- [10] L. Taddia, J. Xavier, F. C. Alcaraz and G. Sierra, “*Entanglement entropies in conformal systems with boundaries*”, *Phys. Rev. B* **88**, 075112 (2013), [arxiv:1302.6222](#).
- [11] I. Affleck, “*Conformal field theory approach to the Kondo effect*”, *Acta Phys. Polon. B* **26**, 1869 (1995), [cond-mat/9512099](#).
- [12] N. Laflorencie, E. S. Sorensen, M.-S. Chang and I. Affleck, “*Boundary effects in the critical scaling of entanglement entropy in 1D systems*”, *Phys. Rev. Lett.* **96**, 100603 (2006), [cond-mat/0512475](#).

- [13] S. Ryu and T. Takayanagi, “*Holographic derivation of entanglement entropy from AdS/CFT*”, *Phys. Rev. Lett.* **96**, 181602 (2006), [hep-th/0603001](#).
- [14] S. Ryu and T. Takayanagi, “*Aspects of Holographic Entanglement Entropy*”, *JHEP* **0608**, 045 (2006), [hep-th/0605073](#).
- [15] A. Karch and L. Randall, “*Locally localized gravity*”, *JHEP* **0105**, 008 (2001), [hep-th/0011156](#).
- [16] T. Takayanagi, “*Holographic Dual of BCFT*”, *Phys. Rev. Lett.* **107**, 101602 (2011), [arxiv:1105.5165](#).
- [17] M. Fujita, T. Takayanagi and E. Tonni, “*Aspects of AdS/BCFT*”, *JHEP* **1111**, 043 (2011), [arxiv:1108.5152](#).
- [18] M. Nozaki, T. Takayanagi and T. Ugajin, “*Central Charges for BCFTs and Holography*”, *JHEP* **1206**, 066 (2012), [arxiv:1205.1573](#).
- [19] G. Penington, “*Entanglement Wedge Reconstruction and the Information Paradox*”, *JHEP* **2009**, 002 (2020), [arxiv:1905.08255](#).
- [20] A. Almheiri, N. Engelhardt, D. Marolf and H. Maxfield, “*The entropy of bulk quantum fields and the entanglement wedge of an evaporating black hole*”, *JHEP* **1912**, 063 (2019), [arxiv:1905.08762](#).
- [21] A. Almheiri, R. Mahajan, J. Maldacena and Y. Zhao, “*The Page curve of Hawking radiation from semiclassical geometry*”, *JHEP* **2003**, 149 (2020), [arxiv:1908.10996](#).
- [22] A. Almheiri, T. Hartman, J. Maldacena, E. Shaghoulian and A. Tajdini, “*Replica Wormholes and the Entropy of Hawking Radiation*”, *JHEP* **2005**, 013 (2020), [arxiv:1911.12333](#).
- [23] G. Penington, S. H. Shenker, D. Stanford and Z. Yang, “*Replica wormholes and the black hole interior*”, *JHEP* **2203**, 205 (2022), [arxiv:1911.11977](#).
- [24] B. Estienne and J.-M. Stéphan, “*Entanglement spectroscopy of chiral edge modes in the Quantum Hall effect*”, *Phys. Rev. B* **101**, 115136 (2020), [arxiv:1911.10125](#).
- [25] B. Estienne, B. Oblak and J.-M. Stéphan, “*Ergodic Edge Modes in the 4D Quantum Hall Effect*”, *SciPost Phys.* **11**, 016 (2021), [arxiv:2104.01860](#).
- [26] V. Crépel, N. Claussen, B. Estienne and N. Regnault, “*Model states for a class of chiral topological order interfaces*”, *Nature Commun.* **10**, 1861 (2019), [arxiv:1806.06858](#).
- [27] V. Crépel, N. Claussen, N. Regnault and B. Estienne, “*Microscopic study of the Halperin–Laughlin interface through matrix product states*”, *Nature Commun.* **10**, 1860 (2019), [arxiv:1904.11023](#).
- [28] M. B. Plenio and S. Virmani, “*An Introduction to entanglement measures*”, *Quant. Inf. Comput.* **7**, 1 (2007), [quant-ph/0504163](#).
- [29] S. Hollands and K. Sanders, “*Entanglement measures and their properties in quantum field theory*”, [arxiv:1702.04924](#).
- [30] I. Peschel and J. Zhao, “*On single-copy entanglement*”, *J. Stat. Mech.* **2005**, P11002 (2005), [quant-ph/0509002](#).

- [31] J. Eisert and M. Cramer, “*Single-copy entanglement in critical quantum spin chains*”, *Phys. Rev. A* **72**, 042112 (2005), [quant-ph/0506250](#).
- [32] R. Orús, J. I. Latorre, J. Eisert and M. Cramer, “*Half the entanglement in critical systems is distillable from a single specimen*”, *Phys. Rev. A* **73**, 060303(R) (2006), [quant-ph/0509023](#).
- [33] C. G. Callan, Jr. and F. Wilczek, “*On geometric entropy*”, *Phys. Lett. B* **333**, 55 (1994), [hep-th/9401072](#).
- [34] C. Holzhey, F. Larsen and F. Wilczek, “*Geometric and renormalized entropy in conformal field theory*”, *Nucl. Phys. B* **424**, 443 (1994), [hep-th/9403108](#).
- [35] A. A. Belavin, A. M. Polyakov and A. B. Zamolodchikov, “*Infinite Conformal Symmetry in Two-Dimensional Quantum Field Theory*”, *Nucl. Phys. B* **241**, 333 (1984).
- [36] J. L. Cardy, “*Conformal Invariance and Surface Critical Behavior*”, *Nucl. Phys. B* **240**, 514 (1984).
- [37] J. L. Cardy, “*Effect of Boundary Conditions on the Operator Content of Two-Dimensional Conformally Invariant Theories*”, *Nucl. Phys. B* **275**, 200 (1986).
- [38] J. L. Cardy, “*Boundary Conditions, Fusion Rules and the Verlinde Formula*”, *Nucl. Phys. B* **324**, 581 (1989).
- [39] J. L. Cardy and D. C. Lewellen, “*Bulk and boundary operators in conformal field theory*”, *Phys. Lett. B* **259**, 274 (1991).
- [40] J. L. Cardy, “*Boundary conformal field theory*”, [hep-th/0411189](#).
- [41] J. L. Cardy, O. A. Castro-Alvaredo and B. Doyon, “*Form factors of branch-point twist fields in quantum integrable models and entanglement entropy*”, *J. Stat. Phys.* **130**, 129 (2008), [arxiv:0706.3384](#).
- [42] L. J. Dixon, D. Friedan, E. J. Martinec and S. H. Shenker, “*The Conformal Field Theory of Orbifolds*”, *Nucl. Phys. B* **282**, 13 (1987).
- [43] A. B. Zamolodchikov, “*Conformal Scalar Field on the Hyperelliptic Curve and Critical Ashkin-teller Multipoint Correlation Functions*”, *Nucl. Phys. B* **285**, 481 (1987).
- [44] M. Bershadsky and A. Radul, “*Conformal Field Theories with Additional $Z(N)$ Symmetry*”, *Int. J. Mod. Phys. A* **2**, 165 (1987).
- [45] V. G. Knizhnik, “*Analytic Fields on Riemann Surfaces. 2*”, *Commun. Math. Phys.* **112**, 567 (1987).
- [46] I. Affleck and A. W. Ludwig, “*Universal noninteger ‘ground state degeneracy’ in critical quantum systems*”, *Phys. Rev. Lett.* **67**, 161 (1991).
- [47] D. Friedan and A. Konechny, “*On the boundary entropy of one-dimensional quantum systems at low temperature*”, *Phys. Rev. Lett.* **93**, 030402 (2004), [hep-th/0312197](#).
- [48] H. Casini, I. Salazar Landea and G. Torroba, “*The g -theorem and quantum information theory*”, *JHEP* **1610**, 140 (2016), [arxiv:1607.00390](#).

- [49] S. Furukawa, V. Pasquier and J. Shiraishi, “*Mutual Information and Compactification Radius in a $c=1$ Critical Phase in One Dimension*”, [Phys. Rev. Lett. 102, 170602 \(2009\)](#), [arxiv:0809.5113](#).
- [50] M. Caraglio and F. Gliozzi, “*Entanglement Entropy and Twist Fields*”, [JHEP 0811, 076 \(2008\)](#), [arxiv:0808.4094](#).
- [51] H. Casini and M. Huerta, “*Reduced density matrix and internal dynamics for multicomponent regions*”, [Class. Quant. Grav. 26, 185005 \(2009\)](#), [arxiv:0903.5284](#).
- [52] P. Calabrese, J. Cardy and E. Tonni, “*Entanglement entropy of two disjoint intervals in conformal field theory*”, [J. Stat. Mech. 0911, P11001 \(2009\)](#), [arxiv:0905.2069](#).
- [53] P. Calabrese, J. Cardy and E. Tonni, “*Entanglement entropy of two disjoint intervals in conformal field theory II*”, [J. Stat. Mech. 1101, P01021 \(2011\)](#), [arxiv:1011.5482](#).
- [54] V. Alba, L. Tagliacozzo and P. Calabrese, “*Entanglement entropy of two disjoint blocks in critical Ising models*”, [Phys. Rev. B 81, 060411 \(2010\)](#), [arxiv:0910.0706](#).
- [55] M. Fagotti and P. Calabrese, “*Entanglement entropy of two disjoint blocks in XY chains*”, [J. Stat. Mech. 1004, P04016 \(2010\)](#), [arxiv:1003.1110](#).
- [56] A. Coser, L. Tagliacozzo and E. Tonni, “*On Rényi entropies of disjoint intervals in conformal field theory*”, [J. Stat. Mech. 1401, P01008 \(2014\)](#), [arxiv:1309.2189](#).
- [57] T. Hartman, “*Entanglement Entropy at Large Central Charge*”, [arxiv:1303.6955](#).
- [58] A. Coser, E. Tonni and P. Calabrese, “*Spin structures and entanglement of two disjoint intervals in conformal field theories*”, [J. Stat. Mech. 1605, 053109 \(2016\)](#), [arxiv:1511.08328](#).
- [59] T. Grava, A. P. Kels and E. Tonni, “*Entanglement of Two Disjoint Intervals in Conformal Field Theory and the 2D Coulomb Gas on a Lattice*”, [Phys. Rev. Lett. 127, 141605 \(2021\)](#), [arxiv:2104.06994](#).
- [60] C. A. Agon, M. Headrick, D. L. Jafferis and S. Kasko, “*Disk entanglement entropy for a Maxwell field*”, [Phys. Rev. D 89, 025018 \(2014\)](#), [arxiv:1310.4886](#).
- [61] C. De Nobili, A. Coser and E. Tonni, “*Entanglement entropy and negativity of disjoint intervals in CFT: Some numerical extrapolations*”, [J. Stat. Mech. 1506, P06021 \(2015\)](#), [arxiv:1501.04311](#).
- [62] B. Estienne, Y. Ikhlef and A. Rotaru, “*Second Rényi entropy and annulus partition function for one-dimensional quantum critical systems with boundaries*”, [SciPost Phys. 12, 141 \(2022\)](#), [arxiv:2112.01929](#).
- [63] M. Mintchev and E. Tonni, “*Modular Hamiltonians for the massless Dirac field in the presence of a boundary*”, [JHEP 2103, 204 \(2021\)](#), [arxiv:2012.00703](#).
- [64] M. Fagotti and P. Calabrese, “*Universal parity effects in the entanglement entropy of XX chains with open boundary conditions*”, [J. Stat. Mech. 1101, P01017 \(2011\)](#), [arxiv:1010.5796](#).
- [65] F. Rottoli, S. Murciano, E. Tonni and P. Calabrese, “*Entanglement and negativity Hamiltonians for the massless Dirac field on the half line*”, [J. Stat. Mech. 2301, 013103 \(2023\)](#), [arxiv:2210.12109](#).

- [66] A. Bastianello, “Rényi entanglement entropies for the compactified massless boson with open boundary conditions”, *JHEP* **1910**, 141 (2019), [arxiv:1909.00806](#).
- [67] A. Bastianello, J. Dubail and J.-M. Stéphan, “Entanglement entropies of inhomogeneous Luttinger liquids”, *J. Phys. A* **53**, 155001 (2020), [arxiv:1910.09967](#).
- [68] H. J. Schnitzer and K. Tsokos, “Partition Functions and Fermi-bose Equivalence for Simple Laced Groups on Compact Riemann Surfaces”, *Nucl. Phys. B* **291**, 429 (1987).
- [69] L. Alvarez-Gaume, G. W. Moore and C. Vafa, “Theta Functions, Modular Invariance and Strings”, *Commun. Math. Phys.* **106**, 1 (1986).
- [70] L. Alvarez-Gaume, J. B. Bost, G. W. Moore, P. C. Nelson and C. Vafa, “Bosonization on Higher Genus Riemann Surfaces”, *Commun. Math. Phys.* **112**, 503 (1987).
- [71] P. H. Ginsparg and C. Vafa, “Toroidal Compactification of Nonsupersymmetric Heterotic Strings”, *Nucl. Phys. B* **289**, 414 (1987).
- [72] S. Hamidi and C. Vafa, “Interactions on Orbifolds”, *Nucl. Phys. B* **279**, 465 (1987).
- [73] R. Dijkgraaf, E. P. Verlinde and H. L. Verlinde, “ $C = 1$ Conformal Field Theories on Riemann Surfaces”, *Commun. Math. Phys.* **115**, 649 (1988).
- [74] D. Bernard, “ Z_2 -twisted fields and bosonization on Riemann surfaces”, *Nucl. Phys. B* **302**, 251 (1988).
- [75] J. J. Atick, L. J. Dixon, P. A. Griffin and D. D. Nemeschansky, “Multi-loop twist field correlation functions for ZN orbifolds”, *Nucl. Phys. B* **298**, 1 (1988).
- [76] P. Calabrese and J. L. Cardy, “Evolution of entanglement entropy in one-dimensional systems”, *J. Stat. Mech.* **0504**, P04010 (2005), [cond-mat/0503393](#).
- [77] P. Calabrese and J. Cardy, “Entanglement and correlation functions following a local quench: a conformal field theory approach”, *J. Stat. Mech.* **0710**, P10004 (2007), [arxiv:0708.3750](#).
- [78] O. A. Castro-Alvaredo and B. Doyon, “Bi-partite entanglement entropy in massive $1+1$ -dimensional quantum field theories”, *J. Phys. A* **42**, 504006 (2009), [arxiv:0906.2946](#).
- [79] B. Estienne, Y. Ikhlef and A. Morin-Duchesne, “Finite-size corrections in critical symmetry-resolved entanglement”, *SciPost Phys.* **10**, 054 (2021), [arxiv:2010.10515](#).
- [80] R. Blumenhagen and E. Plauschinn, “Introduction to conformal field theory: with applications to String theory”, Springer (2009), Berlin Heidelberg.
- [81] E. Alvarez, J. L. F. Barbon and J. Borlaf, “ T duality for open strings”, *Nucl. Phys. B* **479**, 218 (1996), [hep-th/9603089](#).
- [82] C. Schweigert, J. Fuchs and J. Walcher, “Conformal field theory, boundary conditions and applications to string theory”, [hep-th/0011109](#).
- [83] H. M. Farkas and I. Kra, “Riemann surfaces”, Springer (1992).
- [84] H. Casini, C. D. Fosco and M. Huerta, “Entanglement and alpha entropies for a massive Dirac field in two dimensions”, *J. Stat. Mech.* **0507**, P07007 (2005), [cond-mat/0505563](#).

- [85] M. Oshikawa and I. Affleck, “Boundary conformal field theory approach to the critical two-dimensional Ising model with a defect line”, *Nucl. Phys. B* **495**, 533 (1997), [cond-mat/9612187](#).
- [86] C. Restuccia, “Limit theories and continuous orbifolds”, [arxiv:1310.6857](#).
- [87] I. Runkel and G. M. T. Watts, “A Nonrational CFT with $c = 1$ as a limit of minimal models”, *JHEP* **0109**, 006 (2001), [hep-th/0107118](#).
- [88] A. Recknagel and V. Schomerus, “Boundary Conformal Field Theory and the Worldsheet Approach to D-Branes”, Cambridge University Press (2013).
- [89] I. Peschel, “Calculation of reduced density matrices from correlation functions”, *J. Phys. A* **36**, L205 (2003), [cond-mat/0212631](#).
- [90] K. Audenaert, J. Eisert, M. Plenio and R. Werner, “Entanglement Properties of the Harmonic Chain”, *Phys. Rev. A* **66**, 042327 (2002), [quant-ph/0205025](#).
- [91] A. Botero and B. Reznik, “Spatial structures and localization of vacuum entanglement in the linear harmonic chain”, *Phys. Rev. A* **70**, 052329 (2004), [quant-ph/0403233](#).
- [92] M. Plenio, J. Eisert, J. Dreissig and M. Cramer, “Entropy, entanglement, and area: analytical results for harmonic lattice systems”, *Phys. Rev. Lett.* **94**, 060503 (2005), [quant-ph/0405142](#).
- [93] M. Cramer, J. Eisert, M. Plenio and J. Dreissig, “An Entanglement-area law for general bosonic harmonic lattice systems”, *Phys. Rev. A* **73**, 012309 (2006), [quant-ph/0505092](#).
- [94] N. Schuch, J. I. Cirac and M. M. Wolf, “Quantum States on Harmonic Lattices”, *Comm. Math. Phys.* **267**, 65 (2006).
- [95] S. Lievens, N. I. Stoilova and J. Van der Jeugt, “Harmonic oscillator chains as Wigner Quantum Systems: Periodic and fixed wall boundary conditions in $gl(1-n)$ solutions”, *J. Math. Phys.* **49**, 073502 (2008), [arxiv:0709.0180](#).
- [96] P. Calabrese, J. Cardy and E. Tonni, “Entanglement negativity in extended systems: A field theoretical approach”, *J. Stat. Mech.* **1302**, P02008 (2013), [arxiv:1210.5359](#).
- [97] C. Berthiere and W. Witczak-Krempa, “Relating bulk to boundary entanglement”, *Phys. Rev. B* **100**, 235112 (2019), [arxiv:1907.11249](#).
- [98] P. Jain, S. M. Chandran and S. Shankaranarayanan, “Log to log-log crossover of entanglement in $(1+1)$ -dimensional massive scalar field”, *Phys. Rev. D* **103**, 125008 (2021), [arxiv:2103.01772](#).
- [99] I. S. Gradshteyn and I. M. Ryzhik, “Table of Integrals, Series, and Products”, 7th edition, Academic Press (2007), 394p.
- [100] Y. K. Yazdi, “Zero Modes and Entanglement Entropy”, *JHEP* **1704**, 140 (2017), [arxiv:1608.04744](#).
- [101] V. Eisler and I. Peschel, “Evolution of entanglement after a local quench”, *J. Stat. Mech.* **0706**, P06005 (2007), [cond-mat/0703379](#).

- [102] P. Calabrese and J. Cardy, “Quantum quenches in 1 + 1 dimensional conformal field theories”, *J. Stat. Mech.* **1606**, 064003 (2016), [arxiv:1603.02889](#).
- [103] B. Estienne, Y. Ikhlef and A. Rotaru, “Rényi entropies for one-dimensional quantum systems with mixed boundary conditions”, [arxiv:2301.02124](#).
- [104] O. A. Castro-Alvaredo and B. Doyon, “Bi-partite entanglement entropy in massive QFT with a boundary: The Ising model”, *J. Stat. Phys.* **134**, 105 (2009), [arxiv:0810.0219](#).
- [105] J. Dubail, J.-M. Stéphan, J. Viti and P. Calabrese, “Conformal Field Theory for Inhomogeneous One-dimensional Quantum Systems: the Example of Non-Interacting Fermi Gases”, *SciPost Phys.* **2**, 002 (2017), [arxiv:1606.04401](#).
- [106] I. Peschel and V. Eisler, “Exact results for the entanglement across defects in critical chains”, *J. Phys. A* **45**, 155301 (2012), [arxiv:1201.4104](#).
- [107] I. Peschel and V. Eisler, “Exact results for the entanglement across defects in critical chains”, *J. Phys. A* **45**, 155301 (2012), [arxiv:1201.4104](#).
- [108] M. Gutperle and J. D. Miller, “Entanglement entropy at CFT junctions”, *Phys. Rev. D* **95**, 106008 (2017), [arxiv:1701.08856](#).
- [109] M. Mintchev and E. Tonni, “Modular Hamiltonians for the massless Dirac field in the presence of a defect”, *JHEP* **2103**, 205 (2021), [arxiv:2012.01366](#).
- [110] A. Roy and H. Saleur, “Entanglement Entropy in the Ising Model with Topological Defects”, *Phys. Rev. Lett.* **128**, 090603 (2022), [arxiv:2111.04534](#).
- [111] V. Fateev, A. B. Zamolodchikov and A. B. Zamolodchikov, “Boundary Liouville field theory. 1. Boundary state and boundary two point function”, [hep-th/0001012](#).
- [112] A. B. Zamolodchikov and A. B. Zamolodchikov, “Liouville field theory on a pseudosphere”, [hep-th/0101152](#).
- [113] V. Eisler and I. Peschel, “Free-fermion entanglement and spheroidal functions”, *J. Stat. Mech.* **1304**, P04028 (2013), [arxiv:1302.2239](#).
- [114] M. Mintchev, D. Pontello, A. Sartori and E. Tonni, “Entanglement entropies of an interval in the free Schrödinger field theory at finite density”, *JHEP* **2207**, 120 (2022), [arxiv:2201.04522](#).
- [115] M. Mintchev, D. Pontello and E. Tonni, “Entanglement entropies of an interval in the free Schrödinger field theory on the half line”, *JHEP* **2209**, 090 (2022), [arxiv:2206.06187](#).
- [116] A. B. Zamolodchikov, “Conformal symmetry in two-dimensional space: recursion representation of conformal block”, *Theor. Math. Phys.* **73**, 1088 (1987).
- [117] M. A. Rajabpour and F. Gliozzi, “Entanglement Entropy of Two Disjoint Intervals from Fusion Algebra of Twist Fields”, *J. Stat. Mech.* **1202**, P02016 (2012), [arxiv:1112.1225](#).
- [118] P. Ruggiero, E. Tonni and P. Calabrese, “Entanglement entropy of two disjoint intervals and the recursion formula for conformal blocks”, *J. Stat. Mech.* **1811**, 113101 (2018), [arxiv:1805.05975](#).

- [119] J.-M. Stephan and J. Dubail, “*Local quantum quenches in critical one-dimensional systems: entanglement, the Loschmidt echo, and light-cone effects*”, *J. Stat. Mech.* **1108**, P08019 (2011), [arxiv:1105.4846](#).
- [120] H. Casini, M. Huerta and R. C. Myers, “*Towards a derivation of holographic entanglement entropy*”, *JHEP* **1105**, 036 (2011), [arxiv:1102.0440](#).
- [121] A. M. Läuchli, “*Operator content of real-space entanglement spectra at conformal critical points*”, [arxiv:1303.0741](#).
- [122] J. Cardy and E. Tonni, “*Entanglement hamiltonians in two-dimensional conformal field theory*”, *J. Stat. Mech.* **1612**, 123103 (2016), [arxiv:1608.01283](#).
- [123] R. Arias, D. Blanco, H. Casini and M. Huerta, “*Local temperatures and local terms in modular Hamiltonians*”, *Phys. Rev. D* **95**, 065005 (2017), [arxiv:1611.08517](#).
- [124] E. Tonni, J. Rodríguez-Laguna and G. Sierra, “*Entanglement hamiltonian and entanglement contour in inhomogeneous 1D critical systems*”, *J. Stat. Mech.* **1804**, 043105 (2018), [arxiv:1712.03557](#).
- [125] V. Alba, P. Calabrese and E. Tonni, “*Entanglement spectrum degeneracy and the Cardy formula in 1+1 dimensional conformal field theories*”, *J. Phys. A* **51**, 024001 (2018), [arxiv:1707.07532](#).
- [126] V. Eisler and I. Peschel, “*Analytical results for the entanglement Hamiltonian of a free-fermion chain*”, *J. Phys. A* **50**, 284003 (2017), [arxiv:1703.08126](#).
- [127] V. Eisler and I. Peschel, “*Properties of the entanglement Hamiltonian for finite free-fermion chains*”, *J. Stat. Mech.* **2018**, 104001 (2018), [arxiv:1805.00078](#).
- [128] R. E. Arias, H. Casini, M. Huerta and D. Pontello, “*Entropy and modular Hamiltonian for a free chiral scalar in two intervals*”, *Phys. Rev. D* **98**, 125008 (2018), [arxiv:1809.00026](#).
- [129] J. Surace, L. Tagliacozzo and E. Tonni, “*Operator content of entanglement spectra in the transverse field Ising chain after global quenches*”, *Phys. Rev. B* **101**, 241107(R) (2020), [arxiv:1909.07381](#).
- [130] G. Di Giulio and E. Tonni, “*On entanglement hamiltonians of an interval in massless harmonic chains*”, *J. Stat. Mech.* **2003**, 033102 (2020), [arxiv:1911.07188](#).
- [131] G. Di Giulio, R. Arias and E. Tonni, “*Entanglement hamiltonians in 1D free lattice models after a global quantum quench*”, *J. Stat. Mech.* **1912**, 123103 (2019), [arxiv:1905.01144](#).
- [132] V. Eisler, E. Tonni and I. Peschel, “*On the continuum limit of the entanglement Hamiltonian*”, *J. Stat. Mech.* **1907**, 073101 (2019), [arxiv:1902.04474](#).
- [133] V. Eisler, G. Di Giulio, E. Tonni and I. Peschel, “*Entanglement Hamiltonians for non-critical quantum chains*”, *J. Stat. Mech.* **2010**, 103102 (2020), [arxiv:2007.01804](#).
- [134] N. Javerzat and E. Tonni, “*On the continuum limit of the entanglement Hamiltonian of a sphere for the free massless scalar field*”, *JHEP* **2202**, 086 (2022), [arxiv:2111.05154](#).

- [135] V. Eisler, E. Tonni and I. Peschel, “*Local and non-local properties of the entanglement Hamiltonian for two disjoint intervals*”, *J. Stat. Mech.* **2208**, 083101 (2022), [arxiv:2204.03966](#).
- [136] G. Vidal and R. F. Werner, “*Computable measure of entanglement*”, *Phys. Rev. A* **65**, 032314 (2002), [quant-ph/0102117](#).
- [137] P. Calabrese, J. Cardy and E. Tonni, “*Entanglement negativity in quantum field theory*”, *Phys. Rev. Lett.* **109**, 130502 (2012), [arxiv:1206.3092](#).
- [138] P. Calabrese, J. Cardy and E. Tonni, “*Finite temperature entanglement negativity in conformal field theory*”, *J. Phys. A* **48**, 015006 (2015), [arxiv:1408.3043](#).
- [139] A. Coser, E. Tonni and P. Calabrese, “*Towards the entanglement negativity of two disjoint intervals for a one dimensional free fermion*”, *J. Stat. Mech.* **1603**, 033116 (2016), [arxiv:1508.00811](#).
- [140] A. Coser, E. Tonni and P. Calabrese, “*Partial transpose of two disjoint blocks in XY spin chains*”, *J. Stat. Mech.* **1508**, P08005 (2015), [arxiv:1503.09114](#).
- [141] V. Eisler and Z. Zimborás, “*Entanglement negativity in two-dimensional free lattice models*”, *Phys. rev. B* **93**, 115148 (2016), [arxiv:1511.08819](#).
- [142] C. De Nobili, A. Coser and E. Tonni, “*Entanglement negativity in a two dimensional harmonic lattice: Area law and corner contributions*”, *J. Stat. Mech.* **1608**, 083102 (2016), [arxiv:1604.02609](#).
- [143] H. Shapourian, K. Shiozaki and S. Ryu, “*Partial time-reversal transformation and entanglement negativity in fermionic systems*”, *Phys. Rev. B* **95**, 165101 (2017), [arxiv:1611.07536](#).
- [144] V. Eisler and Z. Zimborás, “*On the partial transpose of fermionic Gaussian states*”, *New J. Phys.* **17**, 053048 (2015), [arxiv:1502.01369](#).
- [145] I. R. Klebanov, T. Nishioka, S. S. Pufu and B. R. Safdi, “*On Shape Dependence and RG Flow of Entanglement Entropy*”, *JHEP* **1207**, 001 (2012), [arxiv:1204.4160](#).
- [146] P. Fonda, L. Giomi, A. Salvio and E. Tonni, “*On shape dependence of holographic mutual information in AdS₄*”, *JHEP* **1502**, 005 (2015), [arxiv:1411.3608](#).
- [147] P. Fonda, D. Seminara and E. Tonni, “*On shape dependence of holographic entanglement entropy in AdS₄/CFT₃*”, *JHEP* **1512**, 037 (2015), [arxiv:1510.03664](#).
- [148] D. Seminara, J. Sisti and E. Tonni, “*Corner contributions to holographic entanglement entropy in AdS₄/BCFT₃*”, *JHEP* **1711**, 076 (2017), [arxiv:1708.05080](#).
- [149] D. Seminara, J. Sisti and E. Tonni, “*Holographic entanglement entropy in AdS₄/BCFT₃ and the Willmore functional*”, *JHEP* **1808**, 164 (2018), [arxiv:1805.11551](#).
- [150] P. Bueno, H. Casini, O. L. Andino and J. Moreno, “*Disks globally maximize the entanglement entropy in 2 + 1 dimensions*”, *JHEP* **2110**, 179 (2021), [arxiv:2107.12394](#).
- [151] I. Affleck, “*Edge magnetic field in the XXZ spin-1/2 chain*”, *J. Phys. A* **31**, 2761 (1998).

- [152] B. Nienhuis, “*Critical behavior of two-dimensional spin models and charge asymmetry in the Coulomb gas*”, *J. Stat. Phys.* **34**, 731 (1984).
- [153] S. Eggert and I. Affleck, “*Magnetic impurities in half integer spin Heisenberg antiferromagnetic chains*”, *Phys. Rev. B* **46**, 10866 (1992).
- [154] J. Sully, M. Van Raamsdonk and D. Wakeham, “*BCFT entanglement entropy at large central charge and the black hole interior*”, *JHEP* **2103**, 167 (2021), [arxiv:2004.13088](#).
- [155] B. Chen and J.-q. Wu, “*Universal relation between thermal entropy and entanglement entropy in conformal field theories*”, *Phys. Rev. D* **91**, 086012 (2015), [arxiv:1412.0761](#).
- [156] T. Dupic, B. Estienne and Y. Ikhlef, “*Entanglement entropies of minimal models from null-vectors*”, *SciPost Physics* **4**, 031 (2018).
- [157] B. Estienne, Y. Ikhlef and A. Rotaru, “*The operator algebra of cyclic orbifolds*”, [arxiv:2212.07678](#).
- [158] P. Di Francesco, P. Mathieu and D. Senechal, “*Conformal Field Theory*”, Springer-Verlag (1997), New York.
- [159] A. Coser, E. Tonni and P. Calabrese, “*Entanglement negativity after a global quantum quench*”, *J. Stat. Mech.* **1412**, P12017 (2014), [arxiv:1410.0900](#).